Modeling and Analysis of Modular Multi-level Converter-Based HVDC Systems to Investigate Geomagnetic Disturbance Effects

HAMZEH HOSSEINPOUR

A THESIS SUBMITTED TO THE FACULTY OF GRADUATE STUDIES
IN PARTIAL FULFILMENT OF THE REQUIREMENTS
FOR THE DEGREE OF MASTER OF APPLIED SCIENCE

GRADUATE PROGRAM IN ELECTRICAL ENGINEERING AND COMPUTER SCIENCE
YORK UNIVERSITY
TORONTO, ONTARIO

DECEMBER 2023

Abstract

The MMC-based HVDC systems provide excellent performance. As geomagnetic disturbances (GMD) can be catastrophic events for the power system including MMCs, this research is dedicated to investigating the GMD impacts on the MMC systems. A practical system is selected to provide the most realistic and reliable results. An analytical model is provided to determine the share of the MMC in the harmonics resulting from transformer saturation. Also, a mitigating control block is designed and proposed to eliminate major harmonics in the grid current in the case of GMD. It improves the power quality in the grid, and it reduces the risk of blackout in the system. A control approach is proposed for the reactive power compensation during GMD. It supports grid voltage stability. Simulation results are provided to validate the effectiveness of the proposed methods, which improve the grid power quality and reduce the risk of voltage collapse.

Acknowledgment

I would like to express my sincere gratitude to my advisor, Dr. Afshin Rezaei-Zare, for his expertise, guidance, constant support, and encouragement throughout my research. This work would not have been possible without his supervision. I have been extremely fortunate to work under his supervision and learned much from him with his knowledge, skills, and valuable insights.

Dedication

To those whom I love unconditionally.

Table of Contents

List of Tables

List of Figures

Abbreviations

RES	Renewable Energy Resources
HVDC	High Voltage Direct Current
CSC	Current Source Converter
LCC	Line-Commutated Converters
VSC	Voltage Source Converter
MMC	Modular Multi-level Converter
GMD	Geomagnetic Disturbance
GIC	Geomagnetically Induced Current
NPC	Neutral-Point-Clamped
NLC	The Nearest Level Control
CBA	Capacitor Balancing Algorithm
MCB	Mitigating Control Block
THD	Total Harmonic Distortion

Chapter 1

Introduction

1.1 Motivation

Due to climate change, renewable energy resources (RESs), including solar and wind power, are gaining more and more attention. In 2020, the installed capacity for wind and solar energy surpassed hydropower. At the end of 2021, the total capacity for the RESs reached 3000 GW, mainly comprising solar and wind power, as depicted in Figure 1-1 [1-3].

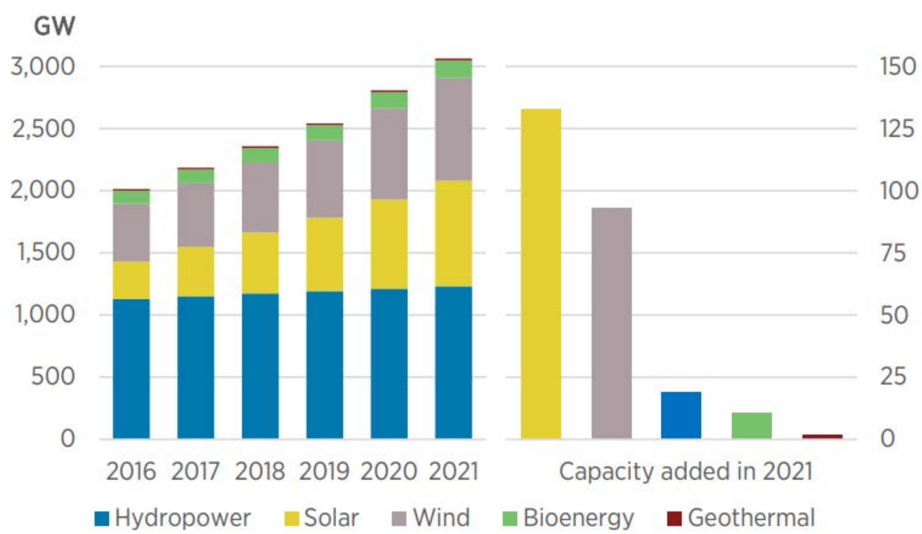

Figure 1-1. Renewable power capacity growth [3].

The RES plants are generally in remote areas, requiring a long transmission of power. Figure 1-2 shows the drastic growth of offshore wind power generation for different countries. In addition to conventional AC transmission lines, high-voltage direct-current (HVDC) based on current source converters (CSC) have been used for decades, and now they have reached the voltage level of hundreds of kV and range up to 2200 km [4]. It has been proved that DC transmission offers more advantages than AC systems in the case of long ranges, bulk power transmission or submarine cables [5].

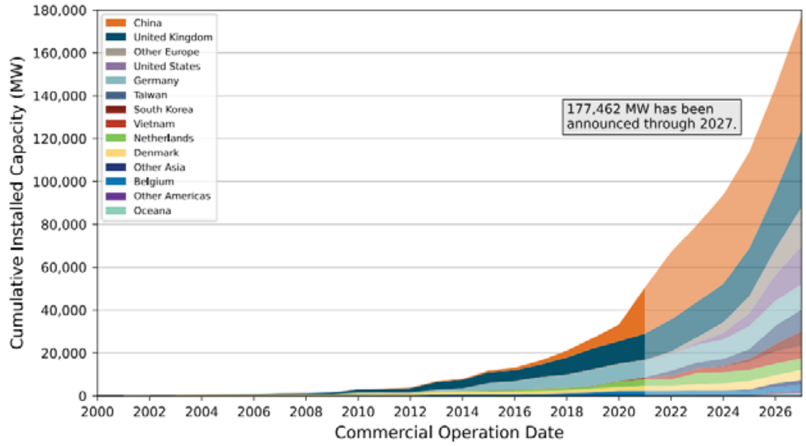

Figure 1-2. Estimated cumulative offshore wind capacity by country [6].

Some disadvantages of line-commutated converters (LCCs) based HVDC systems are low controllability, the need for large filters, and the consumption of reactive power [1]. The development of semiconductor switches, including IGBTs, made the voltage source converter (VSC) HVDC transmission possible. Among the VSCs, the modular multi-level converter (MMC) is dominating the applications as it offers higher efficiency and stability and a lower level of output harmonics, which eliminates the need for bulky filters [7]. Figure 1-3 depicts the history of HVDC systems.

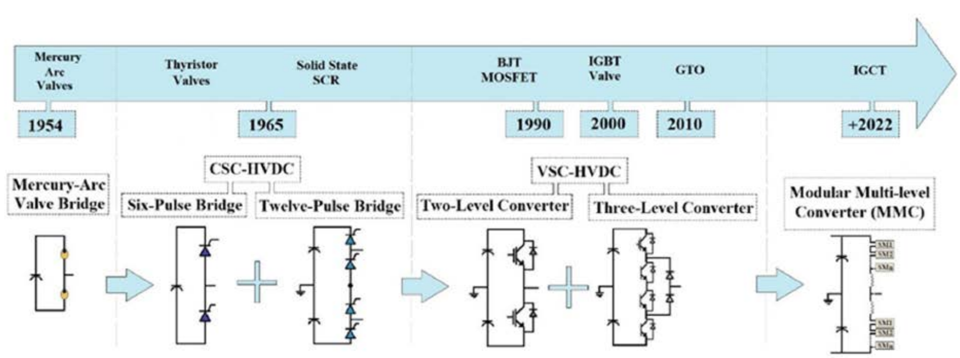

Figure 1-3. The technological evolution of the HVDC systems [5]

One of the risks to the MMC operation is the solar storm. In the case of a geomagnetic disturbance (GMD), the earth's magnetosphere is disturbed, and the earth's magnetic field changes, as depicted in Figure 1-4. The conditions of GMD can last for a few days [8]. Due to this time-varying magnetic field, a voltage is induced in the circuit, including the transmission lines. Consequently, through the transformer ground connection, a current due to the GMD can flow. As the geomagnetically induced current(GIC) flows into the circuit, the power system faces a number of problems [9]. The impacts of the GMD threaten the normal operation of several key elements in the power system. In extreme cases, the GIC can cause a blackout in the system, as it occurred in 1989 in the Hydro-Québec power system [10]. This research aims to investigate the impacts of the GMD on the MMC-based HVDC system.

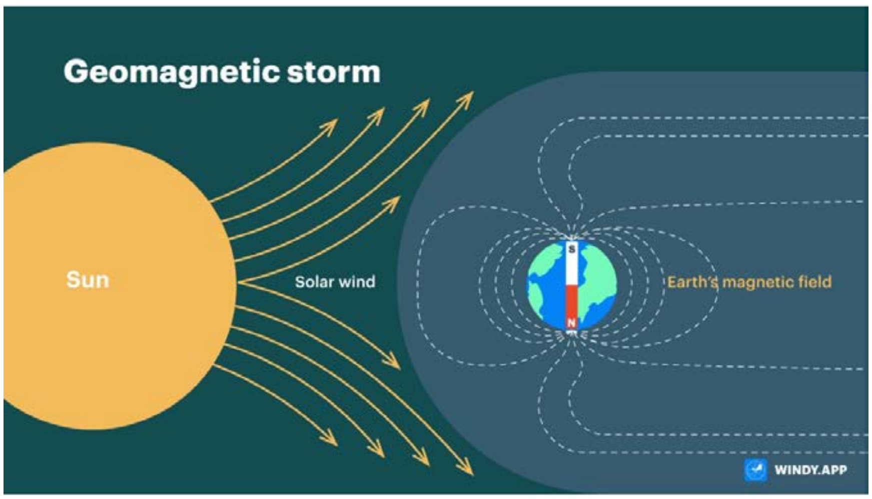

Figure 1-4. Solar wind of charged particles toward earth [11].

1.1.1 Power System Resilience

The resiliency of the power system is gaining importance increasingly as the effect of extreme weather condition is becoming more apparent [12, 13] . These conditions could have a low possibility but the impacts of such events could be huge on the power system [14, 15]. Also due to climate change, the frequency of these condition could increase in the future [16]. The definition and tools for assessment of resiliency have been subject to a number of research projects [17-19]. The effect of harsh weather conditions on the power systems is assessed through the impacts of such events on the reliability of the power system components using special models [16, 20, 21]. A thorough investigation of reliability assessment of components in case of harsh weather can be found in [22-30].

In terms of power system resilience, this research provides analysis of the effects the GMD, which is a weather condition, on the MMC-HVDC systems for the first time and it provides solutions to support power system performance and resiliency. Using the approaches provided in this research improves the grid voltage stability and power system robustness and improves power system resiliency.

The remainder of this report is organized into the following sections:

Chapter 2 is dedicated to the literature review. It provides the background on the effects of GMD on the power system. GIC's effects on different components of the power system are elaborated on in this chapter. Then, it provides a review of the HVDC transmission systems. This chapter explains why the MMC is selected for the study, and it emphasizes the lack of appropriate research in this area.

Chapter 3 explores the details of the study system. Different elements of the MMC station in terms of power components and control systems are examined. Various layers of the control system are reviewed in this chapter. The upper control layer, that is the system-wide control loop that controls the main outputs of the converter, is explained, and also the lower control level, which does the modulation, balancing the SMs voltages and mitigation of the circulation current, is reviewed in detail to provide a comprehensive understanding of the study system.

Chapter 4 is dedicated to the GMD impacts on the MMC system. It states that the resulting harmonics from the saturation of the transformer are distributed between the grid and the MMC. The reactive power demand of the saturated transformer is also discussed. An analytical model is provided in this chapter to determine the share of the MMC in these harmonics. This model considers the internal interactions of the MMC, and it also takes into account the operating point of the converter. Also, a mitigating control block is designed and proposed to eliminate the 2^{nd},4^{th},5^{th},7^{th} and 8^{th} harmonics in the grid current in the case of GMD. This MCB improves the power quality in the grid, and it reduces the risk of blackouts in the system. Finally, a control approach is proposed for the reactive power compensation during GMD. This control approach injects reactive power from the MMC and supports the grid voltage stability.

Chapter 5 includes the simulation results of the study system under GIC. The simulation results are done in the time domain using EMTP software. In this chapter, different levels of GIC are applied to the MMC, and the results are discussed. Also, it is demonstrated that in the presence of GIC, the grid permissible THD for the current and the voltage waveforms are violated. The results from the analytical model and simulations are compared. Lastly, simulation results are provided to prove the efficiency of the proposed control solutions. It is illustrated in this chapter that as the proposed control solutions are activated, the harmonics in the grid current reduce, which is critical for normal operation of the power system components, and the MMC provides reactive power to the saturated transformer instead of the grid. The latter means voltage support for the grid and mitigation of voltage collapse risk.

Chapter 6 is the final section of the thesis devoted to the summary and conclusion of the research. It also provides suggestions and guidelines for future work.

Chapter 2

Geomagnetic Disturbance and MMCs

2.1 Geomagnetically Induced Current

GMD arises from sun activities. Solar coronal holes and coronal mass ejections (CMEs) are the two main classes of events that cause solar magnetic disturbances toward the Earth. CMEs mean the flow of large amounts of charged particles toward the earth, and if they travel directly to the earth, GICs are created, as depicted in Figure 2-1 [31].

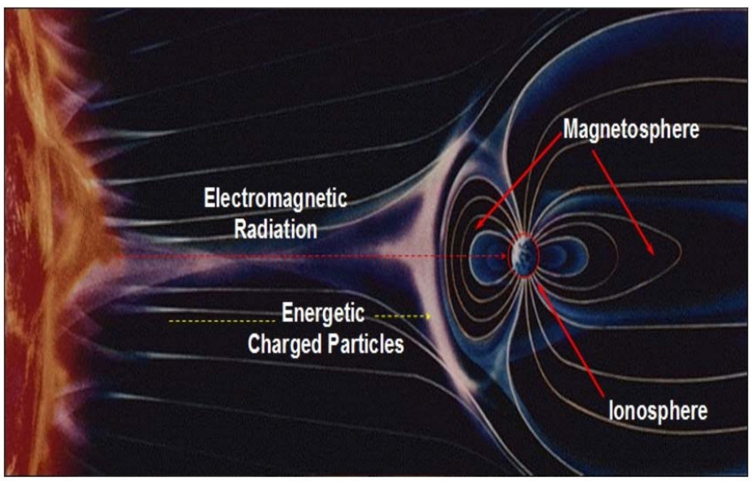

Figure 2-1. Flow of magnetic storm toward earth's atmosphere.

The CME has its currents and magnetic fields, which can change the earth's magnetic field. The charged particles' movement in the conductive part of the atmosphere boosts the currents in the electrojets, which are large currents flowing at a distance to the earth's surface. The result of electrojets is an induced quasi-DC voltage in electrical circuits. Consequently, if an electrical path is provided, the GIC will flow in the power system. GICs are considered quasi-DC currents since their frequency is usually in the range of 0.1 mHz to 0.1 Hz. GMD events can last between 24 to 48 hours. The GIC path is composed of the transmission line, neutral points of the transformer and the ground shown in Figures 2-2 and 2-3 [9]. GIC effects are not limited to the power system, and they can also interfere with the operation of conducting networks, including pipelines and communication cables [32].

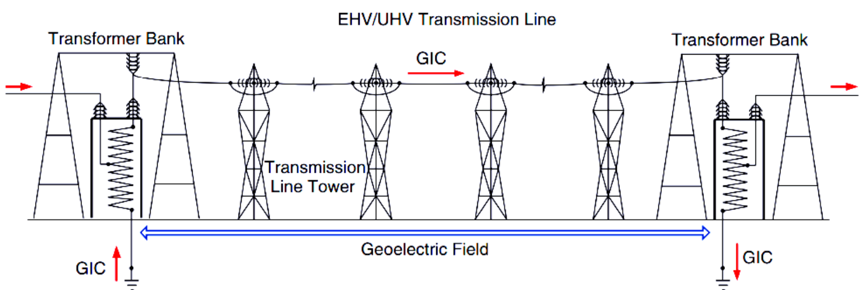

Figure 2-2. GIC path in the power system.

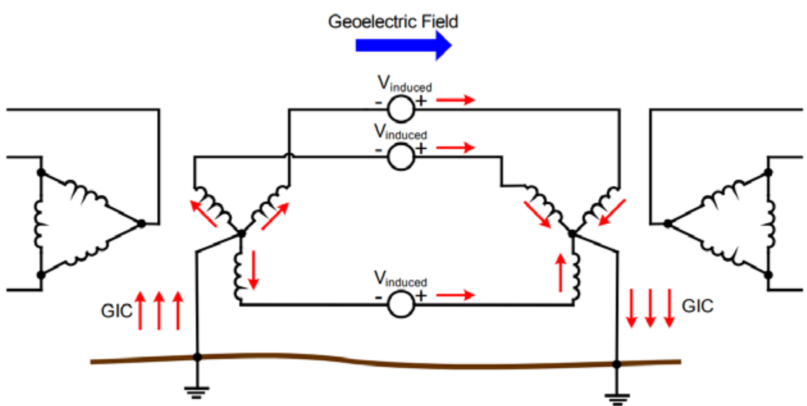

Figure 2-3. GIC flow in the neutral connections of the power transformers [33].

During this period, the GIC level is usually low to moderate, but there are sporadic high peaks in the GIC level [9]. These peaks in the GIC levels impose threats and concerns on the power systems, Figure 2-4 shows the profile for a GMD and associated peaks. The factors that affect the GMD severity involve:

- geomagnetic latitude

- local ground resistivity
- power system configuration along with capabilities of the critical equipment

The first reported GMD effects on power systems occurred in 1940 [32]. Corporates in cities in North America reported disturbances in the power grid. Major and minor effects of GMD on power systems were reported in 1958 and 1972, respectively [8]. On March 13-14, 1989, one of the most Catastrophic GMD events in the century occurred. Several transformers were saturated due to high levels of GIC in the Hydro-Québec power system [10].

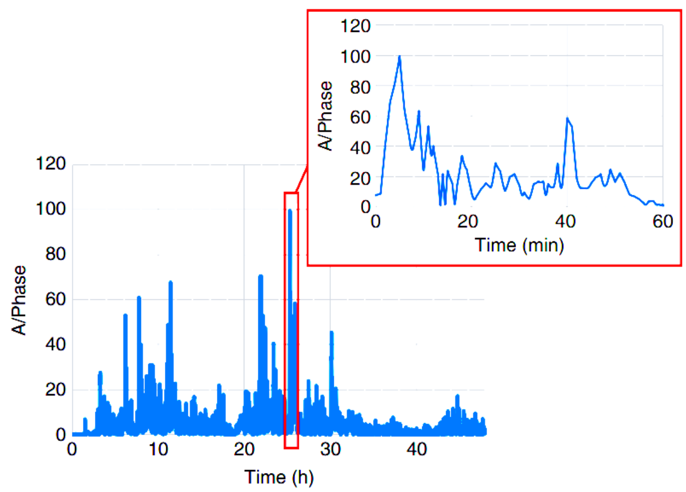

Figure 2-4. Estimated GIC in a large power transformer in a 48-h period [9].

As the resulting harmonic from transformers saturation flew into the power system, the static VAR compensators were tripped by protecting devices. Due to the outage of the VAR compensators that improve the grid stability, a drastic voltage dip occurred in the power system, which was the beginning of the collapse of the power system that happened shortly later [32]. This led to a power outage for 6 million people [34], and the damage was estimated to cost around $6 billion [35]. The following mitigation measures cost $1.2 billion for this network [35]. Damage to two phases of a transformer bank of a nuclear plant was reported in the USA [36]. Also, two high-voltage transformers were damaged in the UK due to this storm [37]. The postevent report from NERC counted more than 200 major anomalies all over the continent due to this one storm [38].

2.2 GIC Impacts on Power System

The impacts of the GIC are studied as the GIC effects on the grid components and subsystems, including [39]:

- Power Transformers
- Protection Systems
- CT Saturation
- Static VAR Compensators
- Generators
- HVDC Transmission Systems

2.2.1 GIC Impacts on Power Transformers

The major effect of the GIC on the power system occurs through the transformer of the transmission lines. If the transformer neutral is connected to the ground, a path is provided for the GIC to flow, and it is distributed among the three phases [39-42].

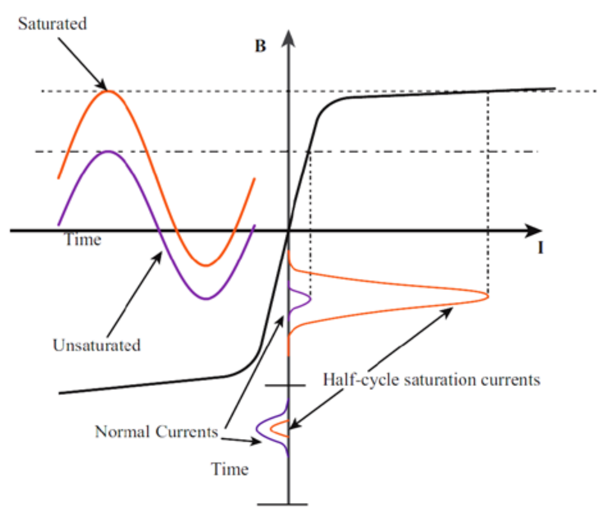

Figure 2-5. Transformer saturation due to GIC.

When this quasi-DC current flows in the winding of the transformer, the transformer flux is shifted, as depicted in Figure 2-5. This unidirectional shift in the flux of the transformer makes the flux saturated in the half cycle, leading to an asymmetric magnetizing current shown in Figure 2-6. Table 2-1 illustrates the relation between the GIC and the magnetizing current peak and RMS. The half-cycle saturation of the flux is the root of the problems [9]. It leads to harmonics generation, transformer heating and a drastic increase in transformer magnetizing current and, ultimately, reactive power consumption [41, 43-48].

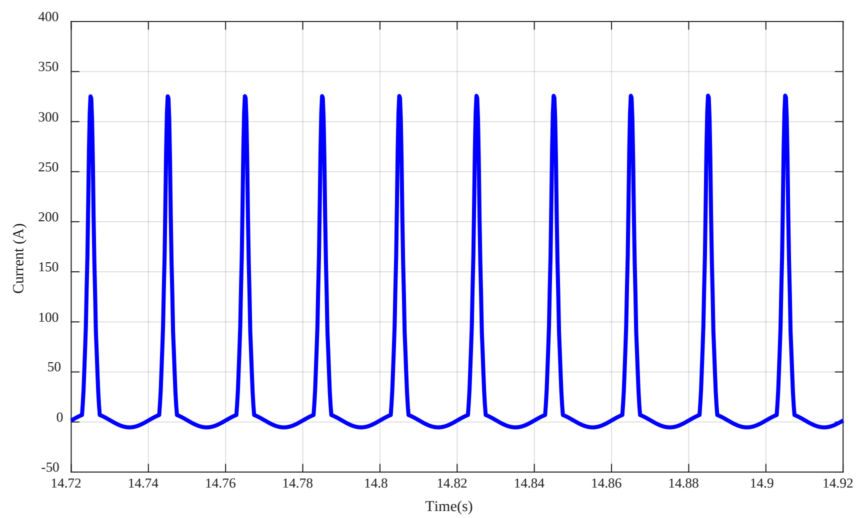

Figure 2-6. Magnetizing current waveform of the transformer exposed to GIC.

Table 2-1. Relation between the GIC level and the peak current in the magnetizing branch [8].

I_{DC}/phase(A)	Peak magnetizing current(A)	RMS magnetizing current (A)
20	390	88
33	570	118
47	745	157

The physical configuration of the transformer affects the magnitude of the DC shift in the flux. The order of vulnerability of the different types of transformers is as follows, and it must be noted that the single-phase transformers are most vulnerable to the GIC [40, 49-51].

- shell-form (conventional) core – most susceptible
- three-phase, seven-leg
- three-phase, five-leg
- three-phase, three-leg – least susceptible

Different types of transformer configurations are depicted in Figure 2-7 [39].

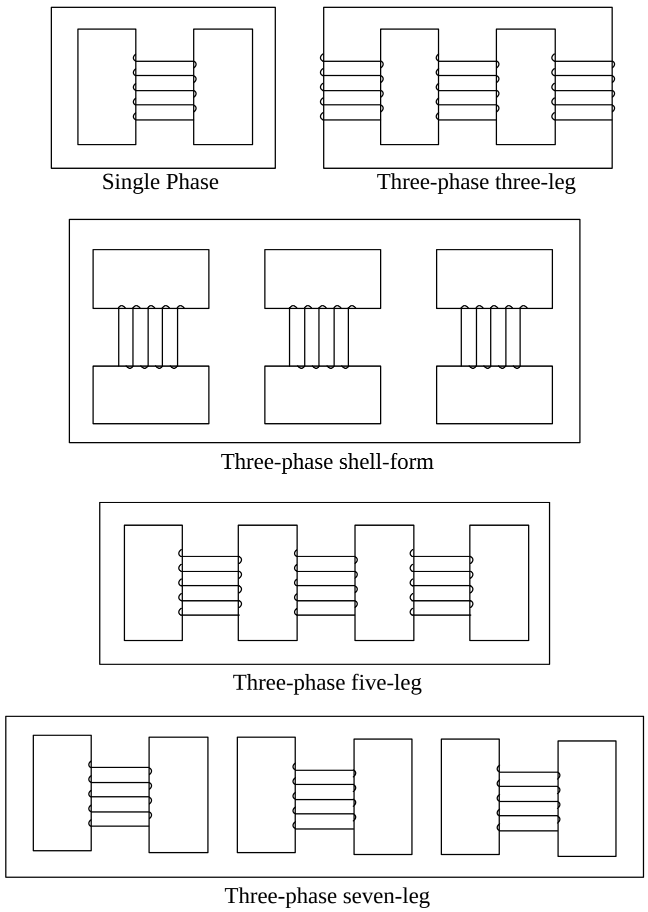

Figure 2-7. Different types of three-phase transformer structures.

Figure 2-8 demonstrates the effect of DC current in the winding of transformers with different core types. One transformer is single phase, and the second one is the three-phase, 3-leg structure. It is clear that for a given DC current, the single-phase transformer is more vulnerable than the three-phase transformer as the magnetic resistance of the single phase is drastically less compared to the magnetic resistance for the DC field of the three-phase transformer.

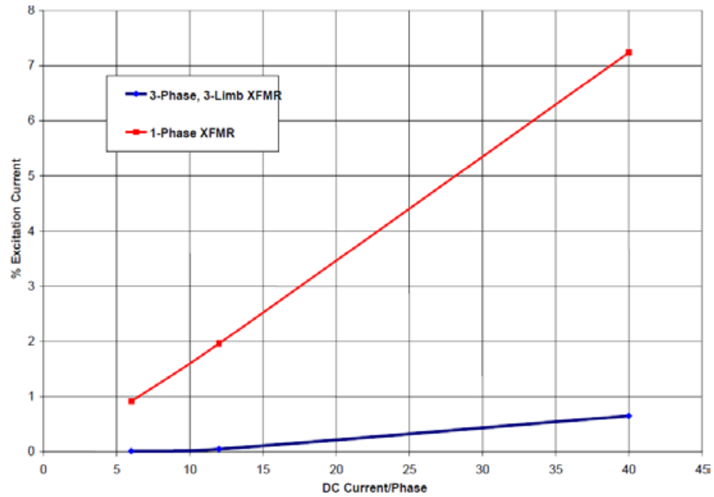

Figure 2-8. RMS of magnetizing current of two transformers exposed to DC current [8].

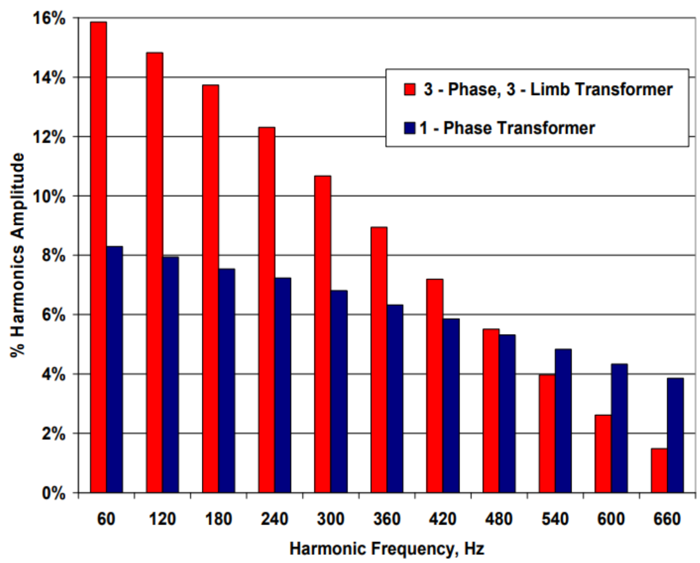

Figure 2-9. Resulting harmonics of two transformers exposed to DC current [52].

Half-cycle saturation due to GIC also creates a spectrum of harmonics, including odd and even ones in the magnetizing current of the transformer [52-54]. Figure 2-9 and Table 2-2, display the produced harmonics in the case of GIC for a simulation study and measured harmonics in an actual GMD event. The increased magnetizing current of the transformer, due to half-cycle saturation, leads to a higher core loss in the transformer, which heats up the core and the other metallic parts [39, 55, 56]. In [45], it is illustrated the temperature rise due to GIC-caused heat could violate the relevant standards. The temperature rises due to the GIC level on a studied transformer is depicted in Figure 2-10.

Table 2-2. Measured harmonics in the Hydro-Québec blackout [57].

Harmonic Order	Voltage Waveform	Current Waveform
1	100 %	100%
2	5.1%	145%
3	3.4%	39%
4	0.5%	90%
5	0.9%	28%
6	0.4%	8%
7	0.2%	3%

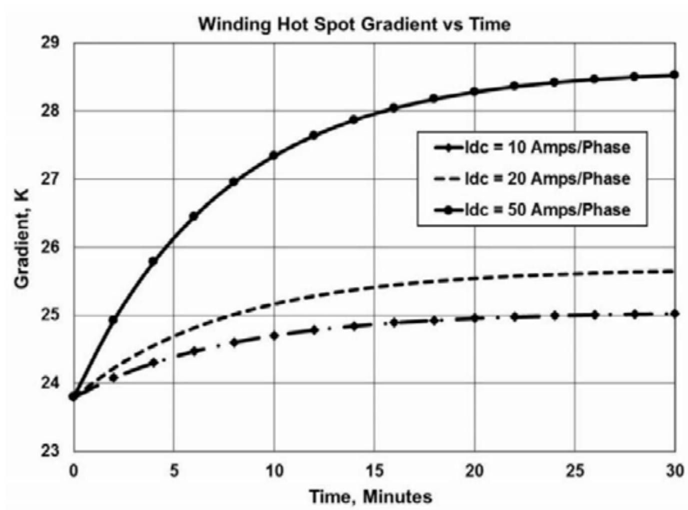

Figure 2-10. Calculated temperature rise of a single phase 250 MVA transformer exposed variant GIC levels [33].

The last important effect of the GIC on the power transformer is the increase in reactive power demand. One major resulting harmonic due to GIC impact on the transformer core is the first harmonic. This effect on the transformer reactive power consumption due to GIC has been studied in several studies [43, 48, 58]. This current lags the transformer voltage by 90 degrees, and it is a purely inductive load on the grid [44]. As the GIC level increases, higher reactive power is demanded by the transformer, as depicted in Figure 2-11.

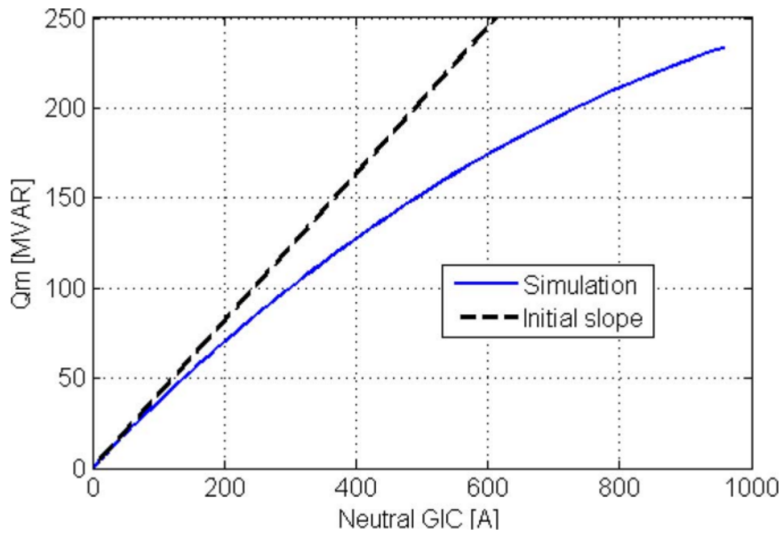

Figure 2-11. Reactive power demand of a 500kV transformer exposed to GIC [44].

2.2.2 GIC Impacts on Protection Systems

The presence of GIC can interfere with the operation of protective relays [59, 60]. It can cause malfunctions in the relays, including neutral overcurrent and overvoltage relays, phase overcurrent, Buchholz relays, and differential relays [61, 62]. If the peak or the average of waveforms are used for calculation, the resulting harmonic from GIC can lower the accuracy [63, 64]. In differential relays, due to the use of a harmonic blocking scheme, undesired blocking can happen during the internal faults in the transformer [59, 60]. The protections of the capacitor banks are also prone to the GIC. The resulting harmonics from half-cycle saturation tend to flow into the capacitor banks as they have lower impedance due to capacitive characteristics [61]. Consequently, the overvoltage and overcurrent relays might trip in this situation [64, 65]. Furthermore, the resulting harmonic can also cause the unbalance protection system to trip [66].

2.2.3 GIC Impacts on Static VAR Compensators

Static VAR compensators (SVCs) are used to control the key buses voltages actively by varying the bus impedance, which results in improving the stability of the grid. The presence of a large level of second harmonic can cause problems in the control unit of SVCs since it results in an asymmetry in the reactor current [39]. This problem is created as the GIC flows in the reactor and causes saturation, and in general, the control system is not able to eliminate the effect of the second harmonic [66]. As the capacitor banks prove a lower path for the harmonics, the GIC can expose the capacitor banks to the following [8]:

- Overcurrent
- Overvoltage
- Unbalance operation
- Resonance

Figure 2-12 displays the overvoltage problem in a capacitor bank due to the GIC level.

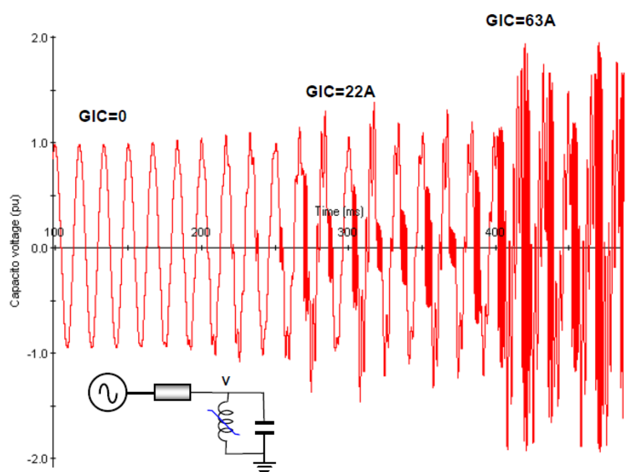

Figure 2-12. Capacitor bank over voltage depending on the GIC level [8].

2.2.4 GIC Impacts on Generators

Since the generators are usually neighbouring the step-up transformer and due to the delta-wye connection of the windings of this transformer, the GIC does not flow in the generators.

Nevertheless, the generator is affected by the increased reactive power demand and also resulting harmonics from core half-cycle saturation, especially the negative sequence currents, including second and fifth harmonics [39]. The field current is increased in the generator to meet the higher demand for reactive power, which results in thermal stress, and it may bring the generator to the limits [61, 67]. The main effect is due to the negative sequence current to which the generators are valuable. The flow of these currents creates heat in the generator's windings and vibration [9, 66, 68-70]. The protecting equipment, including the negative sequence relay, might also malfunction during the GIC [71].

2.2.5 GIC Impacts on HVDC Transmission Systems

In this section, before reviewing the literature on the GIC impacts on HVDC systems, a brief introduction to the history of HVDC systems and the configurations and technologies is provided hereafter.

Due to specific features of HVDC systems, they are considered as superior solutions in long-distance high-volume power transmission, interconnections of different grids and submarine cable projects [72]. In a basic classification, HVDC systems are divided into two main configurations:

- Line-Commutated Converters (LCCs)
- Voltage Source Converters (VSCs)

2.2.5.1 LCC-HVDC Systems

LCCs use thyristors as the control valve in the converters. After the thyristor is on by applying the trigger pulse, it cannot be turned off, and the current must cross zero to have the switch off. The firing angle of thyristors is the relative time it receives the trigger pulse, and it determines when the thyristor turns on. The LCC-HVDC system was first started in the 1970s [73], and most of the HVDC systems in the world now are based on LCCs [74]. Figure 2-13 depicts the structure of a typical LCC-HVDC system.

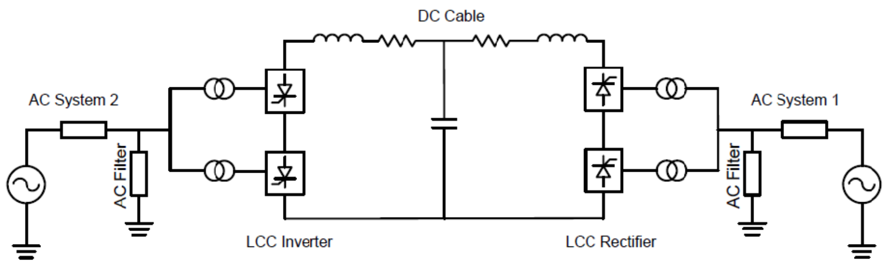

Figure 2-13. Typical LCC-HVDC system.

Each LCC-HVDC system includes the following:

A) HVDC Converters

The primary configuration for the converter is composed of 6 thyristors and is called a 6-pulse bridge. This unit converts AC to DC and the reverse, and it uses a transformer to exchange power to the grid [75]. Each converter could act either as a rectifier or inverter. To form a 12-pulse converter, two 6-pulse bridges must be in series on the DC side, and they must connect in parallel to the AC side. Two bridges are connected to the grid using a wye/wye transformer and a wye/delta transformer that provide a 30-degree phase shift needed for the operation. This configuration is the most common structure in the LCC/HVDC systems, which is depicted in Figure 2-14 [75, 76]. To obtain a 24-pulse converter, four 6-pulse bridges must work in series on the DC side and in parallel on the AC side. There must be a 15-degree phase shift in the input voltage of the bridges that is provided through the transformers as depicted in Figure 2-15 [75].

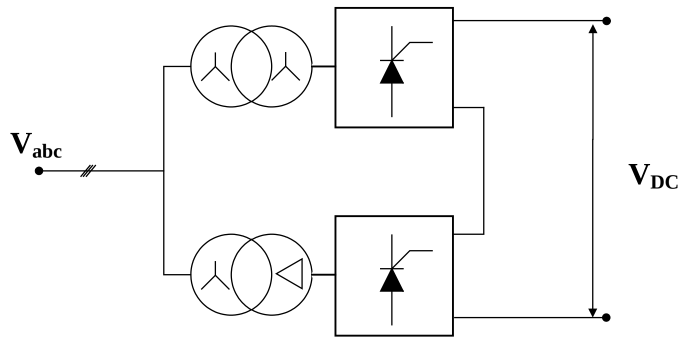

Figure 2-14. 12-pulse LCC configuration.

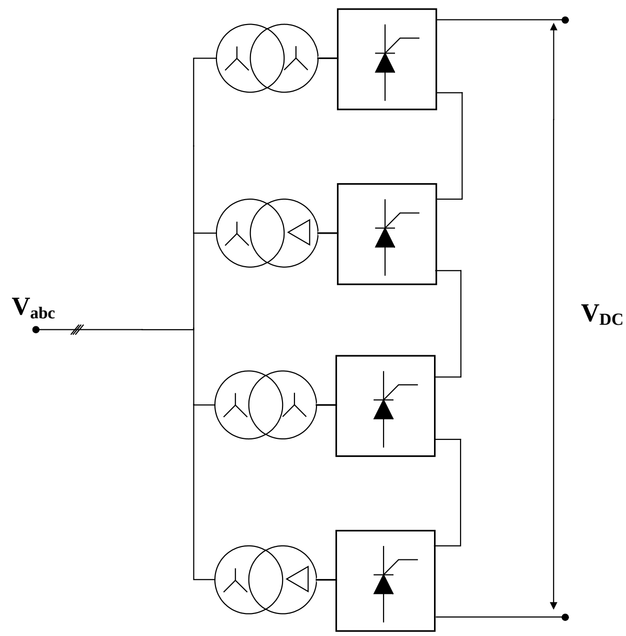

Figure 2-15. 24-pulse LCC system.

B) Filters

Each converter station is equipped with harmonic filters. Since the operation of the converter creates harmonics on both the DC and AC sides, the use of DC and AC filers is mandatory. Three main filters are used in the converter station:

- AC filter that is composed of passive components to provide a low impedance path for harmonics.
- DC filter, which is similar to the AC filter.

- High-frequency filter that is used to prevent the interference of the produced harmonics with the communications that use the power conductors.

C) Reactive Power Compensator

The conventional way of dealing with the high demand for reactive power at the stations of the HVDC is to use switched capacitors or devices that can dynamically compensate for the reactive power, including SVCs, STATCOM and the neighbouring generator excitation control [73].

D) Smoothing Reactor

To smooth the current and decrease the ripple on the DC side, this reactor is used. It also acts as a buffer between the DC side and the converter. This inductor prevents discontinuous current on the DC side in case of low power transfer, and it reduces the stress on the converter due to lightning on the DC lines [75].

There are two main configurations for an LCC-HVDC system: monopolar and bipolar systems, as depicted in Figures 2-16 and 2-17. Monopolar links are mostly used in the long-distance transmission of power or extended submarine cable runs since they offer the lowest cost [5]. The bipolar configuration is composed of two monopolar systems, which is used to reach higher power capacity of higher system security [77, 78].

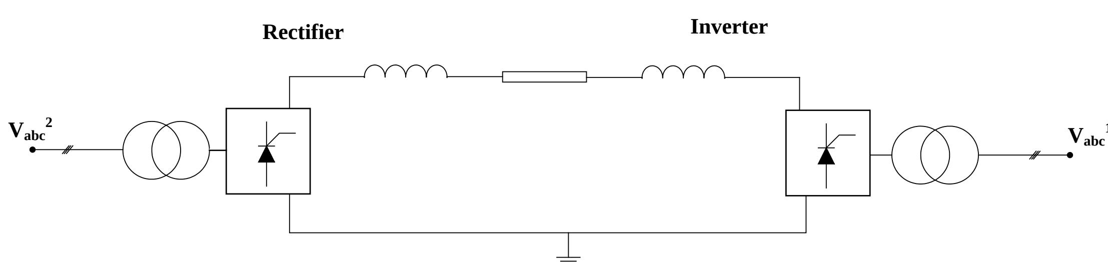

Figure 2-16. Monopolar LCC-HVDC

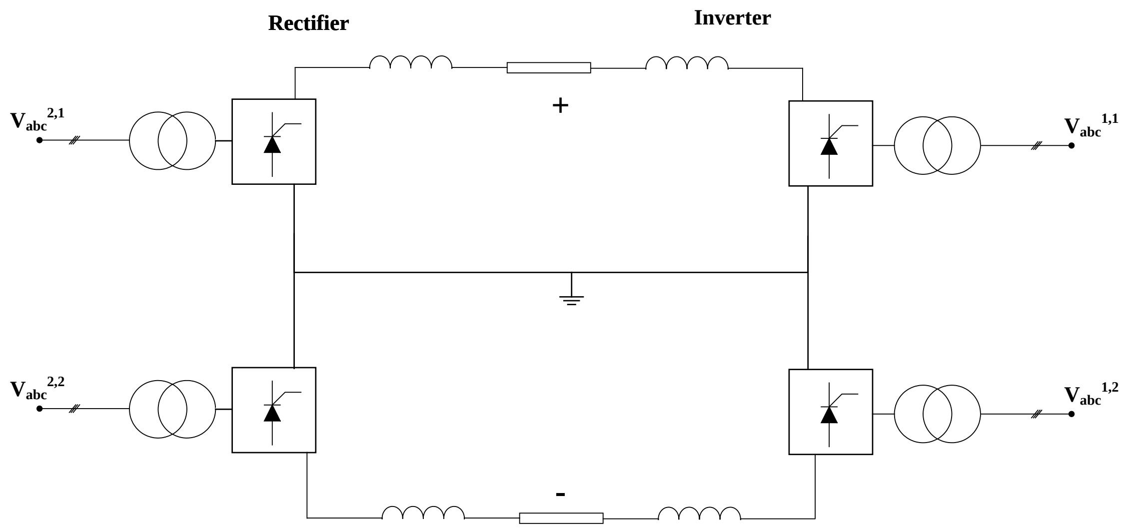

Figure 2-17. Bipolar LCC-HVDC

2.2.5.2 VSC-HVDC Systems

The first implementation of the VSC-HVDC system was done in Sweden in 1999. The operating voltage of the system was ±80 kV, and the power rating was 50 MW, and it was based on the two-level converters based on IGBTs [79]. The VSC-HVDC has been gaining momentum in a way that now the voltage rating of the station has reached ±800 kV and power rating up to 5000 MW [80, 81]. VSC-HVDC has the following major merits compared to the LCC-based solutions [82]:

- There is no need for reactive power compensators. Furthermore, it can support grid stability by providing reactive power compensation.
- The reactive and active power are controlled independently.
- Unlike the LCC-based systems, it can connect passive networks and the start-up problem is solved.
- Generally, the VSC-based systems produce less harmonics, which need less filtering.

Due to these merits, most of the undergoing HVDC projects are based on VSCs [83]. There are three main classes for the VSCs in HVDC systems:

- Two-level VSC
- Three-level VSC
- Modular multi-level converters (MMCs)

2.2.5.2.1 Two-level VSC

The two-level converter is the most common type of VSCs. This configuration includes 6 IGBTs or MOSFETs that come with the antiparallel diodes as in Figure 2-18. This converter produces two voltage levels at the output with reference to the neutral point. Using the PWM

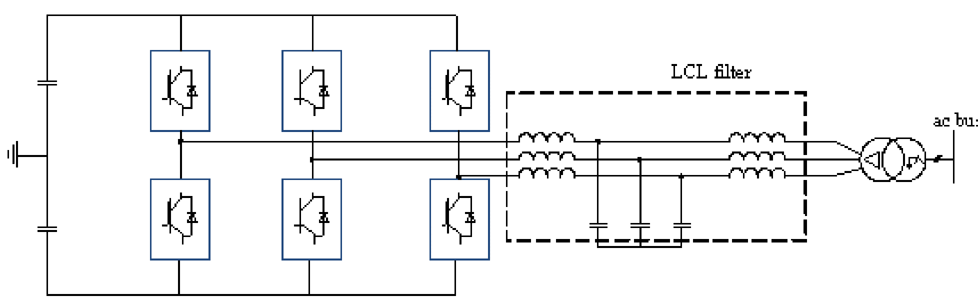

Figure 2-18. Two-level VSC configuration.

techniques, the arbitrary output voltage is created, as shown in Figure 2-19. To achieve higher voltage ratings, the switches can be connected in series. Several HVDC systems based on this topology were built in the 1990s by ABB with a switching frequency in the range of 1950 Hz [82, 84]. The reference signals are compared with the carrier signals, and the gate pulses are produced for the switches. If the reference signal is greater than the carrier signal, the switch is on; otherwise, it is off [85]. Consequently, the output voltage includes a high level of harmonics that needs filtering. To remove the harmonic, an LCL filter is used. If the switching frequency is increased, the center frequency for the output harmonics also increases, which makes the filtering easier, but it means higher power loss on the semiconductors. Typically, the switching frequency for this converter is between 1kHz to 2 kHz [86, 87].

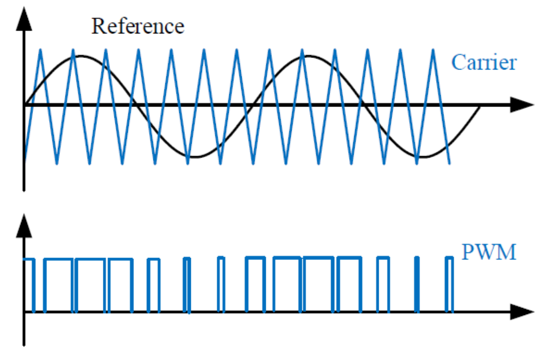

Figure 2-19. PWM technique to generate sinusoidal voltage in the VSCs.

2.2.5.2.2 Three-level VSC

Three-level neutral-point-clamped (NPC) is depicted in Figure 2-20. This configuration was first presented in the 1980s [88, 89]. Since then, it has been widely used in medium power range applications [90, 91]. This topology provides three voltage levels at the output, including 0 level; this means higher quality for the output voltage and less harmonic emission compared to two-level VSC [88]. ABB developed a three-level VCS-based HVDC system that used a harmonic elimination control technique with a switching frequency of 1260 Hz [92].

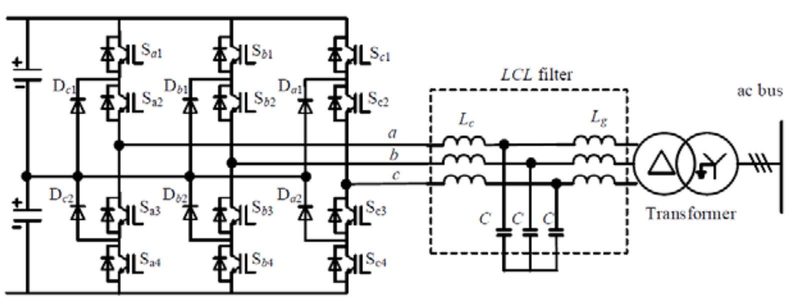

Figure 2-20. Three-level VSC structure.

A setback of this topology is the unbalanced distribution of power loss among the switches [93, 94]. To solve this problem, the three-level active NPC is introduced that replaces the diodes with switches [82, 95]. This topology has been used in several projects with a voltage rating of ±150 kV and power in the range of hundreds of megawatts [96, 97].

2.2.5.2.3 Modular multi-level converter

Modular multi-level converter (MMC) was first introduced in 2003 [98]. The first HVDC system based on this topology was put into service in 2010 in the USA [99]. This project operates with ±200 kV on the DC side and 115 kV and 230 kV on the AC sides, and it is capable of transferring power up to 400 MW [100]. The structure of the MMC can be seen in Figure 2-21. There are three legs in the MMC, and each leg is composed of an upper and a lower arm. There are several sub-modules (SMs) in each arm of the MMC. Depending on the gate signal of an SM, it puts a voltage level at its terminals.

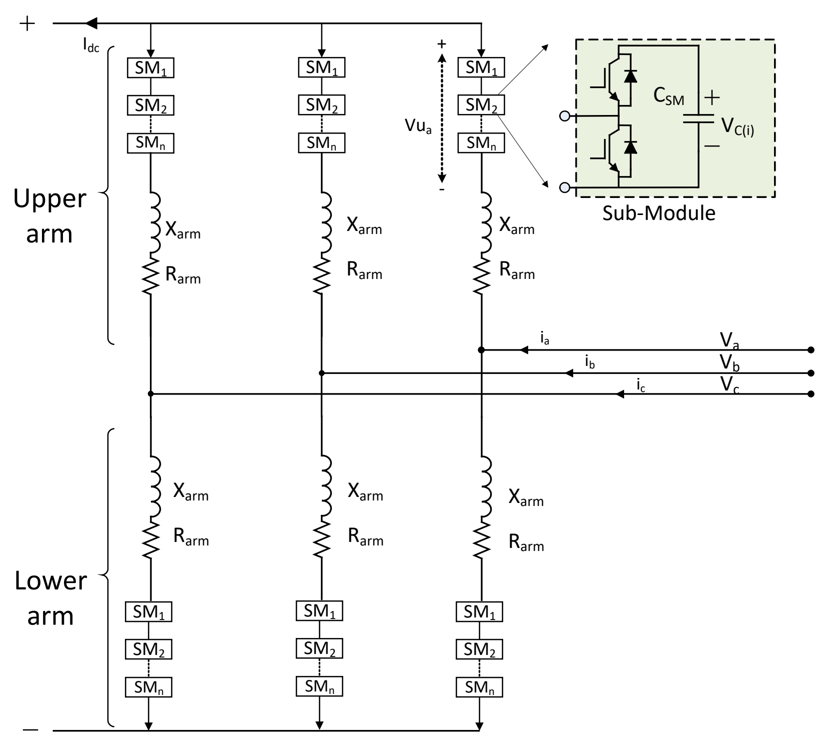

Figure 2-21. MMC configuration.

The efficiency of this converter is relatively high as it creates the least power loss and due to low-speed switching. Also, the need for an output filter for the harmonics is eliminated [101, 102]. Furthermore, there is no concern for uneven voltage distribution among the switches as they only withstand the SMs voltage. Furthermore, the production of the gate signals is less complex [103]. Each SM can be implanted using a half-bridge(HB) or full-bridge(FB) topology, but a half-bridge topology is preferred as it reduces the cost and power loss [104]. The structure of the HB is depicted in Figure 2-22.

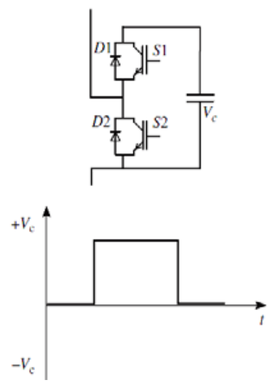

Figure 2-22. Half-bridge converter inside the SM.

If the gate signal is one, the S_1 is on, and the S_2 is off, which means that the output voltage is equal to V_c, but if the gate signal is zero, the S_1 is off, and S_2 is on, and the output voltage of the SM is equal to zero. When the voltages of the SMs accumulate together, the arm voltage is produced, as in Figure 2-23.

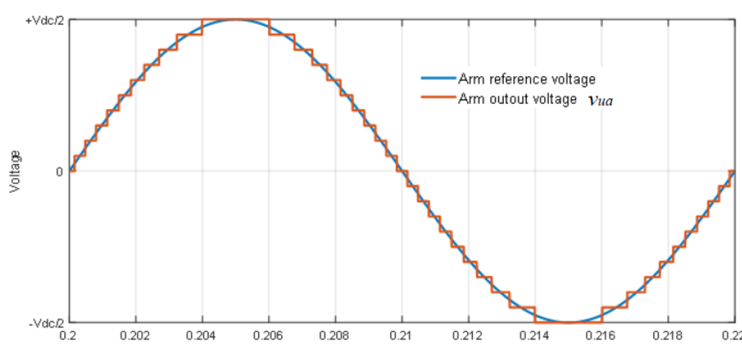

Figure 2-23. The output voltage of the MMC arm with respect to the reference voltage.

The MMC topology has the following merits over the other VSCs:

- This topology is readily expandable for different applications by adjusting the number of SMs [105].
- The emission of harmonics at the output is negligible, and the output waveforms are close to sinusoidal [99, 106-108].
- The switching frequency of the semiconductor is drastically reduced, which lowers the power loss [109-115].
- As the MMC capacitors are distributed among the SMs, and there is no bulk capacitor, they will not discharge during the DC faults [116]. This helps reduce the requirements for the DC breakers [116, 117].

For the VSC-based HVDC system, the following classification also is valid:

- Symmetrical monopole
- Asymmetrical monopole
- Bipolar system

2.2.5.2.4 Symmetrical monopole VSC

The configuration of the symmetrical monopole VSC is depicted in Figure 2-24. In this system, both conductors operate at equal voltage magnitudes but with different polarities. This configuration can be grounded on the DC side or AC side using the grounding reactors to provide a reference point for the converter [118, 119]. In this configuration, with the high impedance grounding, in case of a DC pole to ground fault, the remaining pole will experience double its rated voltage [120, 121].

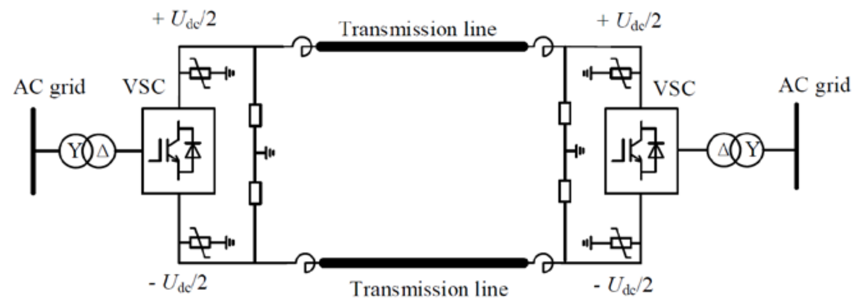

Figure 2-24. VSC-based symmetrical monopole HVDC system [85].

2.2.5.2.5 Asymmetrical monopole VSC

In an asymmetrical monopole configuration, one conductor operates at the nominal voltage of the converter while the other one is grounded, as depicted in Figure 2-25 [85]. Consequently, only one conductor needs insulation. It imposes DC voltage over the power transformer, which makes it more expensive, and also, in the DC faults, the fault current is greatly higher due to low impedance connection to the ground. Consequently, the application of this configuration is limited in the HVDC systems [119].

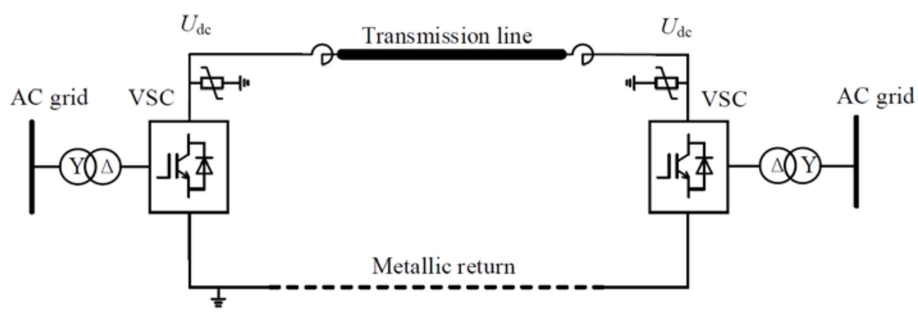

Figure 2-25. Asymmetrical monopole VSC-HVDC system.

2.2.5.2.6 Bipolar HVDC system

The bipolar configuration is a combination of two identical asymmetrical monopole systems. This configuration is shown in Figure 2-26 [85]. This system increases the reliability as in case of failure in one unit; the system is able to continue the operation with half of the rated capacity [122].

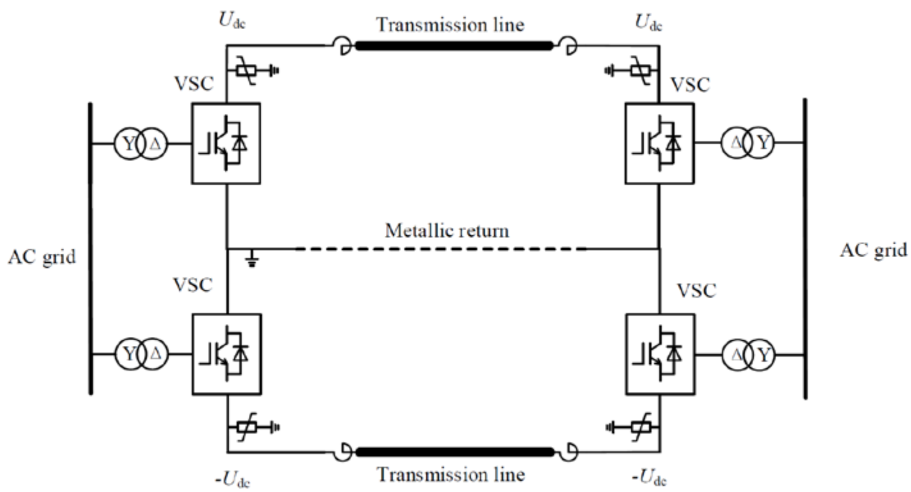

Figure 2-26. Bipolar HVDC system based on VSC technology [85].

2.2.6 GIC Impacts on HVDC Systems

The impact of GIC on the LCC system is studied in [123], and an impedance model is presented for both the DC and AC sides. A model for harmonics arising from GIC and the firing angle of LCC is provided in [124]. Several blocking schemes are also introduced to prevent the flow of GIC in the transformer of the HVDC system [125, 126]. The two-level VCS system in a wind farm is studied in [127], and it is illustrated that the voltage and current distortion is beyond the permissible limits. Furthermore, a passive filter is designed to reduce the distortion at the terminals [127]. In [128], an average model is used, and the PLL configuration is improved to reduce the distortion of the transformer current in an MMC-based HVDC system.

As the applications of the MMC based HVDC systems are growing, especially due to the expanding growth of renewable energies penetration in the grid and considering the lack of extensive studies on GIC impacts on these systems, this research aims to perform a comprehensive study on the topic to model the exact impacts of the GIC on the MMC operation and determine critical situations. Furthermore, this study aims to provide solutions and approaches to mitigate the severe consequences of the GIC in the grid and improve grid stability using the capabilities of the MMC.

Chapter 3

Study System

3.1 Overall System

This chapter provides an introduction to the study system. As stated in the previous section, due to the significant advantages of the MMC, the study system is based on this topology. The overall structure of the system is depicted in Figure 3-1 [129]. This system is based on a practical system that connects the France network to Spain [130, 131]. It has two 401-level MMCs. The

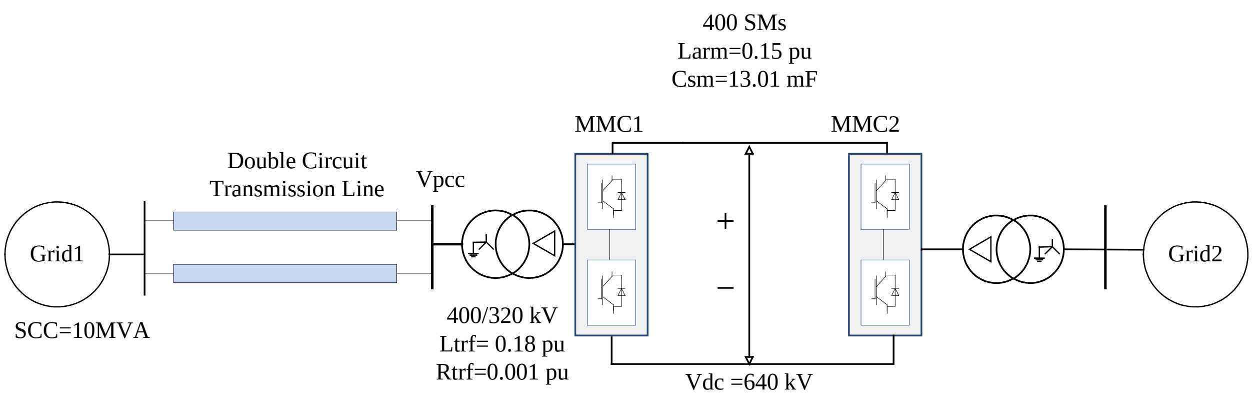

Figure 3-1. The overall structure of the study system.

MMCs are composed of identical SMs that are half-bridge converters. The structure of each MMC is shown in Figure 3-2. The SMs are based on IGBTs. As can be seen, the SMs are in series configuration, and there is an inductor in each arm. The purpose of the inductor is to reduce the fault current and also limit the circulating current in the legs [132]. The MMC transfers power to the grid using a step-up transformer that has a delta/wye configuration. The output of the transformer is connected to the grid using a double-line transmission line in MMC1. At MMC2, the transformer connects to the grid directly.

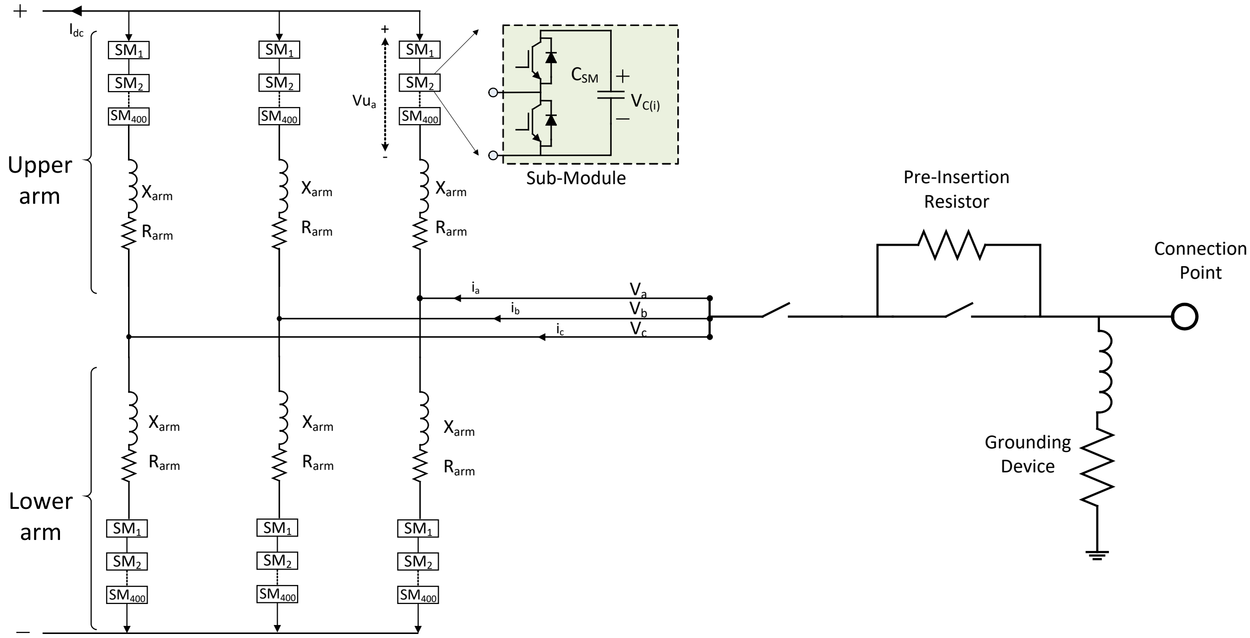

Figure 3-2. MMC converter station.

The grounding device is used to provide a reference point for the MMC [119]. The pre-insertion resistors are used during the start-up for a short time, and they are bypassed during normal operation. These resistors limit the inrush current created by the different capacitors in the converter [119]. Based on the status of the gate signal, each SMs provides a voltage at its terminals that is described in Figure 3-3 and Table 3-1 [119].

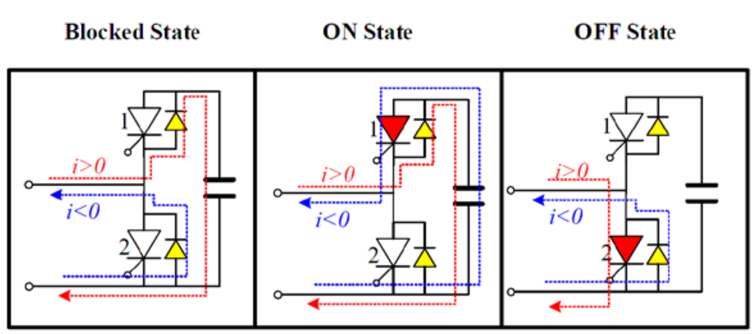

Figure 3-3. The different states of the switches in the SM.

Table 3-1. The output voltage of the SM due to insertion command and the current polarity.

SM State	S1	S2	Output voltage of the SM	
			$I_{SM}>0$	$I_{SM}<0$
Inserted	ON	OFF	V_C	V_C
Bypass	OFF	ON	0	0
Blocked	OFF	OFF	V_C	0

The signal commands for the SMs are issued to provide a staircase output voltage. The output voltage of all the SMs added together provides 401 levels at the arm terminal. Due to the high number of SMs, there is no need to filter the output voltage, and the harmonic emission of MMC is acceptable, as demonstrated in Figure 3-4.

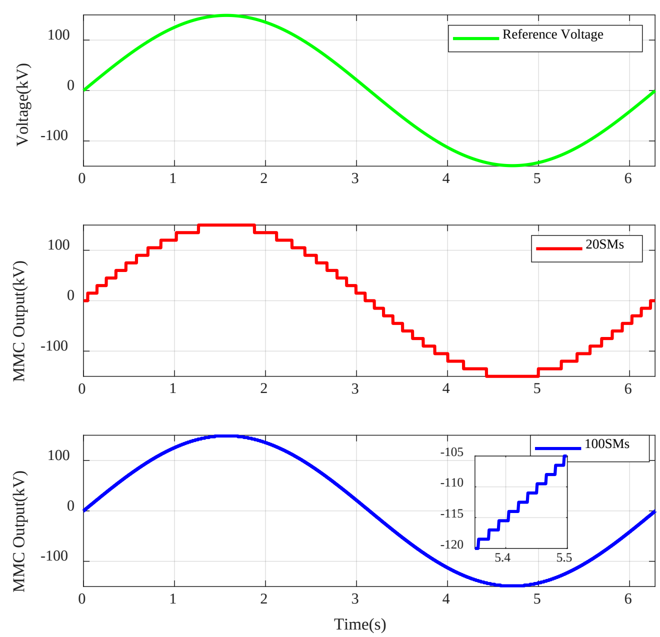

Figure 3-4. Effect of the number of SMs on the output voltage waveform in the MMC.

3.2 Control System

The control system of the MMC is depicted in Figure 3-5. The local control system of the MMC is divided into two main functional levels: the upper level and the lower level. The upper-level control receives commands from the superior controller, and it provides the reference signals for the lower controller. This level of control is independent of the VSC topology, and it is common among the configurations [133].

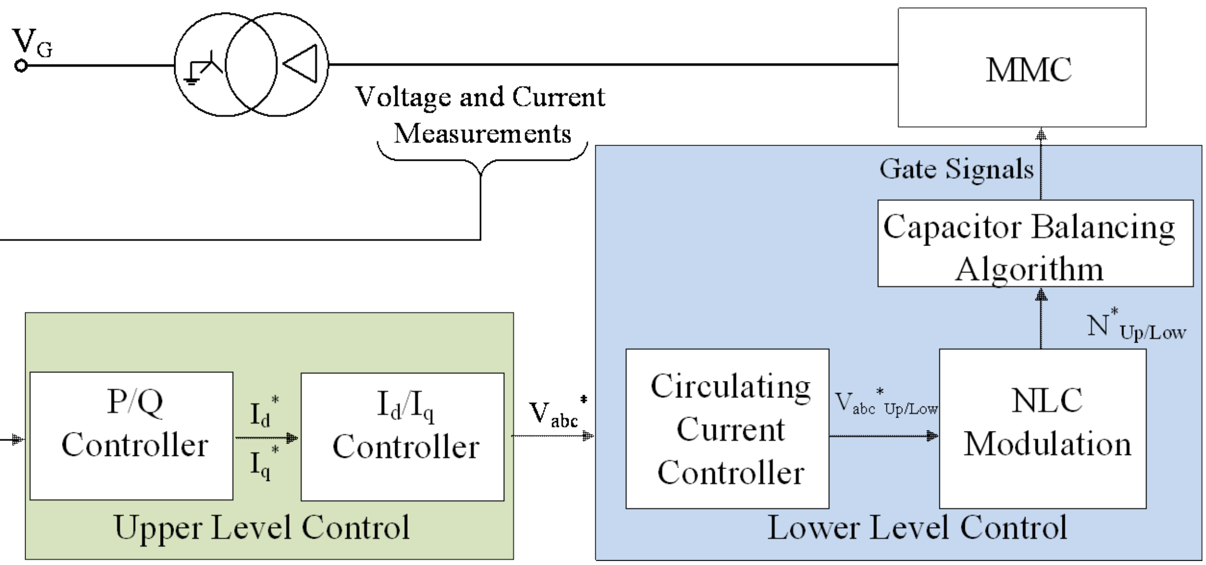

Figure 3-5. The overall control system of the MMC.

3.2.1 Upper-Level Control Layer

The upper-level controller receives the setpoints of P and Q, DC link voltage, and AC voltage (based on the rule) and provides the three-phase voltage references for the downstream controller. In the HVDC system, an MMC is responsible for regulating the active power, while the other is responsible for the DC link voltage control. The controller is implemented in a d-q frame rotating at synchronous speed. To acquire the equation for the control system, based on Figure 3-2, it can be written that:

$$V_{G_{abc}} = V_{C_{abc}} + L\,\frac{di_{abc}}{dt} + R\,i_{abc} \qquad \text{3-1}$$

Where $L=L_{Tr} + L_{Arm}\times 0.5$ in which the L_{Tr} and L_{Arm} are the transformer and arm inductances, respectively, R is the resistance of the system, $V_{G\,abc}$ is the grid voltage at the point of connection to the MMC and $V_{C\,abc}$ is the converter output voltage. Applying the Park's transformation in (3-4) to (3-1) results in:

$$V_{G_d}=V_{C_d}+R\,i_d+L\,\frac{di_d}{dt}-L\,\omega i_q \quad 3\text{-}2$$

$$V_{G_q}=V_{C_q}+R\,i_q+L\,\frac{di_q}{dt}+L\,\omega i_d \quad 3\text{-}3$$

$$T_{dq0}=\frac{2}{3}\begin{bmatrix} cos\theta & cos\,(\theta-\frac{2\pi}{3}) & cos\,(\theta+\frac{2\pi}{3}) \\ -sin\,\theta & -sin\,(\theta-\frac{2\pi}{3}) & -sin\,(\theta+\frac{2\pi}{3}) \\ \frac{1}{2} & \frac{1}{2} & \frac{1}{2} \end{bmatrix} \quad 3\text{-}4$$

where the $\theta=\omega t+\theta_0$ and ω is the base a, thus base speed, thus, (3-2) and (3-3) can be rewritten:

$$V_{C_d}=V_{G_d}-R\,i_d-L\,\frac{di_d}{dt}+L\,\omega i_q \quad 3\text{-}5$$

$$V_{C_q}=V_{G_q}-R\,i_q-L\,\frac{di_q}{dt}-L\,\omega i_d \quad 3\text{-}6$$

Therefore, by substituting the PI controllers' outputs, there will be:

$$V_{C_d}=V_{G_d}-G(s)_{PI}+L\,\omega i_q \quad 3\text{-}7$$

$$V_{C_q}=V_{G_q}-G(s)_{PI}-L\,\omega i_d \quad 3\text{-}8$$

In which the $G(s)_{PI}$ is the PI controller that regulates the d-q currents as follows [134]:

$$G(s)_{PI}=(\frac{k_i}{s}+k_p)\times(i_{d\text{-}q\,Ref}-i_{d\text{-}q}) \quad 3\text{-}9$$

Where K_i and K_p are the controller's coefficients. The reference values for these controllers are set by the outer loop that regulates the active and reactive power, as shown in the following equations, assuming that the grid voltage is aligned on the d-axis and the voltage component on the q-axis is zero.

$$P = i_d \times V_{G_d} \tag{3-10}$$

$$Q = -\, i_q \times V_{G_d} \tag{3-11}$$

To acquire the references for the inner loops, the following equations must be used:

$$i_{d\ Ref} = \frac{1}{V_{G_d}} \left(\frac{k_{i_2}}{s}\right) \times (P_{Ref} - P) \tag{3-12}$$

$$i_{q\ Ref} = -\frac{1}{V_{G_d}} \left(\frac{k_{i_2}}{s}\right) \times (Q_{Ref} - Q) \tag{3-13}$$

DC-link voltage is controlled through the active power loop:

$$C\,\frac{dV_{DC}}{dt} = i_d - I_{DC} \tag{3-14}$$

$$i_{d\ Ref} = \left(k_{p_2} + \frac{k_{i_3}}{s}\right) \times (V_{DC\ Ref} - V_{DC}) \tag{3-15}$$

As demonstrated, the upper-level controller interprets the reference P, Q and DC-link voltage to three-phase voltages that the MMC must follow. Figure 3-6 depicts this control layer. When the reference currents in the d-q frame are determined, a limiter is used to ensure that the converter rating is not exceeded [135]. The current limiter scheme can be seen in Figure 3-7 [133].

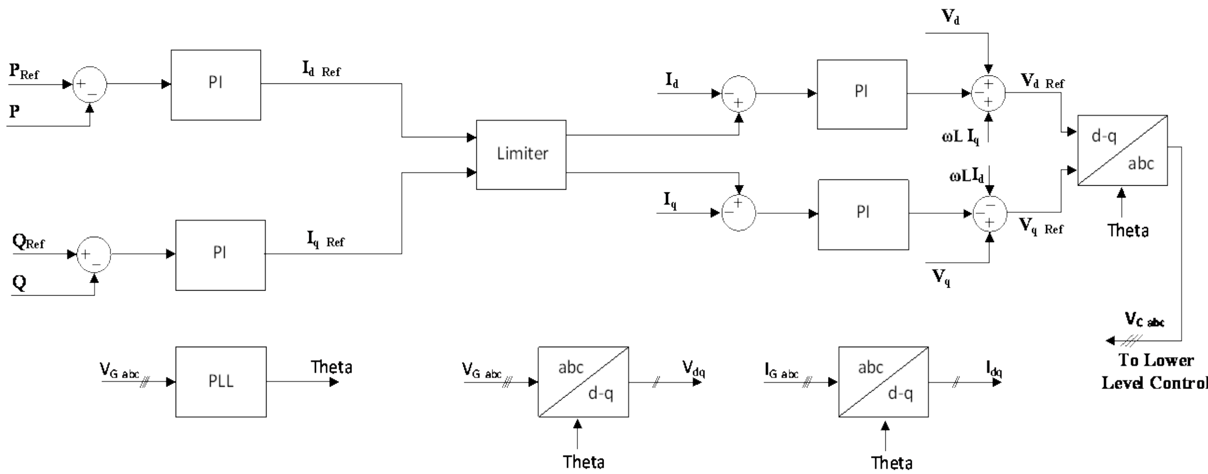

Figure 3-6. Upper-level control layer of the MMC.

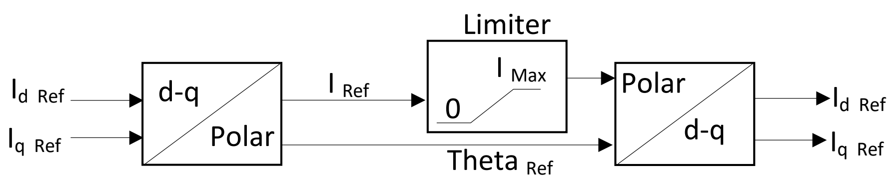

Figure 3-7. Current limiter of the internal control loop.

In this research, the voltages of the system and also the flux shifts by the GIC are considered to be symmetrical in the three phases. Hence, the control system is designed to operate in a balanced condition. However, if the voltages in the system are unbalanced due to factors such as asymmetry in power line transmission, operating in the weak grid, or using three phase transformers instead of three identical single-phase transformer, different types of controllers and control strategies must be used. Such controllers and control strategies can be found in [136-141].

3.2.2 Lower Level Control Layer

The lower-level control creates the demanded three-phase voltages at the output. In the VSC configuration, it is usually composed of the modulation unit, but in MMC, this layer has the following major units:

- Modulation Unit

- Capacitor Voltage Balancing Unit
- Circulating Current Controller

3.2.2.1 Modulation Unit

It has been shown that staircase modulation is more efficient for MMCs with the high number of SMs [142, 143]. The modulation is done using the nearest level control (NLC) technique. In the NLC, the amplitude of the required voltage is divided by the voltage of the SMs, assuming that all the SMs have the same voltage, and the number of the needed SMs is determined, which can be seen in Figure 3-8 [133].

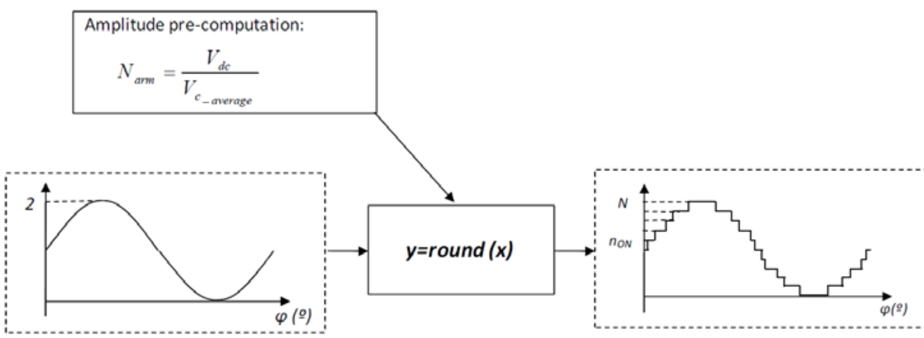

Figure 3-8. Modulation unit in the MMC controller.

3.2.2.2 Capacitor Voltage Balancing Unit

This unit is responsible for stabilizing the capacitor voltage in the SMs. The lack of this controller will result in different voltages in the SMs, which degrades the MMC functionality [133]. This process is done using the capacitor balancing algorithm (CBA) [98]. The CBA receives the number of SMs that need to be inserted in each arm. The voltages of the SMs are measured in small time intervals, and they are sorted based on the voltage level. Then, according to the capacitor voltage level in the SM and the direction of the current in the arm, the required number of SMs are inserted. The adjustment of the SMs capacitor based on the command and the current direction is depicted in Figure 3-9. The CBA logic is simplified in the Table 3-2 [133].

Table 3-2. CBA logic in the lower control layer.

Command	I_{Arm} **is negative**	I_{Arm} **is positive**
Insert SMs	Insert SMs with higher voltage	Insert SMs with the lower voltage
Bypass SMs	Bypass SMs with lower voltage	Bypass SMs with higher voltage

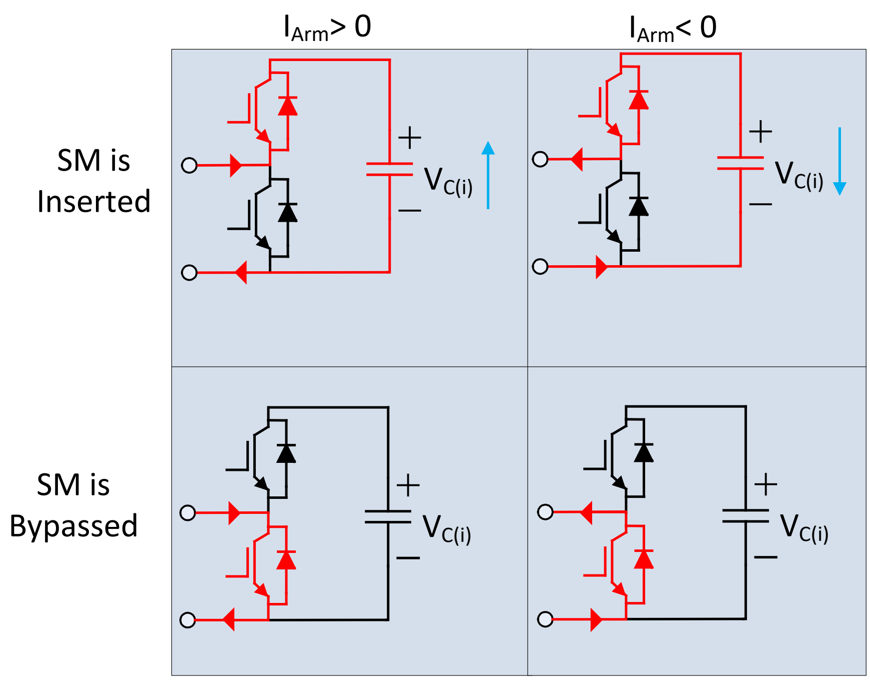

Figure 3-9. Capacitor voltage change in the SM due to current and gate signal.

3.2.2.3 Circulating Current Controller

To eliminate the circulating current in among the MMC legs, a controller is implemented in a d-q frame rotating at 2ω [101, 144]. The cause of the circulating current is the voltage differences in each leg, and they produce negative sequence currents, which leads to an increase in the power loss in the MMC [145-147]. The configuration of the circulating current controller is depicted in Figure 3-10 [101].

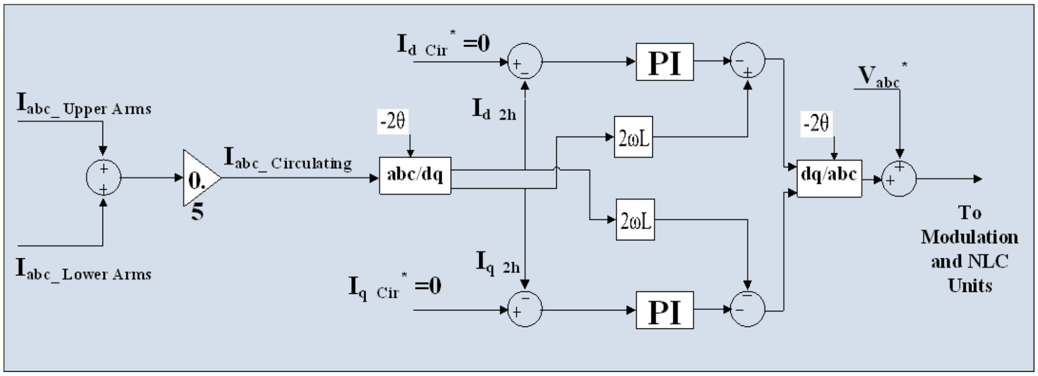

Figure 3-10. The circulating current suppressing controller in the MMC.

From Figure 3-10, it can be noted that this suppressing controller only senses the current that is common in both arms. The directions of currents in the arms are depicted in Figure 3-11. Equations 3-16 and 3-17 demonstrate the relationship between the circulating current, phase current and the currents in the arms.

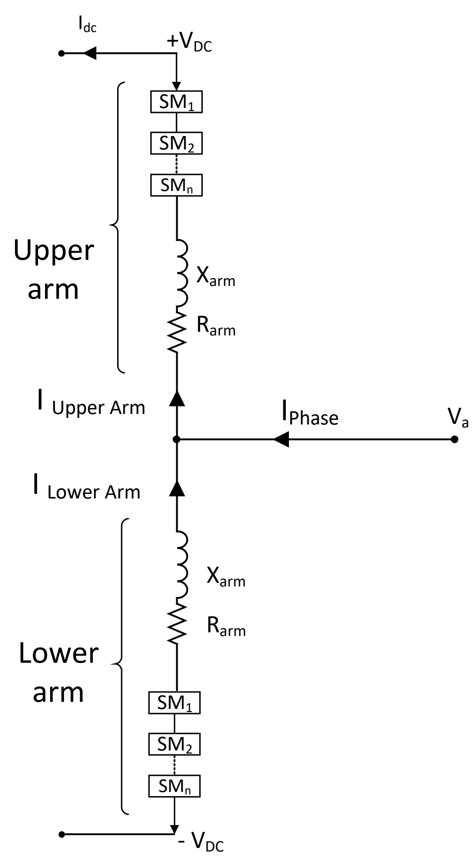

Figure 3-11. Current measurement in the MMC arms.

$$I_{Phase} = I_{Upper\ Arm} - I_{Lower\ Arm} \quad 3\text{-}16$$

$$I_{Circulating} = \frac{I_{Upper\ Arm} + I_{Lower\ Arm}}{2} \quad 3\text{-}17$$

3.3 Transformer Magnetic Characteristics

The last section of this chapter is about transformer modeling and its B-H characteristics. The power transformer in this converter is composed of three identical single-phase units. The single-phase transformer is most vulnerable to the GIC, and it experiences the highest flux shift due to a DC current in comparison to the others. The transformer model is depicted in Figure 3-12. The Z_{Pri} and Z_{Sec} are the equivalent impedances for the primary and secondary sides, respectively. The ratio of the primary impedance to the secondary impedance is 9. The R_{Fe} represents the core losses, and it is 7.4 MΩ. The magnetizing branch is modelled using a non-linear Inductor that has its specific magnetic curve.

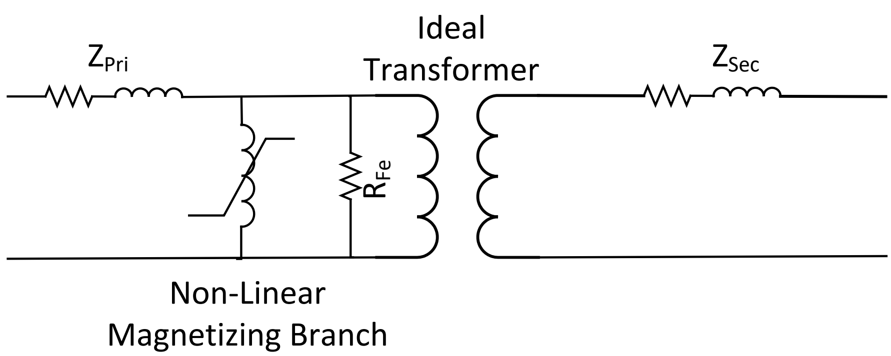

Figure 3-12. The transformer equivalent circuit.

This curve is depicted in Figure 3-13. In normal operating conditions, with the rated voltage applied to the transformer, the magnitude of the flux is around 1030 Wb, which corresponds to 6.99 A of magnetizing current, which is shown in Figure 3-14.

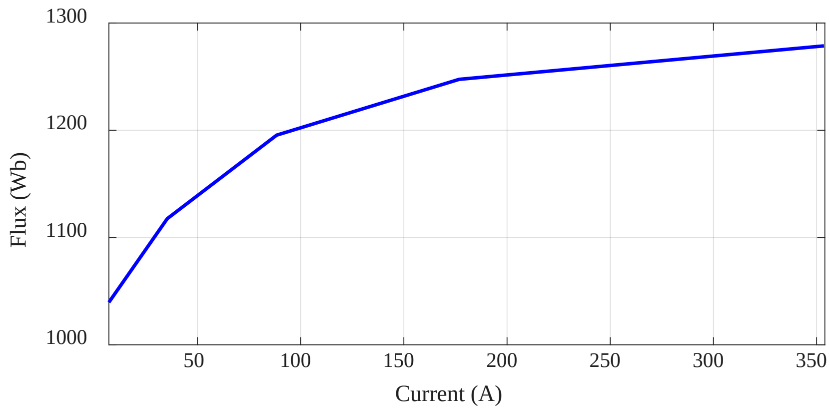

Figure 3-13. Magnetizing curve of the converter unit transformer.

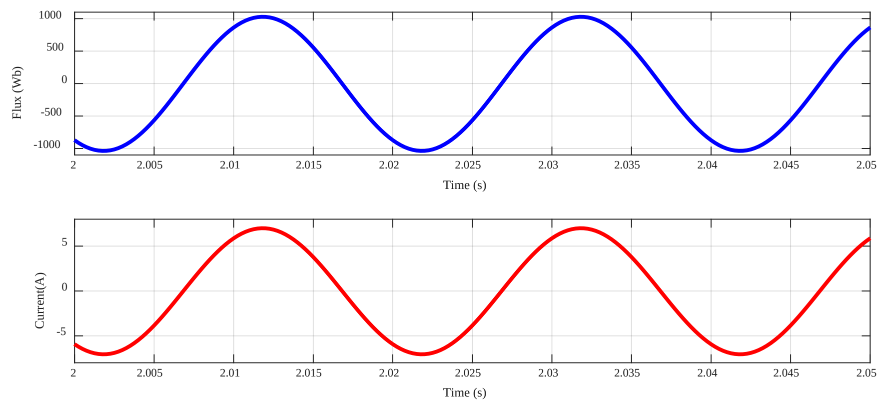

Figure 3-14. Transformer flux and magnetizing current in normal operation.

To summarize this chapter, Table 3-3 provides the study system characteristics in brief:

Table 3-3. Study system characteristics.

HVDC Type	MMC-based symmetrical monopolar system
Rated power	1000 MVA
Grid side AC voltage	400 kV
Grid SCC	10000 MVA
MMC side AC voltage	320 kV
Grounding resistor	7.7 kΩ

Grounding inductance	6500 H
Frequency	50 Hz
DC-link voltage	±320 kV
Transformer reactance	0.18 pu
Transformer resistance	0.001 pu
MMC arm inductance	0.15 pu
Number of SMs per arm	400 half-bridge modules
SMs capacitor	13.0208 mF
Active power controller K_I	30
Reactive power controller K_I	30
Settling Time of outer control loop	100 mS
Inner loop current controller K_I	149.08
Inner loop current controller K_P	0.487
Settling Time of inner control loop	10 mS
Inner loop current controller decoupling coefficient	0.255
Low pass filter cutoff frequency (Second order)	2000 Hz
Low pass filter cutoff frequency (First order)	11 Hz

Chapter 4

MMC Model and GIC Effects

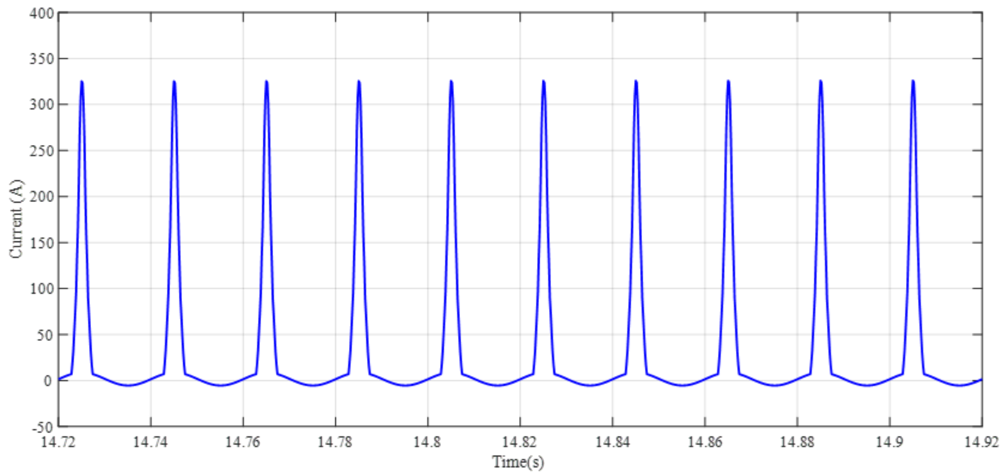

Figure 4-1. Magnetizing current of the saturated transformer due to GIC.

As stated in Chapter 2, when the GIC flows in the transformer neutral, it causes half-cycle saturation, which leads to the generation of harmonics in the magnetizing current. Figure 4-1 shows the magnetic current due to half-cycle saturation, and Figure 4-2 depicts the resulting harmonics in the magnetizing current of the transformer due to 200 A of GIC in the study system. This spectrum starts from the fundamental frequency that lags the fundamental voltage by 90 degrees and includes both even and odd ones. These current harmonics are distributed between the grid and the MMC and distort the voltage and current waveforms. Consequently, a model is needed to investigate the contribution of the MMC and the grid in these harmonics.

4.1 Current Harmonics Distribution

As depicted in Figure 4-2, the resulting harmonic spectrum from GIC starts from the fundamental frequency. This current lags the transformer voltage, and it is an inductive current. Therefore, the fundamental current is associated with the reactive power and creates a reactive load in the power system. The control strategy of the MMC determines how the MMC provides its share of the fundamental current harmonic. Since the MMC typically operates based on a constant P-Q or unity power factor, its reactive current component is constant. Therefore, when

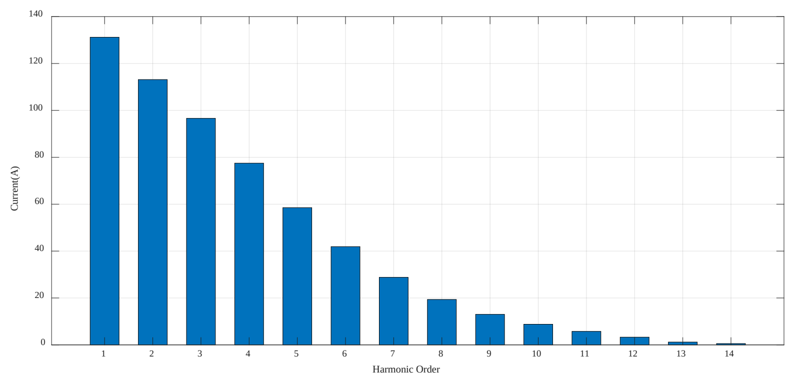

Figure 4-2. Resulting harmonics from 200 A of GIC.

GMD occurs, and the reactive power demand of the converter transformer increases; the grid provides all the demanded reactive power, which means that the total magnitude of the resulting fundamental current harmonic will flow into the grid. To investigate the flow of higher order harmonic, the MMC Thevenin's equivalent must be acquired, which is elaborated on as follows.

4.1.1 MMC Thevenin's Equivalent

The system equivalent is depicted in Figure 4-3. The MMC is modeled using a voltage source and an impedance for each harmonic. The equivalent voltage depends on modulation and the number of MMC levels mostly [148]. Since this system has 400 SMs in each arm, the generated harmonics from MMC are negligible, which means that the Thevenin's voltage can be neglected.

Therefore, only an impedance model is required to determine the harmonic currents in the sides of the transformer.

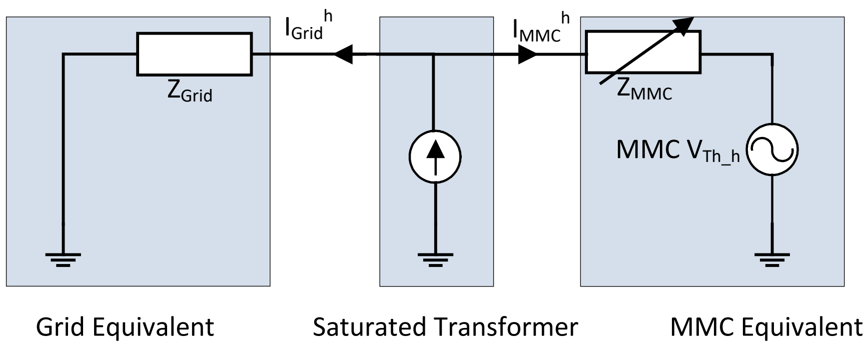

Figure 4-3. Equivalent circuit of the system for harmonic analysis.

4.1.1.1 MMC Impedance Model

The overall control system of the MMC is depicted in Figure 4-4 [129]. The impedance model for MMC has been subject to several studies [149-153]. Since the focus is on frequencies higher than 100Hz, the outer control loops can be neglected as they have a limited effect on those frequencies [154]. As only the AC side impedance is important here, the internal variables, including the circulating current controller and capacitors balancing, could also be neglected [148].

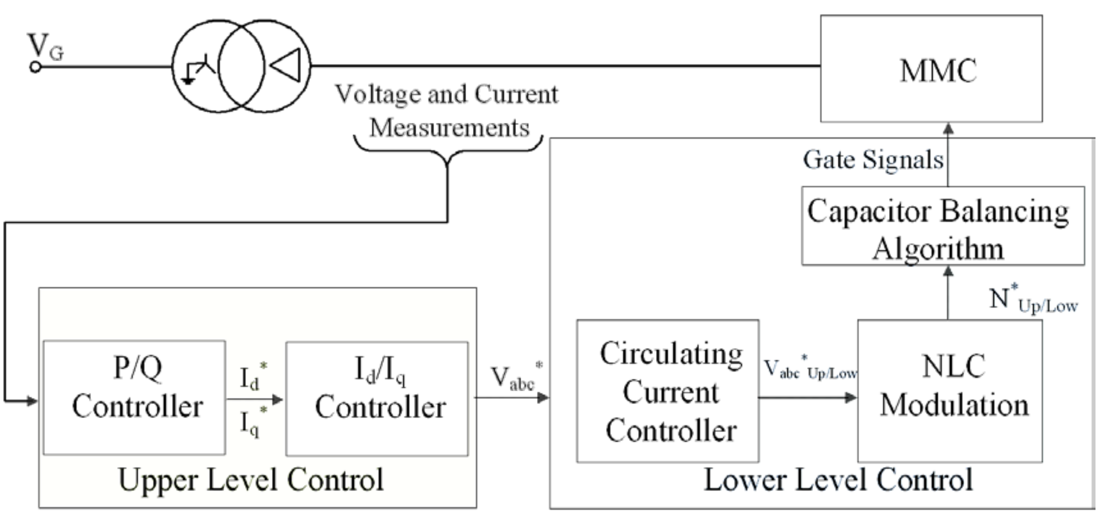

Figure 4-4. MMC control system.

Also, according to [155], the PLL is effective mainly in low frequencies, and it can be disregarded here. Consequently, it can be simplified to the system depicted in Figure 4-5.

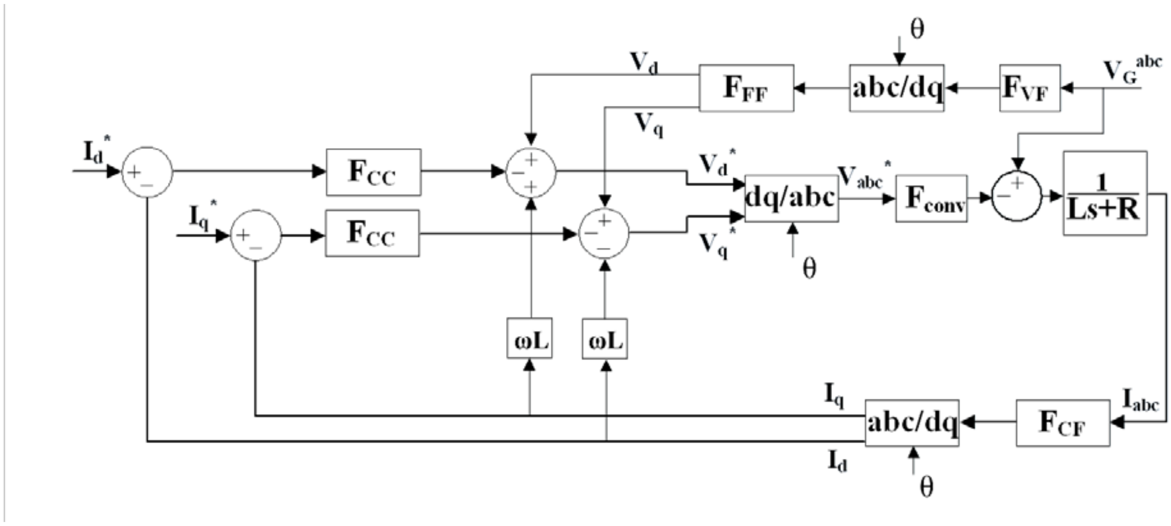

Figure 4-5. Simplified transfer function of the MMC system.

Thus, the following equations can be obtained:

$$V_{G_{abc}}=V_{C_{abc}}+L\frac{di_{abc}}{dt}+Ri_{abc} \quad 4\text{-}1$$

By applying the Park's transformation, there will be:

$$V_{G_d}=V_{C_d}+Ri_d+L\frac{di_d}{dt}\text{-}L\,\omega i_q \quad 4\text{-}2$$

$$V_{G_q}=V_{C_q}+Ri_q+L\frac{di_q}{dt}+L\,\omega i_d \quad 4\text{-}3$$

By neglecting the couplings at $\pm(f_n+2f_1)$ and $\pm(f_p\text{-}2f_1)$, the impedance for the positive and negative sequences will be [154]:

$$Z_p(s)=\frac{F_{conv}\,(s)\left[F_{CC}\left(s\text{-}j2\pi f_1\right)\text{ - }j\,K_d\right]F_{CF}\,(s)+sL+R}{1\text{-}F_{conv}\,(s)\,F_{FF}\,(s)F_{VF}\,(s)} \quad 4\text{-}4$$

$$Z_n(s) = \frac{F_{conv}(s)\left[F_{CC}\left(s+j2\pi f_1\right)+jK_d\right]F_{CF}(s)+sL+R}{1-F_{conv}(s)F_{FF}(s)F_{VF}(s)} \quad 4\text{-}5$$

where $Z_p(s)$ and $Z_n(s)$ are the positive and negative sequence impedance of the converter station, respectively, K_d is the decoupling term in the current controller, $F_{CC}(s)$ is the PI controller for the current loop, $F_{CF}(s)$ is the low-pass filter for the input voltage and $F_{VF}(s)$ *and* $F_{FF}(s)$ low pass filters that filter out high frequencies in the voltage signal. $F_{Conv}(s)$ is the equivalent transfer function for the MMC, which can be considered the total delay from the controller and modulation [148, 156].

$$F_{CC}(s)=k_p^i+\frac{k_i^i}{s} \quad 4\text{-}6$$

$$F_{CF}(s)=\frac{\omega_i^2}{s^2+\zeta\omega_i+\omega_i^2} \quad 4\text{-}7$$

$$F_{VF}(s)=\frac{\omega_v^2}{s^2+\zeta\omega_v+\omega_v^2} \quad 4\text{-}8$$

$$F_{FF}(s)=\frac{\alpha_F}{\alpha_F+s} \quad 4\text{-}9$$

$$F_{conv}(s)=e^{-s\,T_\delta} \quad 4\text{-}10$$

Which is estimated using the Taylor series into the following function:

$$F_{conv}(s)=\frac{1}{T_\delta s+1} \quad 4\text{-}11$$

To increase the accuracy of the model without complicating the impedance equation, a step forward can be taken. The internal interactions of the converter itself without the control loop to the harmonic is as [157]:

$$\begin{bmatrix} b_2 & c_2 & & & & \\ a_4 & b_4 & c_4 & & & \\ & a_6 & b_6 & c_6 & & \\ & & a_8 & b_8 & c_8 & \\ & & & \ddots & \ddots & \ddots \end{bmatrix} \begin{bmatrix} \hat{i}_2 \\ \hat{i}_4 \\ \hat{i}_6 \\ \hat{i}_8 \\ \vdots \end{bmatrix} = \begin{bmatrix} k+\frac{2C}{N} u_2 \\ \frac{2C}{N} u_4 \\ \frac{2C}{N} u_6 \\ \frac{2C}{N} u_8 \\ \vdots \end{bmatrix} \quad \text{4-12}$$

and for the odd harmonics flowing into the MMC, there is:

$$\begin{bmatrix} b_1 & c_1 & & & & \\ a_3 & b_3 & c_3 & & & \\ & a_5 & b_5 & c_5 & & \\ & & a_7 & b_7 & c_7 & \\ & & & \ddots & \ddots & \ddots \end{bmatrix} \begin{bmatrix} \hat{i}_1 \\ \hat{i}_3 \\ \hat{i}_5 \\ \hat{i}_7 \\ \vdots \end{bmatrix} = \begin{bmatrix} \frac{2C}{N} u_1 \\ \frac{2C}{N} u_3 \\ \frac{2C}{N} u_5 \\ \frac{2C}{N} u_7 \\ \vdots \end{bmatrix} \quad \text{4-13}$$

where:

$$a_n = \frac{\widehat{m}^2}{4(n-1)\omega} \sin(n\omega t + \varphi_{n-2}) \quad \text{4-14}$$

$$b_n = \frac{2(n^2-1) + n^2\widehat{m}^2}{2n\omega(n^2-1)} \sin(n\omega t + \varphi_n) \quad \text{4-15}$$

$$c_n = \frac{\widehat{m}^2}{4\omega(n+1)} \sin(n\omega t + \varphi_{n+2}) \quad \text{4-16}$$

Only b_1 is different and given by:

$$b_1 = \left(\frac{8+\widehat{m}^2}{8\omega}\right) \hat{i}_1 \cos(\omega t + \varphi_1) \quad \text{4-17}$$

and:

$$k=\frac{3\hat{m}\,\hat{i}_{a1}}{4\omega}\ sin\ (2\omega t+\varphi_{a1})-\frac{\hat{m}^2 i_{dc}}{2\omega}\ sin\ (2\omega t) \qquad 4\text{-}18$$

in which n is the harmonic order, $\hat{m}$ is the modulation index, C is the submodule capacitance, ω is the base angular speed, N is the number of submodules in the arm, i_{dc} is the DC current in the MMC leg, $\hat{i}_{a1}$ is the half of the peak value of the fundamental frequency and φ_{a1} is the regarding phase angle, $\hat{i}_1$ is the half of the peak value of the fundamental frequency and φ_1 represents the phase angle. In order to increase the accuracy of the impedance model, the diagonal terms are added to the impedance of the arm and the off-diagonal terms are neglected. Consequently, the relation between the current and the voltage in the MMC leg is:

$$\begin{bmatrix} Z_2^{Int} & & & & & \\ & Z_3^{Int} & & & & \\ & & Z_4^{Int} & & & \\ & & & Z_5^{Int} & & \\ & & & & \ddots & \\ & & & & & Z_n^{Int} \end{bmatrix}\begin{bmatrix} i_2 \\ i_3 \\ i_n \\ i_5 \\ \vdots \\ i_n \end{bmatrix}=\begin{bmatrix} u_2 \\ u_3 \\ u_4 \\ u_5 \\ \vdots \\ u_n \end{bmatrix} \qquad 4\text{-}19$$

$$Z_n^{Int}=-j\ \frac{N(n^2-1)+n^2\hat{m}^2}{2n\omega(n^2-1)C} \qquad 4\text{-}20$$

where the Z_n^{Int} is the result of the internal controls of the MMC. This derived impedance can be added to (4-4) and (4-5) to account for internal interactions of the MMC. This impedance is capacitive, which reduces the overall MMC impedance, especially in low frequencies. Consequently, Eq. (4-4) and (4-5) can be rewritten:

$$Z_p(n)=\frac{F_{conv}(n)\ [F_{CC}(n-1)\ -j\ K_d]\ F_{CF}(n)+(nj\omega)L+Z_n^{Int}+R}{1-F_{conv}\ (n)\ F_{FF}\ (n)\ F_{VF}\ (n)} \qquad 4\text{-}21$$

$$Z_n(n)=\frac{F_{conv}(n)\ [F_{CC}(n\text{-}1)+j\ K_d]\ F_{CF}(n)+(nj\omega)L+Z_n^{Int}+R}{1\text{-}F_{conv}\ (n)\ F_{FF}\ (n)\ F_{VF}\ (n)} \quad 4\text{-}22$$

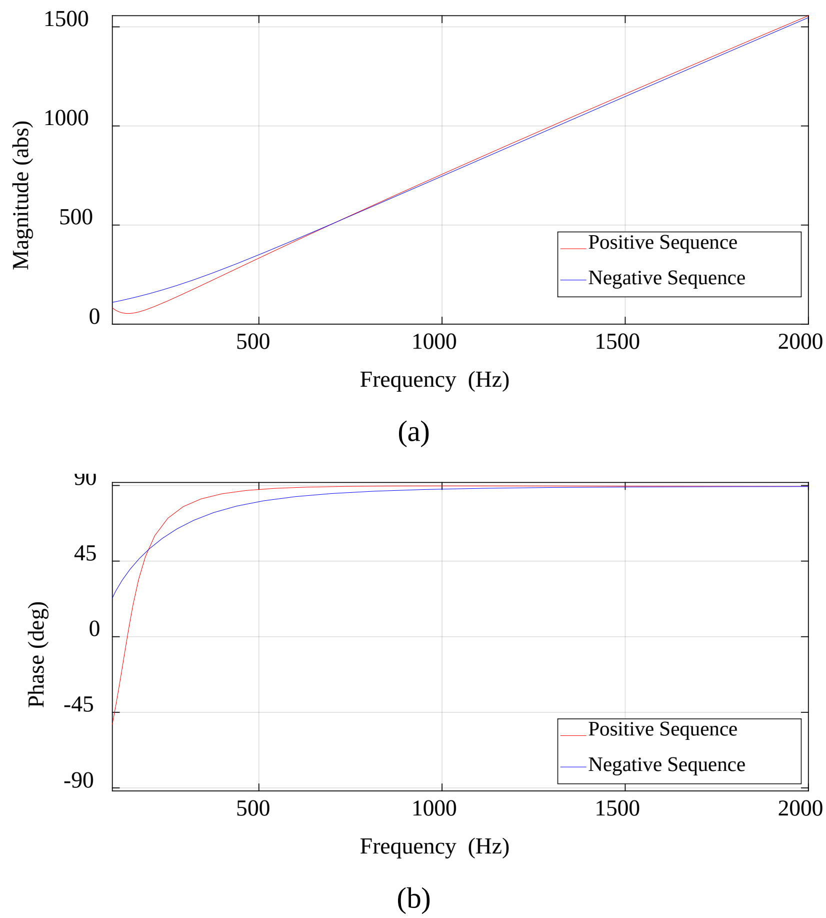

Figure 4-6. The positive and negative sequence impedances: (a) magnitude, (b) phase.

Figure 4-6 shows the positive and negative sequence impedances for different frequencies. Using the derived MMC impedance, the harmonic distribution, in the case of GMD, between the MMC and grid can be formulated as follows:

$$I^n_{mmc}=\frac{Z^n_{grid}}{Z^n_{mmc}+Z^n_{grid}}\ I^n_{transformer} \quad 4\text{-}23$$

Where $I^n_{transformer}$ is the resulting n^{th} order current harmonic from transformer half-cycle saturation, I^n_{mmc} is the n^{th} order current flowing to the MMC, Z^n_{grid} and Z^n_{mmc} are the grid and MMC impedance at the regarding g harmonic order. As these harmonics flow into the grid, they distort the voltage and current waveforms. This could very well lead to a violation of permissible THD values set by the standards. Waveform distortion is not the only effect of the current harmonics flow in the grid; as discussed in the literature, they can cause problems for the generators, SVCs, and protection systems as well. The next section is dedicated to mitigating the severe consequences of the GIC on the grid.

4.2 Mitigating The GIC Effects on The Grid

Two main effects of the GIC on the grid are the flow of current harmonics and the higher demand for reactive power. As the MMC control system provides a wide range of maneuverability, these results can be dealt with. Here, two means of reducing the GIC consequences on the grid are presented. First, eliminating the major harmonics in the grid current is presented, and then a control approach is provided to inject reactive power into the half-cycle saturated transformer from the MMC instead of the grid.

4.2.1 Eliminating the Major Current Harmonics

The spectrum of the harmonics that flow into the grid due to transformer half-cycle saturation starts from the main frequency, and the major harmonics are 2^{nd} to 9^{th} ones. The negative sequence currents cause rotor heating, mal-operation of protective relays, and loss of generation in the generators [123]. Also, the presence of these harmonics could lead to tripping of the protection devices of capacitor banks as they have a low impedance path. As the GIC happens, demand for reactive power increases and outage of the capacitor banks could be the start of voltage collapse in the grid. To reduce the grid current distortion and negative sequence, a mitigating control block (MCB) is proposed. This MCB injects the demanded major current harmonics into the power transformer in the case of GIC, which also reduces the gird distortion. Although this controller is only demonstrated for the second harmonic here, the same procedure is done for harmonics, including the 4th, 5th, 7th and 8th ones. This controller mitigates dominant negative sequence currents, which are especially problematic for the normal operation of the power system components. It must be noted that the internal current controller of the MMC discussed in (3.2.23) that eliminates the circulating current between the legs does not see this harmonic as it only affects the common current in the upper and lower arms. It must be noted that due to transformer winding, the 3rd, 6th, and other zero sequence current harmonics cannot be eliminated in grid current. To start, the (4-1) is rewritten for the second harmonic and the following park's transformation is used.

$$T_{dq0}=\frac{2}{3}\begin{bmatrix} cos\theta_2 & cos\,(\theta_2-\frac{2\pi}{3}) & cos\,(\theta_2+\frac{2\pi}{3}) \\ -sin\,\theta_2 & -sin\,(\theta_2-\frac{2\pi}{3}) & -sin\,(\theta_2+\frac{2\pi}{3}) \\ \frac{1}{2} & \frac{1}{2} & \frac{1}{2} \end{bmatrix} \quad 4\text{-}24$$

This transformation is rotating at -2ω since the goal is to extract the voltage and current signals that are in the form of a negative sequence. This results in the following equations:

$$V_{G\,d}^{\;2h}=V_{C\,d}^{\;2h}+L\frac{d\,I_{G\,d}^{\;2h}}{dt}+R\,I_{G\,d}^{\;2h}-2\omega LI_{G\,q}^{\;2h} \quad 4\text{-}25$$

$$V_{G\,q}^{\;2h}=V_{C\,q}^{\;2h}+L\frac{d\,I_{G\,q}^{\;2h}}{dt}+R\,I_{G\,q}^{\;2h}+2\omega LI_{G\,d}^{\;2h} \quad 4\text{-}26$$

Where $V_{G\,d}^{\;2h}$, $V_{G\,q}^{\;2h}$ $V_{G\,d}^{\;2h}$, $V_{G\,q}^{\;2h}$ and are the grid and converter d-q voltages of the second harmonic respectively, $I_{G\,d}^{\;2h}$ and $I_{G\,q}^{\;2h}$ are also grid d-q currents with double of the base frequency. To get the converter voltage in the d-q frame, the (4-25) and (4-26) need to be rewritten:

$$V_{C\,d}^{2h} = V_{G\,d}^{2h} - L\frac{d\,I_{G\,d}^{2h}}{dt} - R\,I_{G\,d}^{2h} + 2\omega L I_{G\,q}^{2h} \qquad \text{4-27}$$

$$V_{C\,q}^{2h} = V_{G\,q}^{2h} - L\frac{d\,I_{G\,q}^{2h}}{dt} - R\,I_{G\,q}^{2h} - 2\omega L I_{G\,d}^{2h} \qquad \text{4-28}$$

Here, two PI controllers regulate the d-q currents at this harmonic with references equal to zero and two feed-forward signals: $2\omega L I_{G\,q}^{2h}$ and $-2\omega L I_{G\,d}^{2h}$ are added to the outputs of the PI controllers to decouple the d-q currents.

$$V_{C\,d}^{2h} = -G(s)_{PI} + 2\omega L I_{G\,q}^{2h} \qquad \text{4-29}$$

$$V_{C\,q}^{2h} = -G(s)_{PI} - 2\omega L I_{G\,d}^{2h} \qquad \text{4-30}$$

It must be noted that the second harmonic of the grid voltage is zero. The coefficients of the PI controllers are tuned using the modulus optimum as follows [158]:

$$G(s)_{PI} = K_c\left(\frac{1+T_i\,s}{T_i\,s}\right) \qquad \text{4-31}$$

Where $T_i = \frac{L}{R}$, $K_c = \frac{T_i\ R}{2T_a}$ and T_a is the equivalent delay for the MMC. To reduce the bandwidth for this controller as no fast dynamic is needed here, the crossover frequency is also reduced by a decade using an overall gain. The output of this controller is finally added to the main control system and is fed to the converter. To minimize the interference of this extra controller effect on the main control loop, which regulates the converter's active and reactive power, a second-order low pass filter at the output of the Park’s transformation is used with the natural frequency of 9 (Hz) and damping ratio of 0.707.

$$F_{Filter} = \frac{\omega_n^2}{s^2 + 2\,\zeta\omega_n\,s + \omega_n^2} \qquad \text{4-32}$$

Where ω_n is the natural frequency and the ζ is the damping ratio. The frequency response of the low-pass filter can be seen in Figure 4-7.

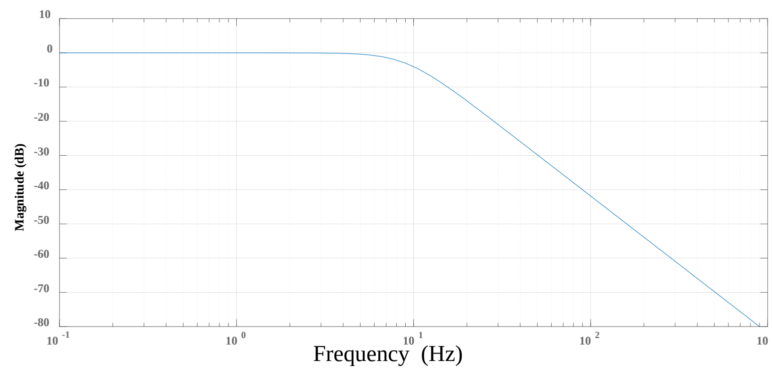

(a)

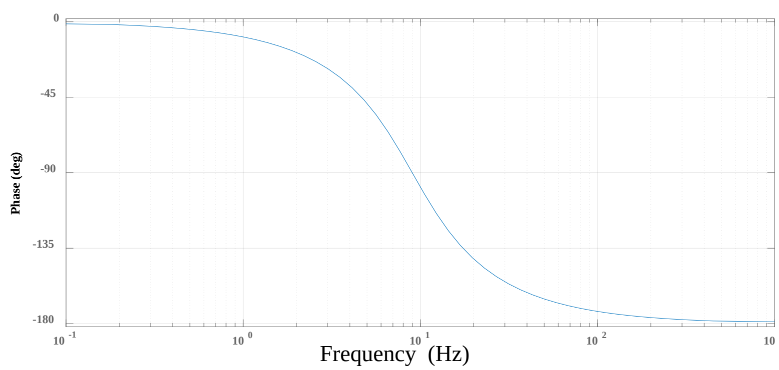

(b)

Figure 4-7. Bode plot of the designed filter for MCB: (a) magnitude, (b) phase.

Since the reference frame is rotating at *-2ω*, the main output current will be transformed into triple frequency and as it passes through the filter, it is attenuated by 50 dB, and the same thing happens to the other harmonics. As this controller is activated, the MMC will provide the second harmonic current needed for the saturated power transformer, which prevents the flow of this negative sequence current into the grid. It must be pointed out that this controller is activated only if GIC is flowing in the system. The second harmonics elimination section of the MCB is depicted in Figure 4-8.

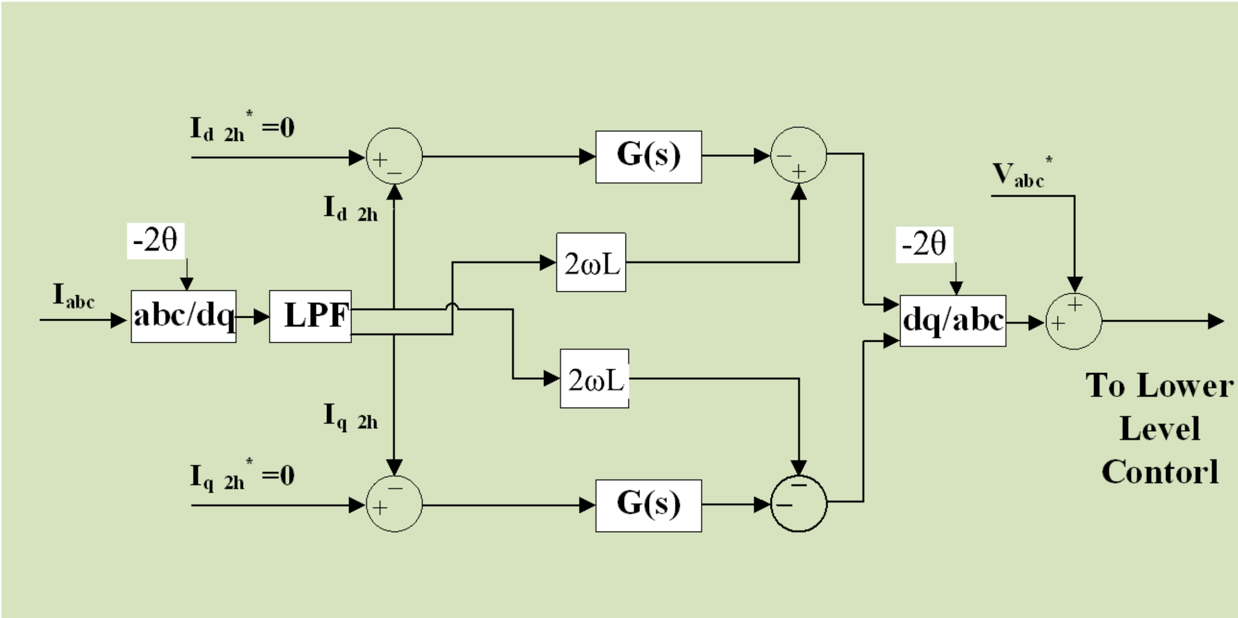

Figure 4-8. Proposed MCB to eliminate the second harmonic in the grid current.

4.2.2 Control Approach to Inject Reactive Power

As the GIC flows in the neutral of the transformer, the transformer magnetizing current and, thus, reactive power loss drastically increases in all affected transformers. Therefore, the availability of sufficient reactive power sources is crucial to maintain the system voltage stability. The reactive power support in power systems is typically the role of shunt capacitor banks. However, during GMDs and high reactive power demands, the capacitor banks can be overloaded and tripped. In the widely presented control system of the MMC, the MMC operates in a constant P-Q mode. Consequently, the control system does not see an increase in the magnetizing current, and the grid is responsible for providing the transformer with escalated reactive power demand. This might be the start of the catastrophic events that lead to voltage collapse in the power grid. To avoid this problem, a control approach is proposed.

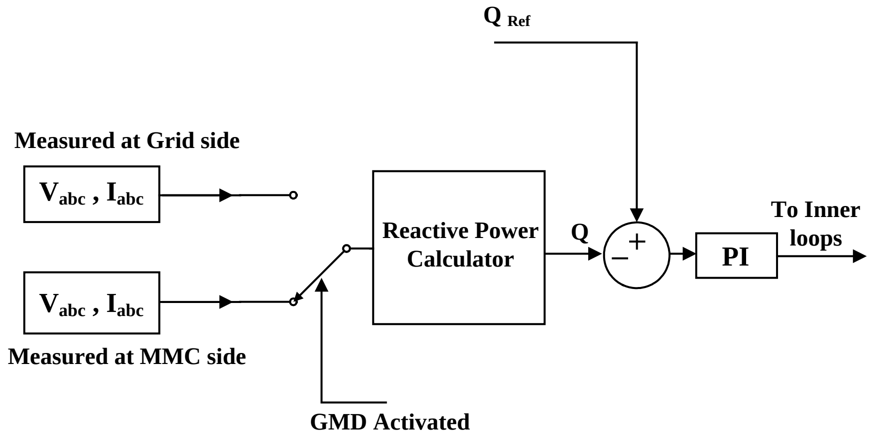

Figure 4-9. Proposed control approach to inject reactive power into the transformer during GMD.

In this approach, the grid side measured voltage and current are used to calculate the reactive power and be compared with the reference values in the control loop. Therefore, during GIC, the control system compensates for the increased magnetizing current in the transformer, and the grid power factor remains unchanged. In other words, by applying the proposed solution, the reactive power is provided from the MMC instead of the grid. This helps the grid voltage stability as it reduces the reactive power demand on the grid side and keeps the system reactive power reserve available for the other transformers and parts of the network that can be affected by the GMD. This control approach is depicted in Figure 4-9.

Chapter 5

Simulation Results

This chapter provides the simulation results of the study system exposed to GIC at different levels. The GIC results from the induced voltage in the circuit that flows in the transmission line, the transformer windings, and the ground as the return path. To model this induced voltage, a DC voltage source is applied at the neutral of the converter transformer. The transmission and transformer resistances limit the GIC magnitude. The GIC triggering voltage source is applied at t=5 s to establish 200 A of GIC flow at the transformer neutral connection [159].

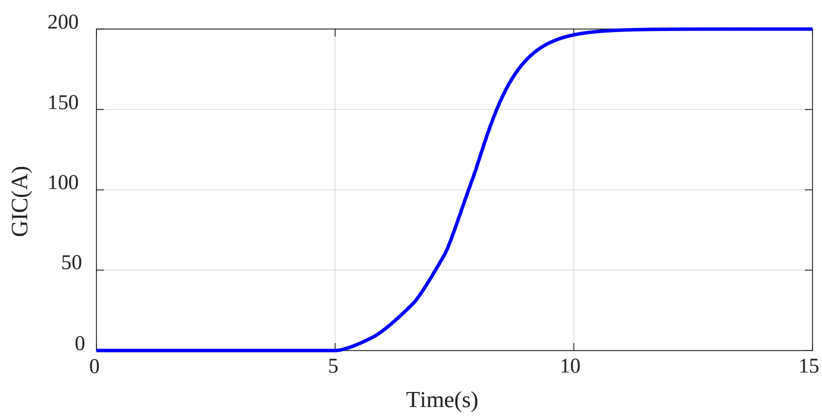

Figure 5-1. Flow of GIC in the neutral of the transformer.

The flow of GIC in the transformer neutral is depicted in Figure 5-1. Since the transformer magnetizing branch is basically a big inductor, there is a relatively long time constant for the DC current to reach the final value; here, it takes 5.8s to have 200A of GIC flowing in the circuit. As the transformer goes into deeper saturation, this inductor reduces and the current change rate increases. Since the DC current increases, flux in the transformer is shifted up, as in Figure 5-2.

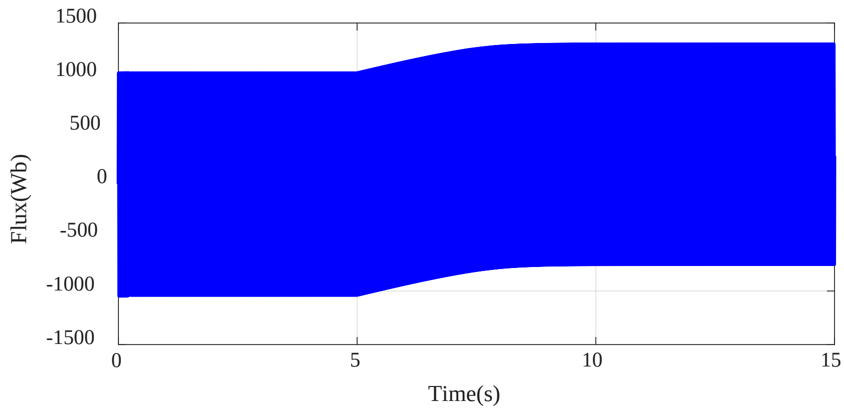

Figure 5-2. Transformer flux shift due to GIC.

This clearly shows the half-cycle saturation in the transformer, which leads to a drastic increase in the magnetizing current. The magnetizing current of the transformer is depicted in Figure 5-3; in the negative half cycle, the current is in the expected range, but as the transformer saturates in the positive half period, there is a high peak in the current that gets to 320 A, this peak is directly related to the GIC level, as the DC current increases, the peak current also increases.

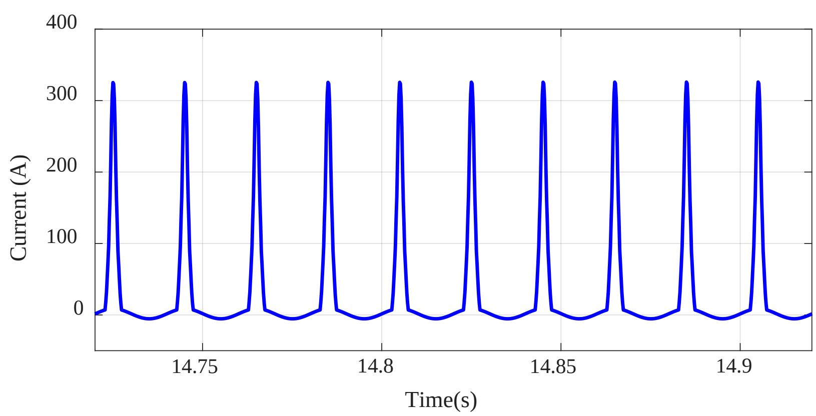

Figure 5-3. Magnetizing current of the transformer exposed to 100 A of GIC.

5.1 GIC level effect on the harmonic's magnitude

The current in the magnetizing branch of the half-cycle saturated transformer includes different harmonics that are depicted in Figure 5-4. As stated before, this spectrum starts from the main frequency of the system; it includes both odd and even harmonics. Also, the effect of the GIC level on the magnitude of the harmonic can be seen. As the GIC level increases, the resulting harmonics will have higher magnitudes since the flux magnitude is increased.

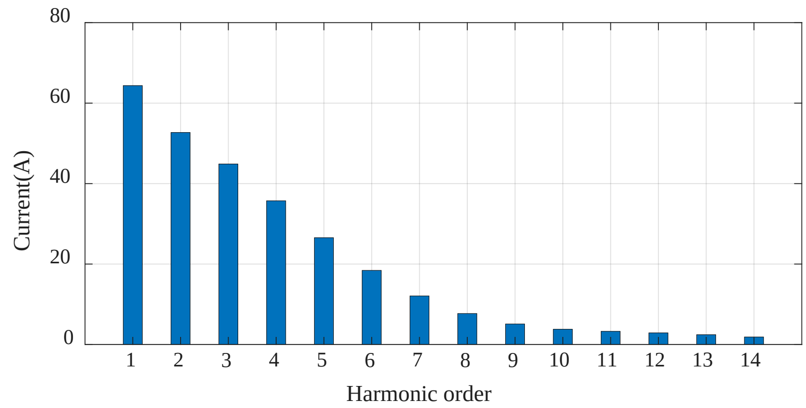

(a)

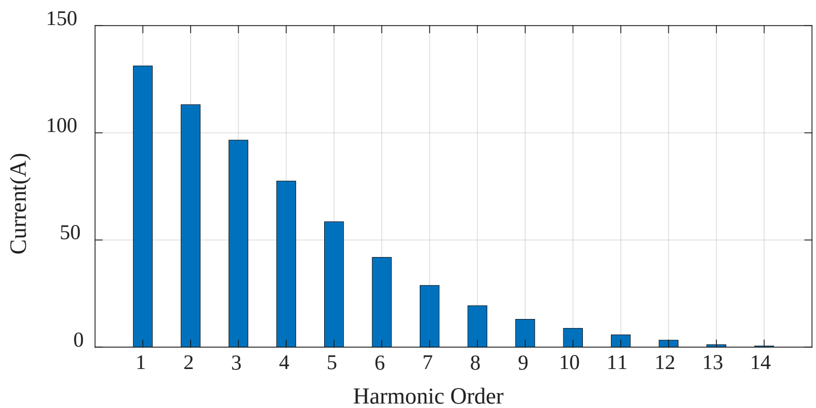

(b)

Figure 5-4. The resulting harmonics in the converter transformer magnetizing branch are due to the GIC of (a) 100 A, (b) 200 A.

5.2 Effect of the MMC loading on the resulting harmonics

To demonstrate the effect of the MMC loading on the resulting harmonics, a comparison is made here. The GIC level is set at 100A, and the operating point of the MMC is changed. Figure 5-5 provides this comparison; in the first situation, the reactive power is constant, and the harmonics magnitude is observed as the active power changes; in the second case, the active power is constant and the reactive power changes.

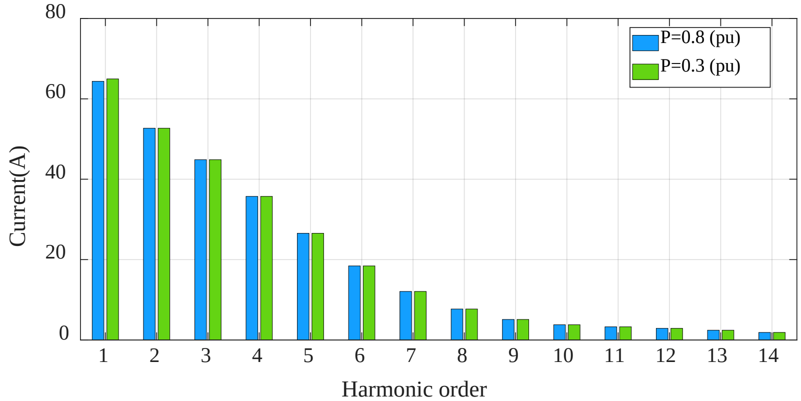

(a)

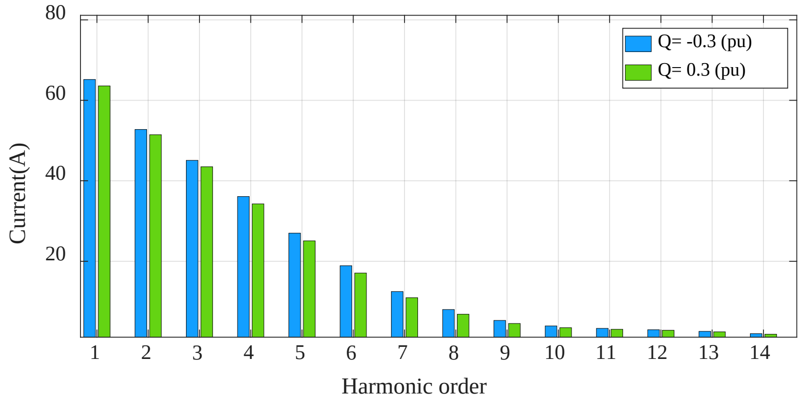

(b)

Figure 5-5. Effect of loading on resulting harmonics. (a) change in active power, (b) reactive power.

It can be seen that the change in the active power transferring from the MMC does not change the produced harmonics; this is expected as the active power is changed mainly through the phase angle according to (5-1). On the other hand, reactive power variation slightly changes the magnitude of the resulting harmonics as it changes the amplitude of the voltage across the magnetizing branch, which changes the flux magnitude, which can be seen in (5-2).

$$P \simeq \frac{V_{grid} V_{conv}}{X} \delta \qquad 5\text{-}1$$

$$Q \simeq \frac{V_{conv}(V_{grid} - V_{conv})}{X} \quad \text{5-2}$$

5.3 GIC Effect on the Control System

Due to the harmonics arising from the GMD, the ripple in the control variables increases. V_q and V_d, which are the grid voltage components in the d-q axis and are supposed to be constant values, show a high magnitude of ripple during GIC. Figure 5-6 shows the waveform of the d-q voltages in the control system of the MMC.

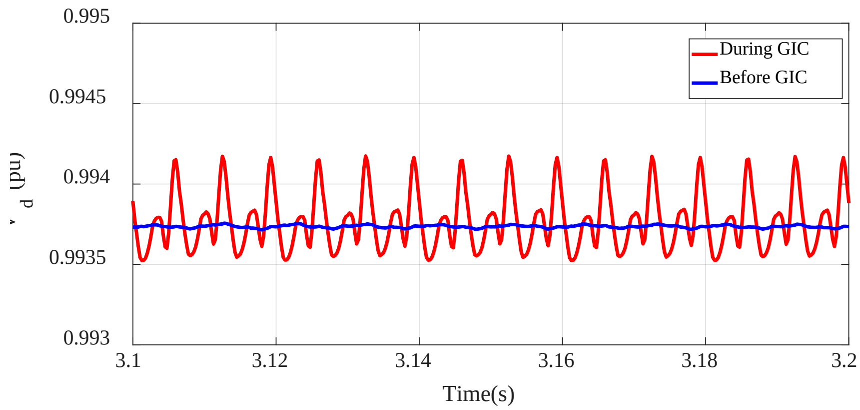

(a)

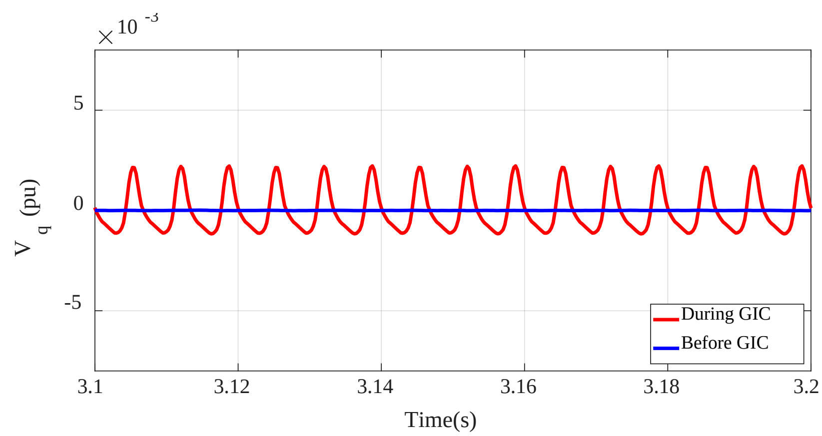

(b)

Figure 5-6. Voltage fluctuations in d-q due to GIC=200A: (a) V_d,

(b) V_q .

Although two low-pass filters are used to remove the high-frequency ripple from these variables, during the GIC, the ripple in these quantities increases drastically. The I_q and I_d that control the reactive and active power, respectively, are expected to be DC values in a steady state with very small variation, but due to GIC, they suffer from the same thing, and they start to oscillate as depicted in Figure 5-7.

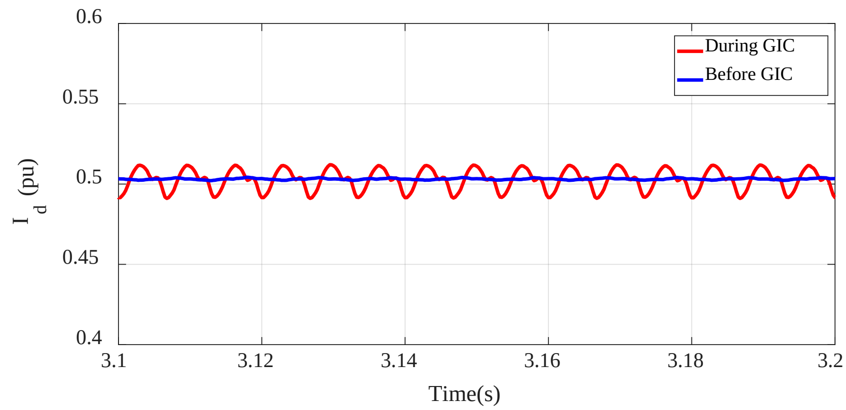

(a)

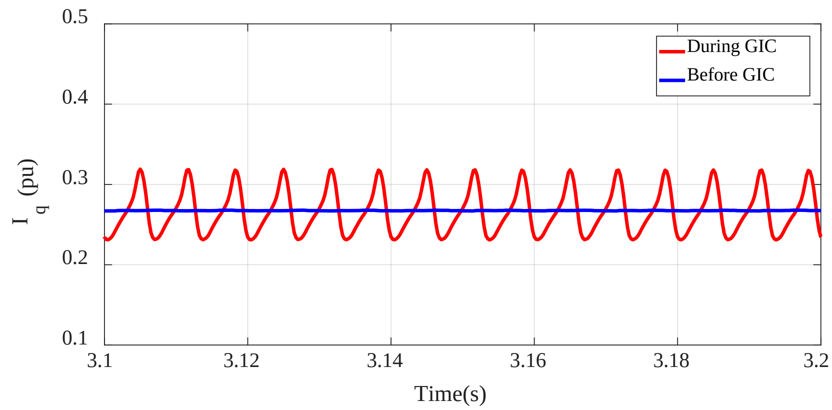

(b)

Figure 5-7. Fluctuation in d-q currents due to GIC=200A: (a) I_d oscillation (Reference=0.5 pu), (b) I_q oscillation (Reference= 0.27 pu).

The operation of PLL unit is crucial for the control system to be synchronized with the grid and if PLL operation is interfered, it could be the start of instability in the MMC. Figure 5-8 shows the

PLL output frequency normal operation and in case of GIC. As it appears, the output of the PLL is not affected by the GIC and PLL is able to continue to its operation with minimum error.

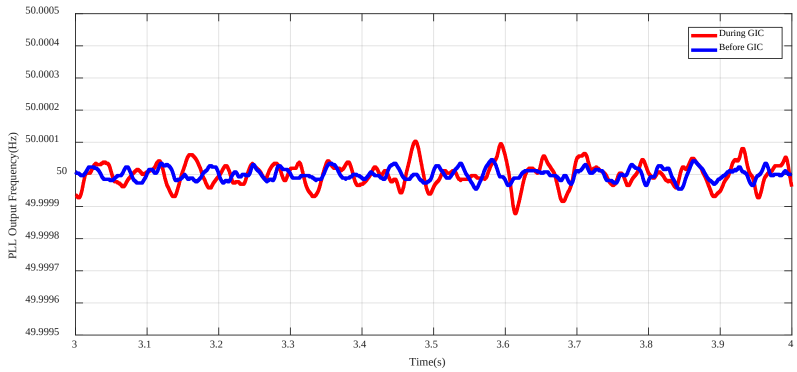

Figure 5-8. PLL output frequency

However, higher ripple in control parameters is not limited to the d-q components. During the GIC, the DC link current and voltage experience higher ripple in comparison to normal operation. As depicted in Figures 5-9 and 5-10, ripple slightly increases in the current and voltage of the link, which is mainly due to the third harmonic current that appears in the MMC legs.

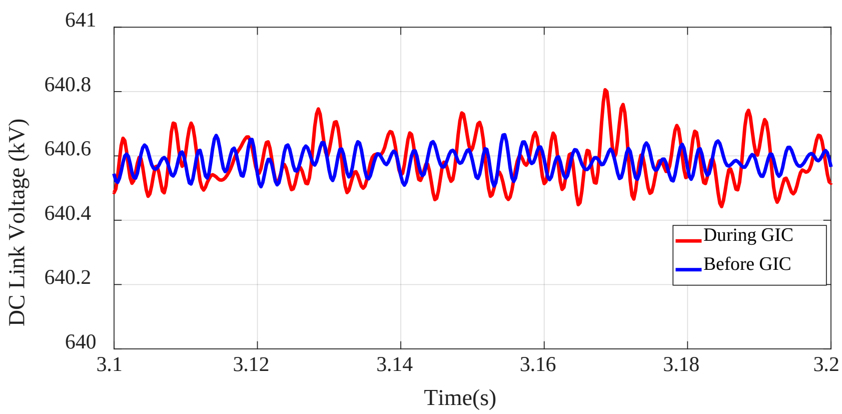

Figure 5-9. DC Link voltage (I_d =0.5 pu)

Another aspect of the control system that is affected during the GIC is the internal circulating current suppressing controller. This unit adds a voltage with double frequency to the main voltage of the phases to make sure that no circulating current is flowing between the legs. As the GIC flows, the added voltage in upper and lower arms that were equal, start to deviate depicted in Figure 5-11. This voltage increases in the lower arm but in the upper arm, it decreases. The reason for this difference is the flow of the second harmonic of the current into the MMC from the saturated transformer.

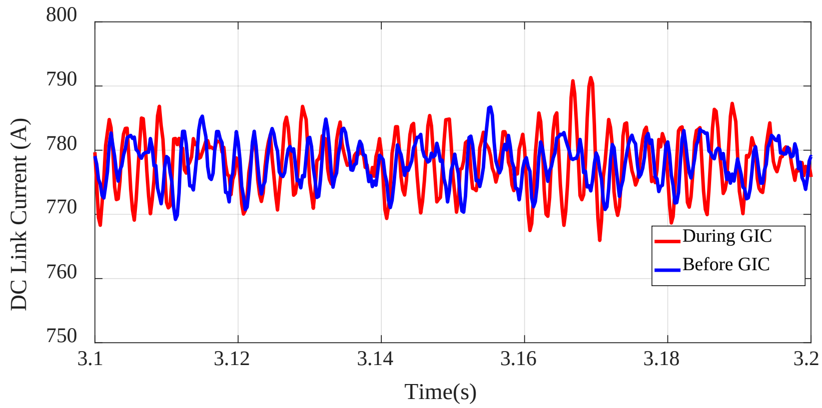

Figure 5-10. DC Link current (I_d =0.5 pu)

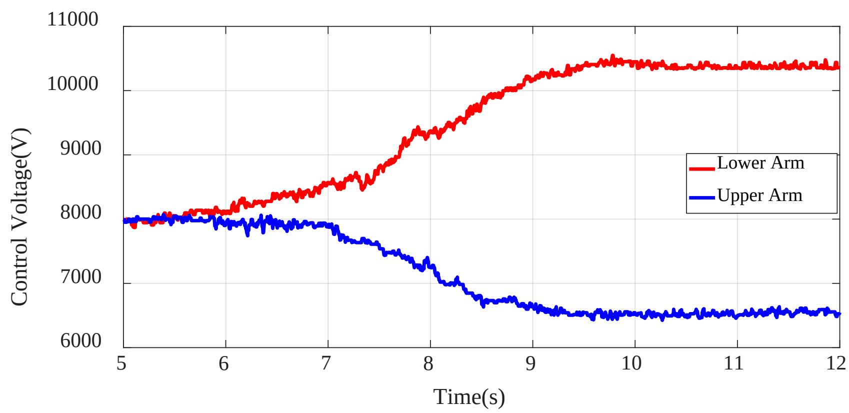

Figure 5-11. Output of circulating current suppressing controller due to GIC.

5.4 Transformer reactive power demand in presence of GIC

The 1st harmonic, i.e., the fundamental frequency component arising from transformer saturation, lags the transformer voltage and thus it behaves like an inductive current. Therefore, the fundamental current is associated with the reactive power and represents the transformer as a reactive load in the power system. The control strategy of the MMC determines how the MMC provides its share of the fundamental harmonic current. Since the MMC typically operates based on a constant P-Q or unity power factor, its reactive current component is constant. Therefore, when the GMD occurs and the reactive power demand of the converter transformer increases, the grid provides all the augmented reactive power demand as depicted in Figure 5-12.

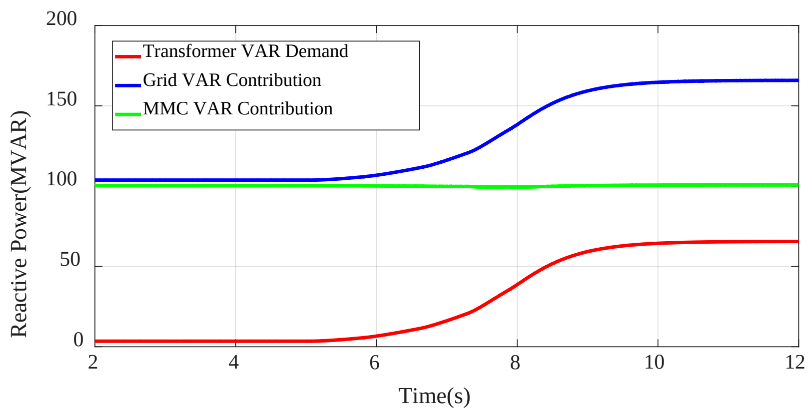

Figure 5-12. Variation in the reactive power transfer of the transformer, grid and the MMC in presence of the GIC.

Figure 5-12 shows that as the GIC flows, the reactive power transfer of MMC remains constant and the grid is balancing the reactive power equation. The GIC level is also determining the reactive power demand of the transformer and as it increases, higher reactive power must be injected into the transformer. This is a very serious effect of the GIC since in the case of GIC, the capacitor banks or SVCs that provide reactive power could be out of service. Therefore, increasing reactive demand from the grid might endanger the voltage stability in the grid. The effect of GIC level on the reactive power demand of the transformer is depicted in Figure 5-13. The time constant difference in different levels of GIC is due to the fact that as the transformer goes to higher saturation, the equivalent inductance decreases which means the time constant of

R-L circuit, decreases. This explains why for higher levels of GIC, the circuit reaches the final value in a shorter time.

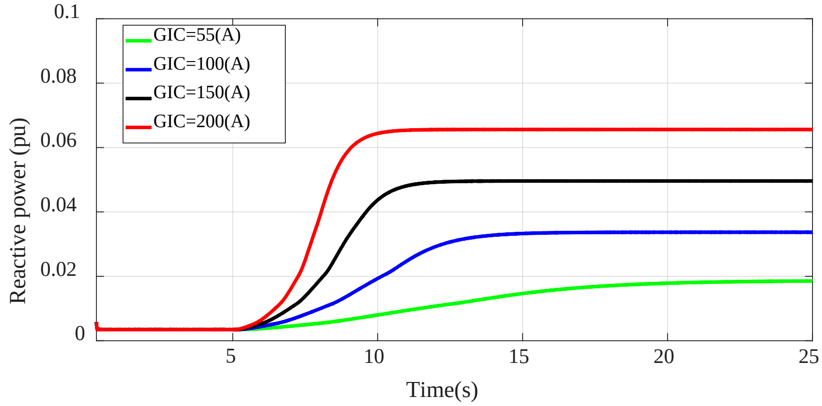

Figure 5-13. Reactive power demand due to different levels of GIC.

5.5 Harmonic distribution during GIC

As discussed before, when the GIC flows, the harmonics will be distributed between the grid and the MMC. Figures 5-14 and 5-15 show the grid and MMC side harmonics due to 200A of GIC respectively.

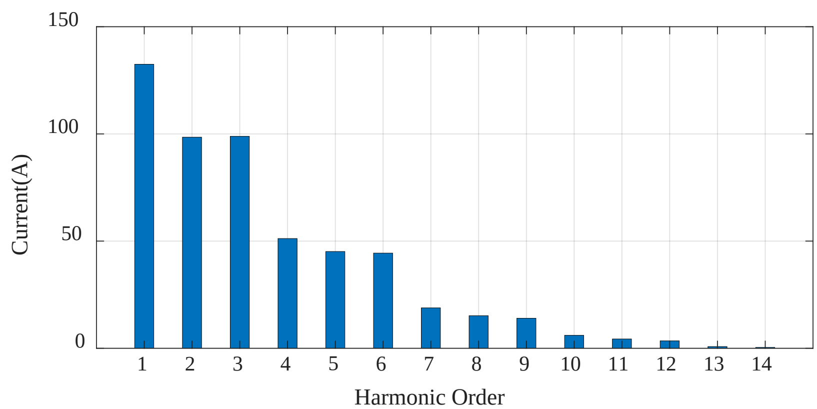

Figure 5-14. The current harmonics on the grid side under 200A of GIC.

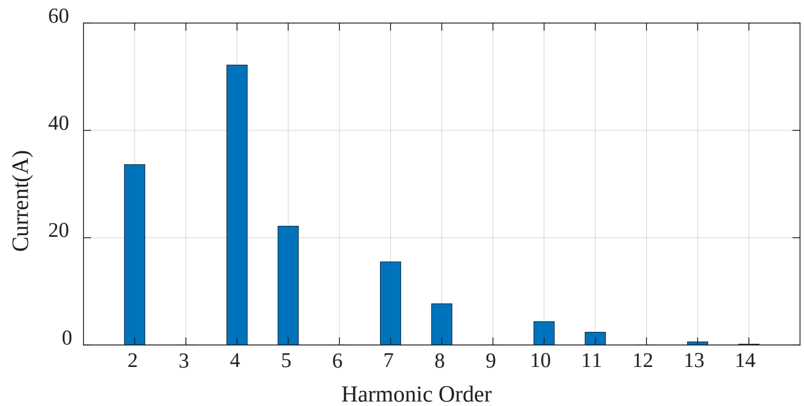

Figure 5-15. The current harmonics at the MMC terminals under 200A of GIC.

It is worth noting that the delta connection of the transformer at the MMC side prevents the flow of the 3rd harmonic, and its multiplies harmonic currents. However, Figure 5-16 illustrates that these harmonics are present in the MMC arms. The reason for having these currents is that the multiplication of $N_{up}(t)$ which is the number of inserted SMs in the arm, and SM's voltage term resulting from second and forth harmonic, creates the zero sequence voltage sources that result in these circulating currents.

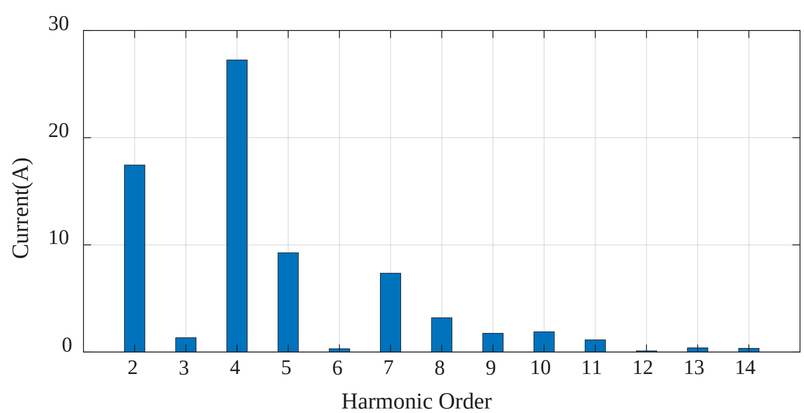

Figure 5-16. The current harmonics in the MMC arm due to 200A of GIC.

The circulating current among the MMC legs creates a voltage shift in the SMs capacitor voltages as shown in Figure 5-17. Before the GIC, the voltages in the capacitors in the upper arm and lower arm have the same voltage magnitude and have the same waveforms. However, due to

GIC, these voltages are not equal anymore. The capacitors voltage in the upper arm increases during the GIC while the average voltage is constant, which is expected since the average voltage is affected by the DC link voltage and the number of the SMs.

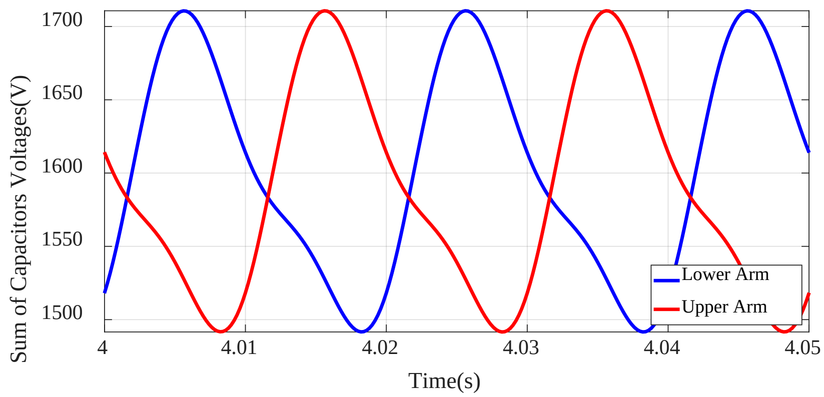

(a)

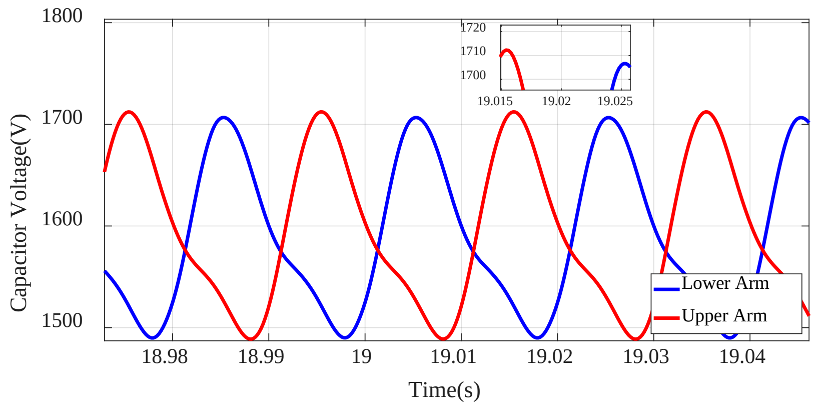

(b)

Figure 5-17. The SMs' capacitors voltage :(a), before GIC, (b) during GIC (200A of GIC).

5.5.1 Verification of harmonics distribution model

To validate the impedance model and the model for current sharing between the MMC and the grid, the current harmonics derived from the analytical model are compared with the results measured in the simulation. Figure 5-18 shows the calculated magnitude and phase of the MMC current harmonics and the simulation results for 100 (A) of GIC. In this case, the MMC receives

30% active power and no reactive power from the grid. In the second case for evaluating the model, the GIC level is increased to 200 (A) and the operating point is set to have 0.9 (pu) active and 0.3 (pu) reactive power in the MMC. The results of the analytical model and simulation results are compared in Figure 5-19.

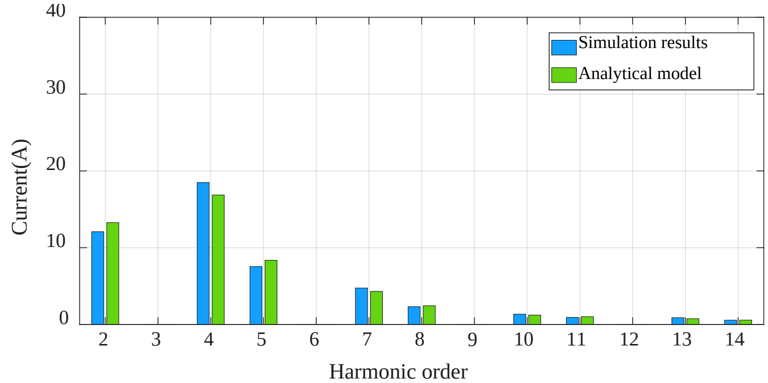

(a)

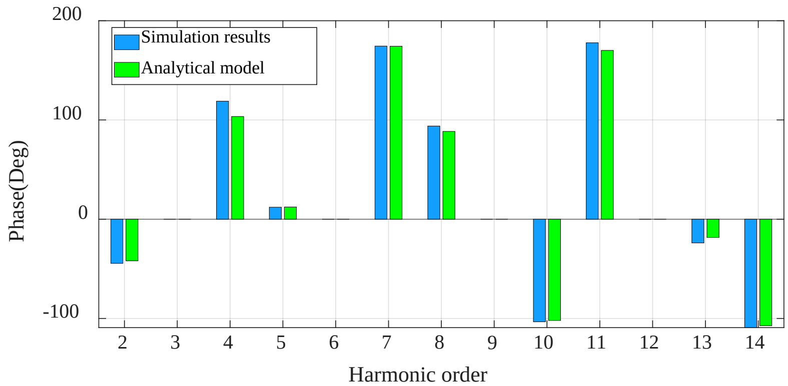

(b)

Figure 5-18. The MMC side current harmonics due to 100A of GIC (P=0.9 pu, Q=0.3). (a) magnitude, (b) phase.

The operating point affects the model through the modulation index, which, depending on the change in the reactive power, can increase or decrease. As the MMC shows capacitive behaviour and provides reactive power to the grid, the modulation index increases, leading to an increase in the equivalent capacitor of the MMC, which ultimately provides a path with lower impedance for the harmonics to flow. This effect is more visible in the low frequencies since, with high frequencies, the effect of the equivalent capacitor diminishes, and the arm inductor becomes dominant. Despite the minor differences between the analytical model and the simulation results, which are mainly due to neglecting the internal control loops, including circulating current suppressing and outer control loops of active and reactive power to simplify the impedance model, the model accuracy is acceptable. It must be noted that due to the delta winding of the transformer at the MMC side, the zero sequence currents cannot flow into the MMC side, and inevitably, these harmonics are fed to the grid.

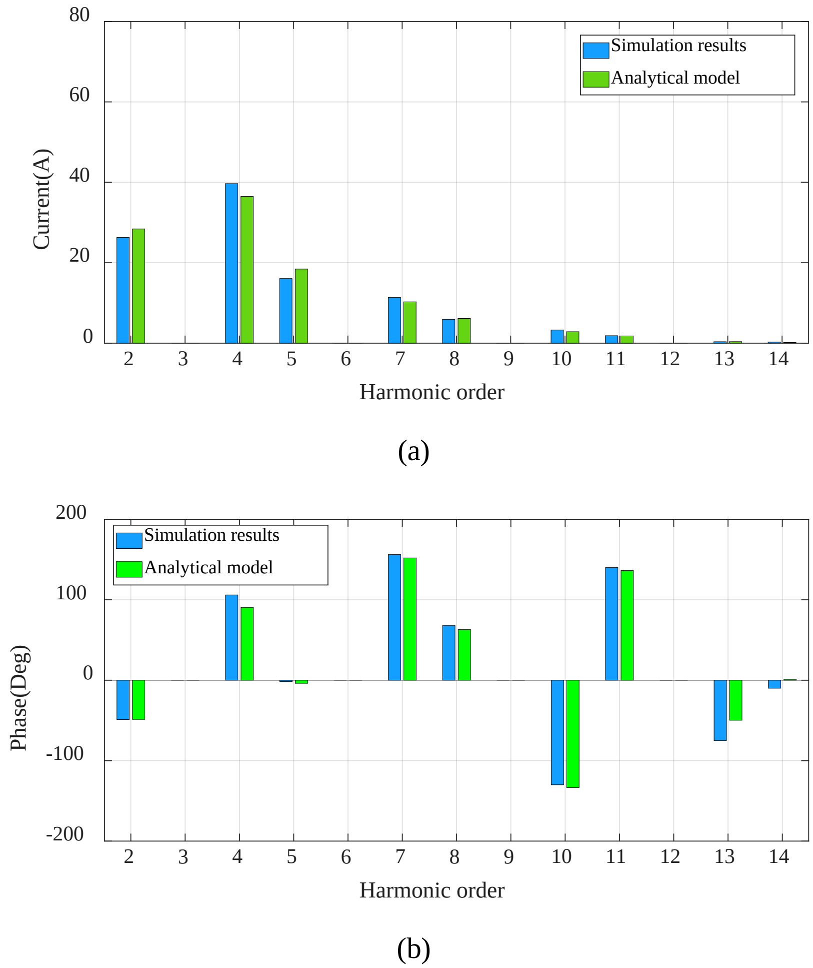

Figure 5-19. The MMC side current harmonics due to 200A of GIC (P=0.3 pu, Q=0). (a) magnitude. (b) phase.

5.6 Voltage and Current Distortion Due to GIC

The presence of the harmonics arising from transformer half-cycle saturation distorts the grid and MMC voltages, especially current waveforms. This effect can be seen in Figure 5-20 for the grid side and in Figure 5-21 for the MMC side waveforms. Since a higher portion of the harmonics flow into the grid rather than the MMC, the distortion in the grid parameter is more severe. From these figures, it can be seen that the distortion in the grid voltage is more noticeable than the MMC voltage waveform distortion. The effects of loading on the total harmonic distortion (THD) are also depicted in Figures 5-22 and 5-23. As the output power of the MMC decreases, the THD increases adversely. The reason for this effect is that the resulting harmonics from saturation during the GIC are almost independent of the MMC loading. The standards provide maximum permissible limits for voltage and current harmonics to maintain the system power quality in an acceptable condition. Table 5-1 provides the permissible THD limits of the IEEE Std 519 [160]. It can be seen that THDs of the current and voltage violate the permissible standard limits under different loading conditions. The grid is subjected to more distortion as it provides a path with lower impedance for the current harmonics.

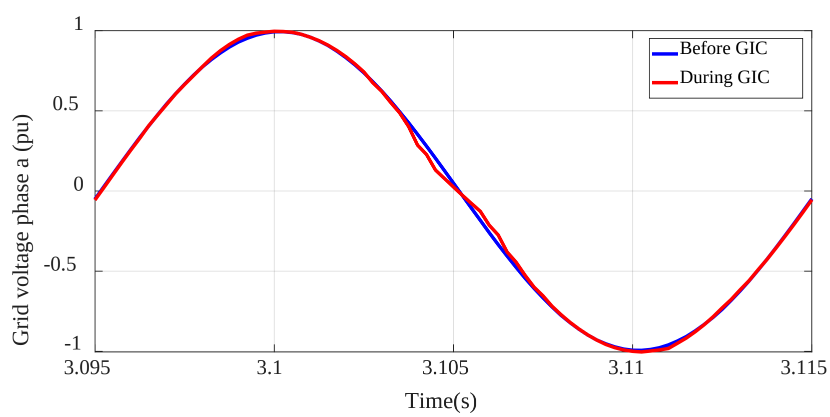

Figure 5-20. Grid voltage waveform.

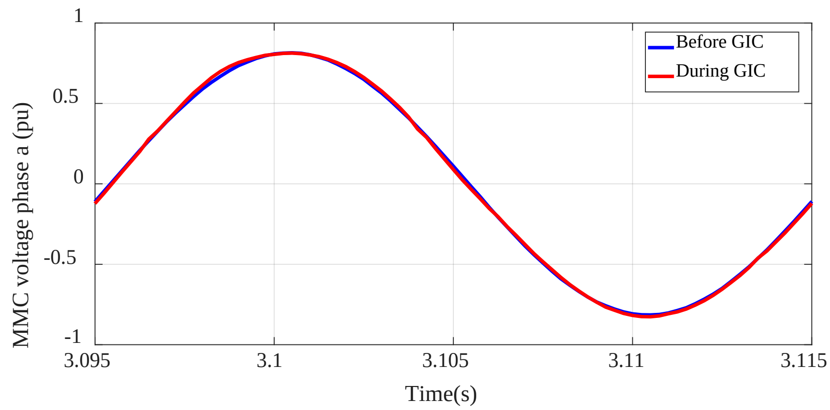

Figure 5-21. MMC voltage waveform.

Table 5-1. Permissible standard limits for total harmonic distortion (THD)

System Type	Voltage THD	Current THD
Transmission Level	1.5 %	3.75 %

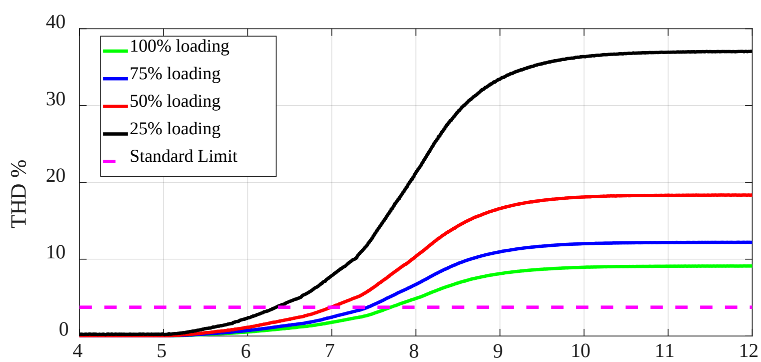

(a)

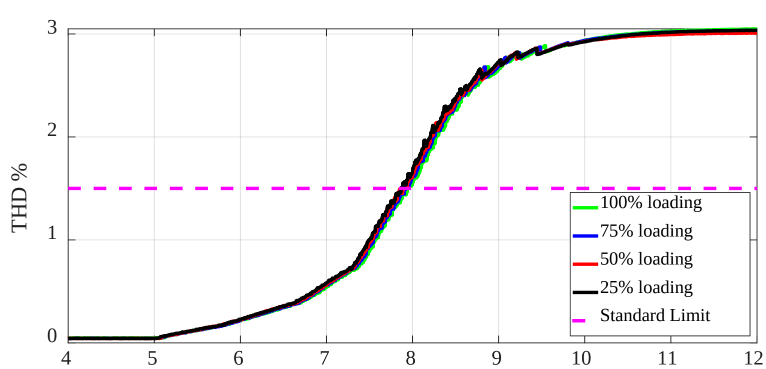

(b)

Figure 5-22. Grid side distortion during 200 A of GIC: (a) Current THD, (b) Voltage THD.

Figure 5-25 states that even if the grid power exchange to the MMC is at the nominal capacity, during the 200 A of the GIC, the THD values are beyond the permissible values. The grid voltage THD violates the standard value regardless of the loading. Voltage and current distortion are less tolerable in high voltage transmission levels as it threatens the operation of the power system. For current waveforms, the situation is even worse; if the MMC is loaded with a quarter of the nominal capacity due to the same level of the GIC, THD in grid current reaches to 38 %, which is way beyond the value in Table 5-1. The magnitudes of the first 10 harmonics in the grid voltage and current are presented in Table 5-2.

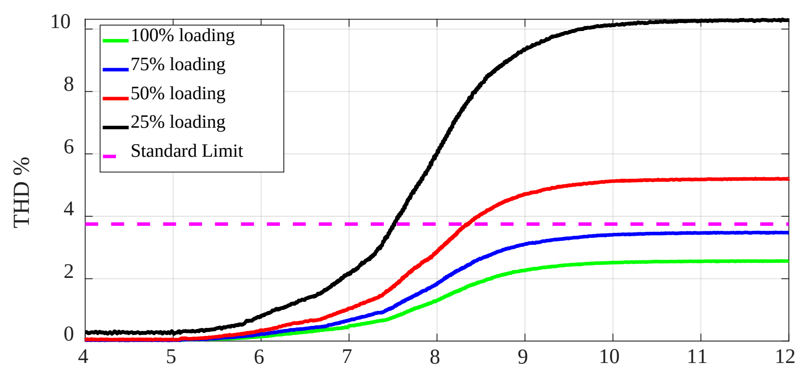

(a)

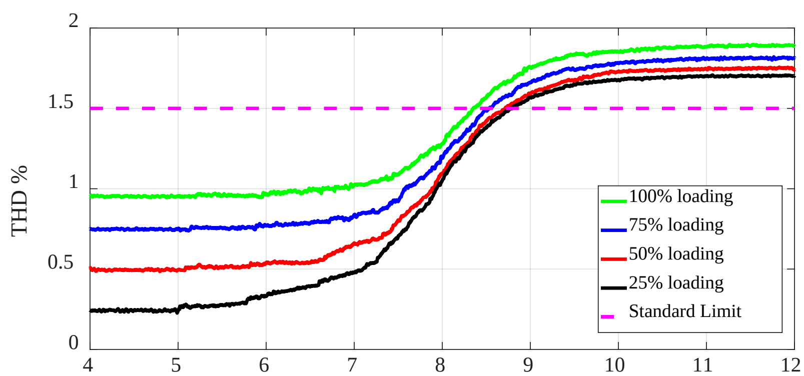

(b)

Figure 5-23. MMC side distortion during 200 A of GIC: (a) Current THD, (b) Voltage THD.

Even though THD values for the MMC are lower, they still are higher than accepted levels of distortion. In the worst for the current waveform, the THD for the MMC side reaches 11 %. It must be mentioned it is preferred to make the grid waveforms close to sinusoidal even if it costs distorting the MMC parameters. The first 10 harmonics are also presented for the MMC side in Table 5-3. Tables 5-2 and 5-3 show that harmonics tend to flow into the grid instead of the MMC, which results in deeper distortion in the grid voltage and current waveforms.

Table 5-2. Magnitude of grid voltage and current harmonics in phase a for GIC=200A.

Harmonic Order	**Voltage (pu)**	**Current (A)**
1	99.38	1027
2	0.0096	98.49
3	0.0142	98
4	0.0095	50.09
5	0.0103	44.62
6	0.0126	44.05
7	0.0056	18.4
8	0.0051	14.62
9	0.0057	13.81
10	0.0023	5.82

Table 5-3. Magnitude of MMC voltage and current harmonics in phase a for GIC=200A.

Harmonic Order	**Voltage (pu)**	**Current (A)**
1	1.007	1293.53
2	0.0087	33.63
3	0.0002	0.017
4	0.013	52.96
5	0.0058	21.54
6	0.0006	0.08
7	0.0013	15.36

8	0.0028	7.93
9	0.0005	0.17
10	0.0004	4.48

5.7 Mitigating Control Block Response

The mitigating control block (MCB) is designed to eliminate the 2nd, 4th, 5th,7th and 8th harmonics in the grid current. These harmonics threaten the operation of power system components. The design goal is that as the MCB is used, these harmonics flow entirely into the MMC instead of the grid. To validate the MCB performance, it is activated at t= 12 s after the GIC has reached the final value of 200 A. As depicted in Figure 5-24, this controller successfully eliminates those harmonics in the Grid current, and it satisfies the design goals. The waveform of the grid current is depicted in Figure 5-25; as the MCB is in the system, the distortion of the current reduces.

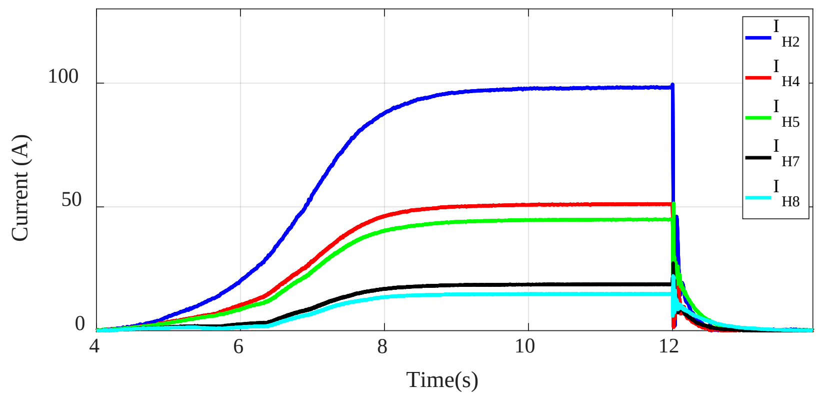

Figure 5-24: Effect of the MCB activation on the magnitude of the targeted harmonics (GIC=200 A)

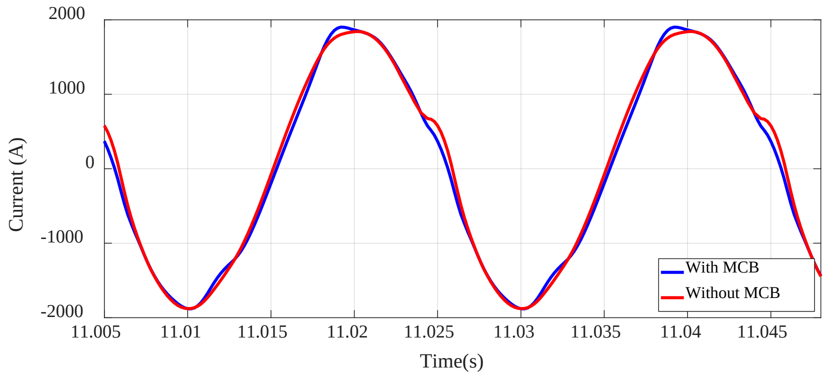

(a)

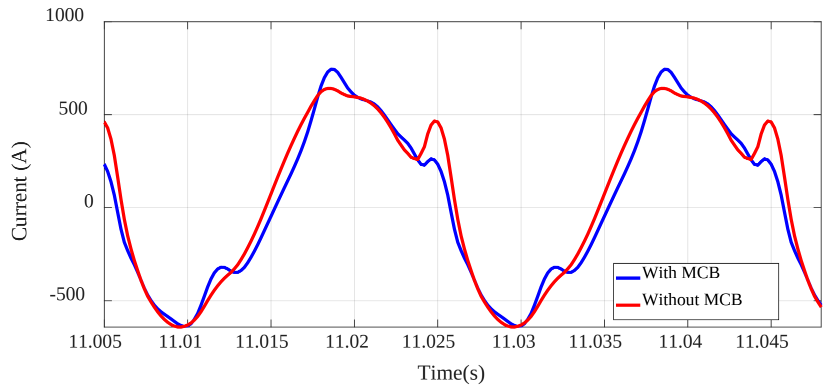

(b)

Figure 5-25. Grid current waveform due to 200 A of GIC: (a) P=0.9 pu , (b) P=0.3 pu.

To prove that the effect of the MCB is minimized on the main control loop of the system, two cases are compared. In the first step, the reference of active power is changed from 0.3(pu) to 0.8(pu), and finally, it goes back to 0.2(pu). This procedure is done in two scenarios; first only the main control loop is regulating the system, and in the second one, the GIC is flowing, and the proposed control block is activated, eliminating the targeted harmonics from the grid current. The system response in both scenarios is depicted in Figure 5-26. There are small fluctuations in the system with active MCB due to the presence of current harmonics as the result of the GIC, and a simple low pass filter is used to remove them for demonstration. Also, the same procedure is done for reactive power loop. The reference for reactive power goes from zero to -0.2(pu), and eventually, it settles on 0.2(pu). The system responses are compared to evaluate the effect of the proposed control block. It can be seen in Figure 5-26(a) and Figure 5-26(b) that the dynamic of the system is the same, and the settling time is 100 (ms) in both cases, which means that the operation of the MCB unit is not affecting the main control loop. The reason for similar for main control loop responses with and without the MCB is that the MCB has a very narrow bandwidth, which minimizes the interference of the two controllers. It must be noted that the internal current control loops of the MMC, which regulate the I_d and $I_{q,}$ are about seventy times faster than the added control block, and they have a settling time of 10(ms) and the responses depicted here are for the outer control loop which must be slower than inner ones.

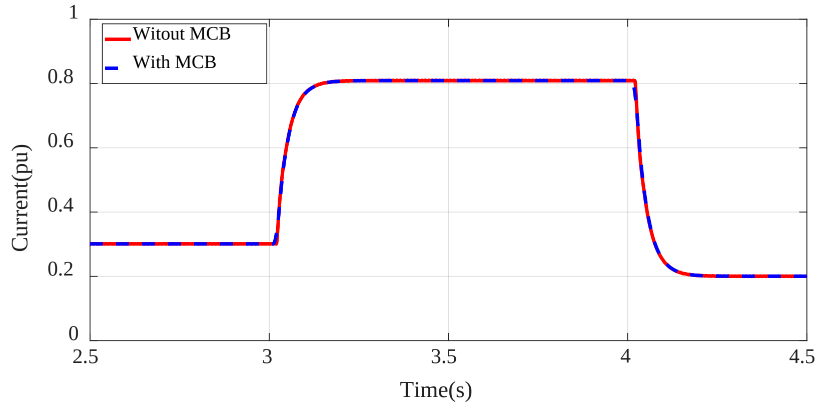

(a)

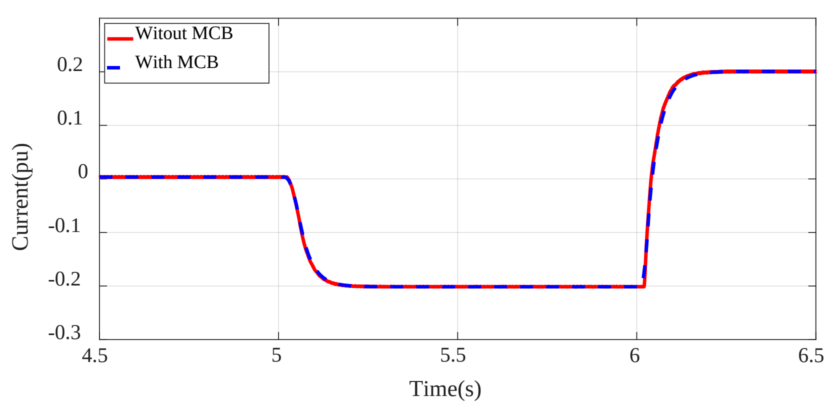

(b)

Figure 5-26. MMC response to reference change, (a) active power reference, (b) reactive power reference.

5.7.1 MMC Derating in Presence of GIC Due to MCB

In the case of a GMD, as the MCB is activated, the MMC will eliminate the major resulting harmonics from the grid side. This means that the MMC is used to absorb current harmonics. As these currents flow into the MMC arms and, eventually, the semiconductors, power loss increases in these components. Consequently, the MMC's capacity for transferring active and reactive power is decreased. As depicted in Figure 5-27, at GIC level of 200 A, the capacity of MMC for reactive and active power is reduced to 85 %.

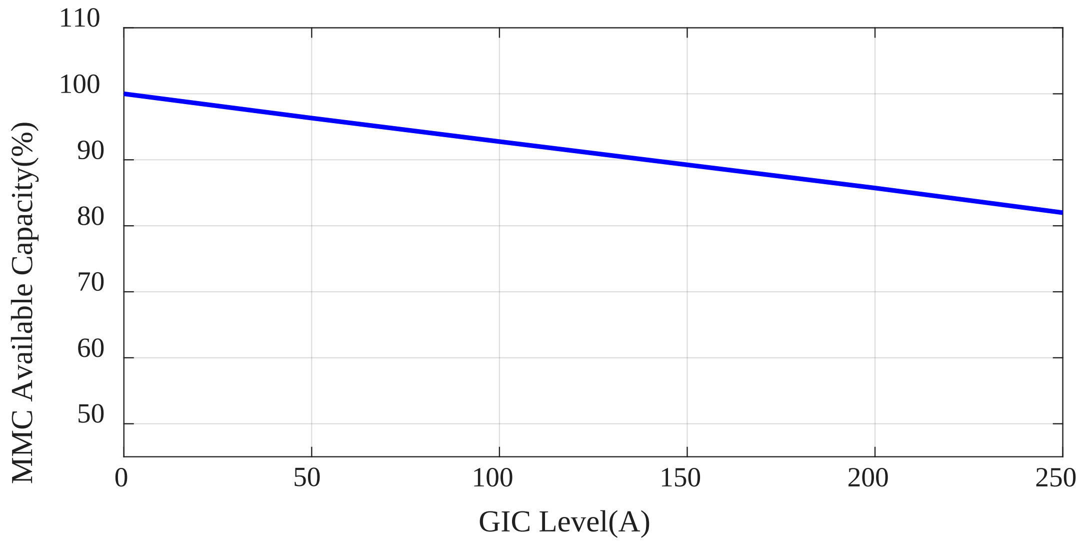

Figure 5-27. MMC derating in case of GIC due to MCB.

5.8 Response of Control Approach to Inject Reactive Power

As stated in the previous chapter, a severe result of the GMD is the increase in the reactive power in the grid due to transformer saturation, which is emphasized in section (5.3). To reduce the chance of a grid blackout, a control approach was presented to inject reactive power from the MMC in Chapter 4. The simulation results in Figure 5-28 with the proposed control scheme show that as the GIC flows in the system, the grid reactive power exchange does not change, whereas the MMC injects higher reactive power to the transformer, which accounts for the magnetizing current rise. This means that the proposed control scheme successfully reduces the risk of voltage collapse in the grid under GMD conditions.

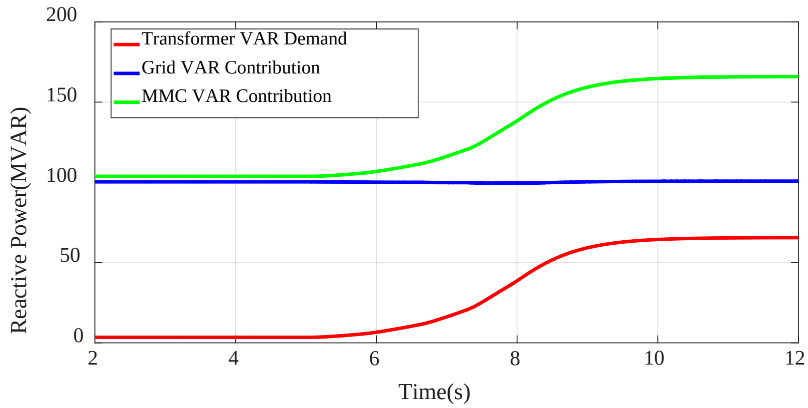

Figure 5-28. Effect of the proposed control scheme on the MMC and grid reactive power injection during 200 A of GIC.

Chapter 6

Conclusion and Future Works

6.1 Conclusion

The VSC-HVDC transmission systems are gaining more and more attention as they offer higher performance for long distances and offshore power transfer. The MMC-based HVDC system provides excellent performance in terms of harmonic emissions, reliability, scalability and efficiency. This research presents a novel analysis of the performance of the MMC-based HVDC system in the event of a solar storm. Chapter 1 provides the motivation for this research. It emphasizes that due to global attention to renewable energy sources, the application of MMC technology will be expanding. It states that GMD can be a catastrophic event for the power system, and this research is dedicated to investigating the GMD impacts on the MMC systems.

Chapter 2 provides a literature review on the GMD effects on the power system. The effects of GMD on different power system components are explored, and it is pinpointed that the transformers are most vulnerable in the presence of the GIC. An introduction to the background of the HVDC systems, including LCC and VSC based systems, is provided in this chapter. After examining different topologies of LCCs and VSCs, it is clearly inferred that the MMC is the most promising configuration for the HVDC transmission systems due to its significant intrinsic merits.

Finally, it emphasizes the lack of research on the MMC-based HVDC configuration exposed to GMD.

Chapter 3 explores the details of the study system. Different elements of the MMC station in terms of power components and control systems are examined. Various layers of the control system are reviewed in this chapter. The upper control layer, that is the system-wide control loop that controls the main outputs of the converter, is explained and the lower control level, which does the modulation, balancing the SMs voltages and mitigation of the circulation current, is reviewed in detail to provide a comprehensive understanding of the study system.

Chapter 4 starts with the GMD impacts on the MMC system. It states that the resulting harmonics from the saturation of the transformer are distributed between the grid and the MMC. The reactive power demand of the saturated transformer is also discussed. An analytical model is provided in this chapter to determine the share of the MMC in these harmonics. This model considers the internal interactions of the MMC, and it also considers the operating point of the converter. Also, a mitigating control block is designed and proposed to eliminate the 2^{nd},4^{th}, 5^{th},7^{th} and 8^{th} harmonics in the grid current in the case of GMD. This MCB improves the power quality in the grid, and it reduces the risk of blackouts in the system. Finally, a control approach is proposed for the reactive power compensation during GMD. This control approach injects reactive power from the MMC and supports the grid voltage stability.

Chapter 5 is dedicated to the simulation results. In this chapter, the effect of the GIC level on the magnitude of the harmonic spectrum and the demanded reactive power by the transformer is illustrated. Also, the impact of the MMC operating point on the resulting harmonics from the transformer saturation is explored. It is illustrated that the THD of the current and voltage violated the permissible values in both the grid and MMC for different loading. This chapter compares the analytical results for the MMC current harmonics with the measured values for different GIC levels and various MMC operating points, and it proves the effectiveness of the provided analytical model. The MCB effect on the targeted harmonics is observed, and it proves the expected performance. Also, simulation results are presented to make sure the operation of the MCB does not interfere with the main control loop of the system. The effect of the MCB on the MMC capacity is also discussed in this chapter, and appropriate derating is provided. Finally, the effectiveness of the proposed control approach for reactive power compensation is demonstrated using simulation results.

The proposed control schemes support the gird in the following aspects:

- The stability of the grid voltage is improved as the MMC injects reactive power into the saturated transformer instead of the grid.
- As the major current harmonics are removed from the grid current, the risk of outage of power components, including capacitor banks, generators, and SVCs, is reduced.
- Grid power quality is increased as the harmonics are removed.
- The distortion of the grid current and voltage waveforms is reduced.

6.2 Future Works

As suggestions for future works, the following can be noted:

- Research on how to reduce the distortion due to zero sequence currents in the grid.
- Investigating the harmonic spectrum and other impacts of asymmetrical saturation in three phases due to a mismatch in the phase’s resistance.

- Effect of the line frequency-dependent model on the system behaviour in the case of GMD.
- Improving the analytical impedance model by accounting for all the control loops, CBA, and circulating current controller.
- Exploring any other effect of MCB on the main system.

References

[1] F. Blaabjerg, Y. Yang, K. A. Kim, and J. Rodriguez, "Power Electronics Technology for Large-Scale Renewable Energy Generation," *Proceedings of the IEEE*, vol. 111, no. 4, pp. 335-355, 2023.

[2] Global Direct Primary Energy Consumption [Online]. Available: https://ourworldindata.org/grapher/global-primary-energy?stackMode=relative&time=800.2019&country=OWID_WRL

[3] "Renewable capacity highlights " International Renewable Energy Agency (IRENA)11 April 2022, Available: https://www.irena.org/-/media/Files/IRENA/Agency/Publication/2022/Apr/IRENA_-RE_Capacity_Highlights_2022.pdf?la=en&hash=6122BF5666A36BECD5AAA2050B011ECE255B3BC7.

[4] M. Barnes, D. V. Hertem, S. P. Teeuwsen, and M. Callavik, "HVDC Systems in Smart Grids," *Proceedings of the IEEE*, vol. 105, no. 11, pp. 2082-2098, 2017.

[5] A. Stan, S. Costinaș, and G. Ion, "Overview and Assessment of HVDC Current Applications and Future Trends," *Energies*, vol. 15, no. 3. doi: 10.3390/en15031193

[6] "Offshore Wind Market Report: 2022 Edition," US Department of EnergyAUGUST 16, 2022, Available: https://www.energy.gov/sites/default/files/2022-09/offshore-wind-market-report-2022-v2.pdf.

[7] B. Gemmell, J. Dorn, D. Retzmann, and D. Soerangr, "Prospects of multilevel VSC technologies for power transmission," in *2008 IEEE/PES Transmission and Distribution Conference and Exposition*, 2008, pp. 1-16.

[8] "Effects of geomagnetic disturbances on the bulk power systems," in "Special Reliability Assessment Interim Report," North American Electric Reliability Corporation (NERC)2012.

[9] "Geomagnetic Disturbances: Their Impact on the Power Grid," *IEEE Power and Energy Magazine,* vol. 11, no. 4, pp. 71-78, 2013.

[10] D. H. Boteler, "The Evolution of Québec Earth Models Used to Model Geomagnetically Induced Currents," *IEEE Transactions on Power Delivery,* vol. 30, no. 5, pp. 2171-2178, 2015.

[11] What is geomagnetic storm [Online]. Available: https://windy.app/textbook/what-is-geomagnetic-storm-explanation-in-simple-words.html

[12] N. Bhusal, M. Abdelmalak, M. Kamruzzaman, and M. Benidris, "Power System Resilience: Current Practices, Challenges, and Future Directions," *IEEE Access,* vol. 8, pp. 18064-18086, 2020.

[13] M. Panteli, P. Mancarella, D. N. Trakas, E. Kyriakides, and N. D. Hatziargyriou, "Metrics and Quantification of Operational and Infrastructure Resilience in Power Systems," *IEEE Transactions on Power Systems,* vol. 32, no. 6, pp. 4732-4742, 2017.

[14] M. Panteli, C. Pickering, S. Wilkinson, R. Dawson, and P. Mancarella, "Power System Resilience to Extreme Weather: Fragility Modeling, Probabilistic Impact Assessment, and Adaptation Measures," *IEEE Transactions on Power Systems,* vol. 32, no. 5, pp. 3747-3757, 2017.

[15] I. P. O. C. J. A. Change, "Climate change 2007: The physical science basis," vol. 6, no. 07, p. 333, 2007.

[16] R. Billinton and K. E. Bollinger, "Transmission System Reliability Evaluation Using Markov Processes," *IEEE Transactions on Power Apparatus and Systems,* vol. PAS-87, no. 2, pp. 538-547, 1968.

[17] F. H. Jufri, V. Widiputra, and J. J. A. e. Jung, "State-of-the-art review on power grid resilience to extreme weather events: Definitions, frameworks, quantitative assessment methodologies, and enhancement strategies," vol. 239, pp. 1049-1065, 2019.

[18] A. Gholami, T. Shekari, M. H. Amirioun, F. Aminifar, M. H. Amini, and A. Sargolzaei, "Toward a Consensus on the Definition and Taxonomy of Power System Resilience," *IEEE Access*, vol. 6, pp. 32035-32053, 2018.

[19] A. Hussain, V.-H. Bui, and H.-M. J. A. e. Kim, "Microgrids as a resilience resource and strategies used by microgrids for enhancing resilience," vol. 240, pp. 56-72, 2019.

[20] M. Panteli and P. J. I. S. J. Mancarella, "Modeling and evaluating the resilience of critical electrical power infrastructure to extreme weather events," vol. 11, no. 3, pp. 1733-1742, 2015.

[21] Y. Liu and C. Singh, "Reliability Evaluation of Composite Power Systems Using Markov Cut-Set Method," *IEEE Transactions on Power Systems*, vol. 25, no. 2, pp. 777-785, 2010.

[22] M. Panteli and P. J. E. P. S. R. Mancarella, "Influence of extreme weather and climate change on the resilience of power systems: Impacts and possible mitigation strategies," vol. 127, pp. 259-270, 2015.

[23] W. Yuan, J. Wang, F. Qiu, C. Chen, C. Kang, and B. Zeng, "Robust Optimization-Based Resilient Distribution Network Planning Against Natural Disasters," *IEEE Transactions on Smart Grid*, vol. 7, no. 6, pp. 2817-2826, 2016.

[24] M. Ouyang, L. Dueñas-Osorio, and X. J. S. s. Min, "A three-stage resilience analysis framework for urban infrastructure systems," vol. 36, pp. 23-31, 2012.

[25] R. Francis, B. J. R. e. Bekera, and s. safety, "A metric and frameworks for resilience analysis of engineered and infrastructure systems," vol. 121, pp. 90-103, 2014.

[26] M. Ouyang and L. J. C. A. I. J. o. N. S. Dueñas-Osorio, "Time-dependent resilience assessment and improvement of urban infrastructure systems," vol. 22, no. 3, 2012.

[27] M. Ouyang and L. J. S. S. Duenas-Osorio, "Multi-dimensional hurricane resilience assessment of electric power systems," vol. 48, pp. 15-24, 2014.

[28] A. J. E. Kwasinski, "Quantitative model and metrics of electrical grids’ resilience evaluated at a power distribution level," vol. 9, no. 2, p. 93, 2016.

[29] M. Panteli, D. N. Trakas, P. Mancarella, and N. D. Hatziargyriou, "Boosting the Power Grid Resilience to Extreme Weather Events Using Defensive Islanding," *IEEE Transactions on Smart Grid,* vol. 7, no. 6, pp. 2913-2922, 2016.

[30] S. Espinoza, M. Panteli, P. Mancarella, and H. J. E. P. S. R. Rudnick, "Multi-phase assessment and adaptation of power systems resilience to natural hazards," vol. 136, pp. 352-361, 2016.

[31] Geo-magnetic Disturbances (GMD): Monitoring, Mitigation, and Next Steps [Online]. Available: https://www.epri.com/research/products/000000000001024629

[32] D. H. Boteler, "Geomagnetic Hazards to Conducting Networks," *Natural Hazards,* vol. 28, no. 2, pp. 537-561, 2003/03/01 2003.

[33] "IEEE Guide for Establishing Power Transformer Capability while under Geomagnetic Disturbances," *IEEE Std C57.163-2015,* pp. 1-50, 2015.

[34] N. R. Council, *Severe Space Weather Events: Understanding Societal and Economic Impacts: A Workshop Report*. Washington, DC: The National Academies Press, 2008, p. 144.

[35] Centra Technology. Inc., "Geomagnetic Storms”," *produced for the OECD/IFP Futures Project on “Future Global Shocks,”* January 14, 2011.

[36] J. N. Wrubel, "Monitoring for geomagnetic induced current flow effects using existing EMS telemetering," in *[Proceedings] Conference Papers 1991 Power Industry Computer Application Conference,* 1991, pp. 45-49.

[37] S. M. I. A. Erinmez, C. Rogers, T. Yasuhiro, S. Ogawa, H. Swahn, and J. G. Kappenman, "Application of modelling techniques to assess geomagnetically induced current risks on the NGC transmission system," presented at the CIGRÉ = International Conference on Large High Voltage Electric Systems, Paris, France, March 26, 2002.

[38] Metatech Corporation for Oak Ridge National Laboratory, "Geomagnetic Storms and Their Impacts on the U.S. Power Grid," *Meta‐R‐319,* January 2010.

[39] Berge Jonathan E., "Impact of Geomagnetically Induced Currents on Power Transformers," Electronic Thesis and Dissertation Repository, 132, 2011.

[40] N. Takasu, T. Oshi, F. Miyawaki, S. Saito, and Y. Fujiwara, "An experimental analysis of DC excitation of transformers by geomagnetically induced currents," *IEEE Transactions on Power Delivery*, vol. 9, no. 2, pp. 1173-1182, 1994.

[41] M. Lahtinen and J. Elovaara, "GIC occurrences and GIC test for 400 kV system transformer," *IEEE Transactions on Power Delivery,* vol. 17, no. 2, pp. 555-561, 2002.

[42] Z. M. Khurshid, N. F. A. Aziz, Z. A. Rhazali, and M. Z. A. A. Kadir, "Impact of Geomagnetically Induced Currents on High Voltage Transformers in Malaysian Power Network and Its Mitigation," *IEEE Access*, vol. 9, pp. 167204-167217, 2021.

[43] A. Rezaei-Zare, "Behavior of Single-Phase Transformers Under Geomagnetically Induced Current Conditions," *IEEE Transactions on Power Delivery*, vol. 29, no. 2, pp. 916-925, 2014.

[44] A. Rezaei-Zare, "Reactive Power Loss Versus GIC Characteristic of Single-Phase Transformers," *IEEE Transactions on Power Delivery*, vol. 30, no. 3, pp. 1639-1640, 2015.

[45] M. Akbari, M. Mostafaei, and A. Rezaei-Zare, "Estimation of Hot-Spot Heating in OIP Transformer Bushings Due to Geomagnetically Induced Current," *IEEE Transactions on Power Delivery*, vol. 38, no. 2, pp. 1277-1285, 2023.

[46] S. Lu, Y. Liu, and J. D. L. Ree, "Harmonics generated from a DC biased transformer," *IEEE Transactions on Power Delivery,* vol. 8, no. 2, pp. 725-731, 1993.

[47] P. R. Price, "Geomagnetically induced current effects on transformers," *IEEE Transactions on Power Delivery,* vol. 17, no. 4, pp. 1002-1008, 2002.

[48] D. Xuzhu, L. Yilu, and J. G. Kappenman, "Comparative analysis of exciting current harmonics and reactive power consumption from GIC saturated transformers," in *2001 IEEE Power Engineering Society Winter Meeting. Conference Proceedings (Cat. No.01CH37194)*, 2001, vol. 1, pp. 318-322 vol.1.

[49] A. P. S. Meliopoulos, E. N. Glytsis, G. J. Cokkinides, and M. Rabinowitz, "Comparison of SS-GIC and MHD-EMP-GIC effects on power systems," *IEEE Transactions on Power Delivery,* vol. 9, no. 1, pp. 194-207, 1994.

[50] S. Lu and Y. Liu, "FEM analysis of DC saturation to assess transformer susceptibility to geomagnetically induced currents," *IEEE Transactions on Power Delivery,* vol. 8, no. 3, pp. 1367-1376, 1993.

[51] P. S. M. M.A.S. Masoum, "Impact of balanced and unbalanced direct current bias on harmonic distortion generated by asymmetric three-phase three-leg transformers," *IET Electric Power Applications*, vol. 4, no.4, pp. 507-515, 2010.

[52] R. Girgis and K. Vedante, "Effects of GIC on power transformers and power systems," in *PES T&D 2012*, 2012, pp. 1-8.

[53] J. Ramírez, J. H. Rodríguez–Rodríguez, and R. Mijarez, "Simple Geomagnetic Induced Current Detection and Monitoring in Power Transformers," vol. 49, no. 7, pp. 230-233, 2016.

[54] R. S. Girgis and K. B. Vedante, "Impact of GICs on Power Transformers: Overheating is not the real issue," *IEEE Electrification Magazine,* vol. 3, no. 4, pp. 8-12, 2015.

[55] R. Girgis, C.-D. Ko, and D. Scott, "Analysis of transformer overheating due to geomagnetically induced currents," in *Proceedings of the American Power Conference;(United States)*, 1991, vol. 53, no. CONF-9104106-.

[56] L. Marti, A. Rezaei-Zare, and A. Narang, "Simulation of Transformer Hotspot Heating due to Geomagnetically Induced Currents," *IEEE Transactions on Power Delivery,* vol. 28, no. 1, pp. 320-327, 2013.

[57] "1989 NERC Hydro Quebec GMD Event Report," 1989, Available: https://www.nerc.com/pa/Stand/Geomagnetic%20Disturbance%20Resources%20DL/NERC_1989-Quebec-Disturbance_Report.pdf.

[58] R. A. Walling and A. N. Khan, "Characteristics of transformer exciting-current during geomagnetic disturbances," *IEEE Transactions on Power Delivery,* vol. 6, no. 4, pp. 1707-1714, 1991.

[59] J. G. Kappenman, V. D. Albertson, and N. Mohan, "Current Transformer and Relay Performance in the Presence of Geomagnetically-Induced Currents," *IEEE Transactions on Power Apparatus and Systems,* vol. PAS-100, no. 3, pp. 1078-1088, 1981.

[60] R. Fan, Y. Liu, A. Umana, Z. Tan, L. Sun, and Y. An, "The impact of solar storms on protective relays for saturable-core transformers," in *2017 IEEE Power & Energy Society General Meeting*, 2017, pp. 1-5.

[61] V. N. Rajput, D. H. Boteler, N. Rana, M. Saiyed, S. Anjana, and M. Shah, "Insight into impact of geomagnetically induced currents on power systems: Overview, challenges and mitigation," *Electric Power Systems Research,* vol. 192, p. 106927, 2021/03/01/ 2021.

[62] B. Ahmadzadeh-Shooshtari and A. Rezaei-Zare, "Advanced Transformer Differential Protection Under GIC Conditions," *IEEE Transactions on Power Delivery,* vol. 37, no. 3, pp. 1433-1444, 2022.

[63] L. Bolduc, P. Langlois, D. Boteler, and R. Pirjola, "A study of geoelectromagnetic disturbances in Quebec. II. Detailed analysis of a large event," *IEEE Transactions on Power Delivery,* vol. 15, no. 1, pp. 272-278, 2000.

[64] B. Bozoki *et al.*, "The effects of GIC on protective relaying," *IEEE Transactions on Power Delivery*, vol. 11, no. 2, pp. 725-739, 1996.

[65] R. P. Jayasinghe, P. G. McLaren, and T. Gouldsborough, "Effect of GIC on overcurrent protection for filter banks," in *IEEE WESCANEX 93 Communications, Computers and Power in the Modern Environment - Conference Proceedings*, 1993, pp. 36-42.

[66] L. Bolduc, A. Gaudreau, and A. Dutil, "Saturation time of transformers under dc excitation," *Electric Power Systems Research*, vol. 56, no. 2, pp. 95-102, 2000/11/01/ 2000.

[67] P. Jankee, D. T. O. Oyedokun, and H. K. Chisepo, "Dynamic Response of Power Systems With Real GICs: Impact on Generator Excitation Control," *IEEE Transactions on Power Delivery*, vol. 37, no. 6, pp. 4911-4922, 2022.

[68] W. B. Gish, W. E. Feero, and G. D. Rockefeller, "Rotor heating effects from geomagnetic induced currents," *IEEE Transactions on Power Delivery*, vol. 9, no. 2, pp. 712-719, 1994.

[69] P. Jankee, D. T. O. Oyedokun, and H. Chisepo, "Harmonic Sequences Affecting Synchronous Generator Response to GIC," in *2022 IEEE PES/IAS PowerAfrica*, 2022, pp. 1-5.

[70] A. Rezaei-Zare and L. Marti, "Generator thermal stress during a Geomagnetic Disturbance," in *2013 IEEE Power & Energy Society General Meeting*, 2013, pp. 1-5.

[71] Z. M. K. Abda, N. F. A. Aziz, M. Z. A. A. Kadir, and Z. A. Rhazali, "A Review of Geomagnetically Induced Current Effects on Electrical Power System: Principles and Theory," *IEEE Access*, vol. 8, pp. 200237-200258, 2020.

[72] M. P. Bahrman and B. K. Johnson, "The ABCs of HVDC transmission technologies," *IEEE Power and Energy Magazine*, vol. 5, no. 2, pp. 32-44, 2007.

[73] D. V. Hertem, O. Gomis-Bellmunt, and J. Liang, *HVDC Grids: For Offshore and Supergrid of the Future*. Wiley-IEEE Press, 2016, p. 528.

[74] G. Lagrotteria, D. Pietribiasi, and M. Marelli, "HVDC Cables - The technology boost," in *2019 AEIT HVDC International Conference (AEIT HVDC)*, 2019, pp. 1-5.

[75] M. Eremia, C.-C. Liu, and A.-A. Edris, *Advanced Solutions in Power Systems: HVDC, FACTS, and Artificial Intelligence*. 2016, p. 1072.

[76] C.-K. Kim, V. K. Sood, G.-S. Jang, S.-J. Lim, and S.-J. Lee, *HVDC Transmission: Power Conversion Applications in Power Systems*. Wiley-IEEE Press, 2009, p. 352.

[77] S. Kuruganty, "HVDC transmission system models for power system reliability evaluation," in *IEEE WESCANEX 95. Communications, Power, and Computing. Conference Proceedings*, 1995, vol. 2, pp. 501-507 vol.2.

[78] J. Chitode, *Power Electronics*. Technical Publications, 2020.

[79] H. Nee, L. Harnefors, and K. Sharifabadi, *Design, control, and application of modular multilevel converters for HVDC transmission systems*. Chichester, West Sussex: IEEE Press, 2016.

[80] *Kunliulong DC Project has been placed into operation*. Available: http://eng.csg.cn/Press_release/News_2021/202101/t20210105_316697.html

[81] *Kunliulong UHV hybrid multi-terminal HVDC transmission project was successfully put into operation*. Available: https://www.nrec.com/en/index.php/about/newsInfo/83.html

[82] N. Flourentzou, V. G. Agelidis, and G. D. Demetriades, "VSC-Based HVDC Power Transmission Systems: An Overview," *IEEE Transactions on Power Electronics*, vol. 24, no. 3, pp. 592-602, 2009.

[83] D. Guo, "Modelling of MMC-HVDC system for EMT study," http://purl.org/coar/resource_type/c_db06, 2020.

[84] ABB. *HVDC Light® reference list*. Available: https://new.abb.com/systems/hvdc/references

[85] W.Liu, "OPERATION AND PROTECTION OF VSC-HVDC GRIDS," PhD dissertation, CARDIFF UNIVERSITY, 2022.

[86] *Evolution of HVDC light*. Available: https://new.abb.com/news/detail/4224/evolution-of-hvdc-lightr

[87] B. R. Andersen, L. Xu, and K. T. G. Wong, "Topologies for VSC transmission," in *Seventh International Conference on AC-DC Power Transmission*, 2001, pp. 298-304.

[88] A. Nabae, I. Takahashi, and H. Akagi, "A New Neutral-Point-Clamped PWM Inverter," *IEEE Transactions on Industry Applications*, vol. IA-17, no. 5, pp. 518-523, 1981.

[89] J. Rodriguez, S. Bernet, P. K. Steimer, and I. E. Lizama, "A Survey on Neutral-Point-Clamped Inverters," *IEEE Transactions on Industrial Electronics*, vol. 57, no. 7, pp. 2219-2230, 2010.

[90] R. Sommer, A. Mertens, C. Brunotte, and G. Trauth, "Medium voltage drive system with NPC three-level inverter using IGBTs," in *IEE Seminar PWM Medium Voltage Drives (Ref. No. 2000/063)*, 2000, pp. 3/1-3/5.

[91] R. Sommer, A. Mertens, M. Griggs, H. J. Conraths, M. Bruckmann, and T. Greif, "New medium voltage drive systems using three-level neutral point clamped inverter with high voltage IGBT," in *Conference Record of the 1999 IEEE Industry Applications Conference. Thirty-Forth IAS Annual Meeting (Cat. No.99CH36370)*, 1999, vol. 3, pp. 1513-1519 vol.3.

[92] D. Kidd, B. Mehraban, B. Ekehov, J. Ulleryd, and A. Edris, "Eagle pass back to back VSC installation and operation," in *2003 IEEE Power Engineering Society General Meeting (IEEE Cat. No.03CH37491)*, 2003, vol. 3, pp. 1829-1833 Vol. 3.

[93] O. S. Senturk, L. Helle, S. Munk-Nielsen, P. Rodriguez, and R. Teodorescu, "Power Capability Investigation Based on Electrothermal Models of Press-Pack IGBT Three-Level NPC and ANPC VSCs for Multimegawatt Wind Turbines," *IEEE Transactions on Power Electronics*, vol. 27, no. 7, pp. 3195-3206, 2012.

[94] T. Bruckner, S. Bernet, and H. Guldner, "The active NPC converter and its loss-balancing control," *IEEE Transactions on Industrial Electronics*, vol. 52, no. 3, pp. 855-868, 2005.

[95] T. Bruckner and S. Bemet, "Loss balancing in three-level voltage source inverters applying active NPC switches," in *2001 IEEE 32nd Annual Power Electronics Specialists Conference (IEEE Cat. No.01CH37230)*, 2001, vol. 2, pp. 1135-1140 vol.2.

[96] The world’s longest underground power transmission system [Online]. Available: https://www.hitachiabb-powergrids.com/references/hvdc/murraylink

[97] Cross Sound Cable [Online]. Available: http://www.crosssoundcable.com/

[98] A. Lesnicar and R. Marquardt, "An innovative modular multilevel converter topology suitable for a wide power range," in *2003 IEEE Bologna Power Tech Conference Proceedings*, 2003, vol. 3, p. 6 pp. Vol.3.

[99] T. WESTERWELLER, K. FRIEDRICH, U. ARMONIES, A. ORINI, D. PARQUET, and S. WEHN, "Trans bay cable – world's first HVDC system using multilevel voltage-sourced converter," in *CIGRE Conference*, Paris, August 2010.

[100] S. P. Teeuwsen, "Modeling the Trans Bay Cable Project as Voltage-Sourced Converter with Modular Multilevel Converter design," in *2011 IEEE Power and Energy Society General Meeting*, 2011, pp. 1-8.

[101] Q. Tu, Z. Xu, and L. Xu, "Reduced Switching-Frequency Modulation and Circulating Current Suppression for Modular Multilevel Converters," *IEEE Transactions on Power Delivery*, vol. 26, no. 3, pp. 2009-2017, 2011.

[102] Q. Tu and Z. Xu, "Power losses evaluation for modular multilevel converter with junction temperature feedback," in *2011 IEEE Power and Energy Society General Meeting*, 2011, pp. 1-7.

[103] A. Dekka, B. Wu, N. R. Zargari, and R. L. Fuentes, "Dynamic Voltage Balancing Algorithm for Modular Multilevel Converter: A Unique Solution," *IEEE Transactions on Power Electronics*, vol. 31, no. 2, pp. 952-963, 2016.

[104] R. Marquardt, "Modular Multilevel Converter: An universal concept for HVDC-Networks and extended DC-Bus-applications," in *The 2010 International Power Electronics Conference - ECCE ASIA -*, 2010, pp. 502-507.

[105] A. Lesnicar and R. Marquardt, "An innovative modular multilevel converter topology suitable for a wide power range," in *2003 IEEE Bologna Power Tech Conference Proceedings*, 2003, vol. 3, p. 6.

[106] S. Allebrod, R. Hamerski, and R. Marquardt, "New transformerless, scalable Modular Multilevel Converters for HVDC-transmission," in *2008 IEEE Power Electronics Specialists Conference*, 2008, pp. 174-179.

[107] M. Glinka and R. Marquardt, "A new AC/AC-multilevel converter family applied to a single-phase converter," in *The Fifth International Conference on Power Electronics and Drive Systems, 2003. PEDS 2003.*, 2003, vol. 1, pp. 16-23 Vol.1.

[108] S. Li, F. Xingang, E. Alonso, M. Fairbank, and D. C. Wunsch, "Neural-network based vector control of VSCHVDC transmission systems," in *2015 International Conference on Renewable Energy Research and Applications (ICRERA)*, 2015, pp. 173-180.

[109] Y. Zhang, G. P. Adam, T. C. Lim, S. J. Finney, and B. W. Williams, "Voltage source converter in high voltage applications: Multilevel versus two-level converters," in *9th IET International Conference on AC and DC Power Transmission (ACDC 2010)*, 2010, pp. 1-5.

[110] P. Li, G. P. Adam, D. Holliday, and B. Williams, "Controlled Transition Full-Bridge Hybrid Multilevel Converter With Chain-Links of Full-Bridge Cells," *IEEE Transactions on Power Electronics*, vol. 32, no. 1, pp. 23-38, 2017.

[111] D. A. N. Jacobson, P. Wang, M. Mohaddes, M. Rashwan, and R. Ostash, "A preliminary look at the feasibility of VSC HVdc in Manitoba," in *2011 IEEE Electrical Power and Energy Conference*, 2011, pp. 80-85.

[112] G. P. Adam, I. Abdelsalam, J. E. Fletcher, G. M. Burt, D. Holliday, and S. J. Finney, "New Efficient Submodule for a Modular Multilevel Converter in Multiterminal HVDC Networks," *IEEE Transactions on Power Electronics*, vol. 32, no. 6, pp. 4258-4278, 2017.

[113] G. Asplund, "Application of HVDC Light to power system enhancement," in *2000 IEEE Power Engineering Society Winter Meeting. Conference Proceedings (Cat. No.00CH37077)*, 2000, vol. 4, pp. 2498-2503 vol.4.

[114] U. Astrom, B. Westman, V. Lescale, and G. Asplund, "Power transmission with HVDC at voltages above 600 kV," in *2005 IEEE Power Engineering Society Inaugural Conference and Exposition in Africa*, 2005, pp. 44-50.

[115] B. Jacobson, P. Karlsson, G. Asplund, L. Harnefors, and T. U. Jonsson, "VSC-HVDC Transmission with Cascaded Two-Level Converters," in *CIGRE*, 2010.

[116] G. P. Adam, I. A. Gowaid, S. J. Finney, D. Holliday, and B. W. Williams, "Review of dc–dc converters for multi-terminal HVDC transmission networks," vol. 9, no. 2, pp. 281-296, 2016.

[117] G. P. Adam, S. J. Finney, K. Bell, and B. W. Williams, "Transient capability assessments of HVDC voltage source converters," in *2012 IEEE Power and Energy Conference at Illinois*, 2012, pp. 1-8.

[118] W. Su, X. Zhou, and F. Cai, "Application analysis of dc grounding resistance used in the Nanhui flexible HVDC," *Power Energ*, vol. 34, Dec. 2013 Art. no. 6.

[119] "Working Group B4.70, "Guide for electromagnetic transient studies involving VSC converters," *CIGRE Technical Brochure*, vol. 832, 2021.

[120] K. Sano and H. Nakayama, "An Overvoltage-Less Protection Method for Pole-to-Ground Faults in Symmetrical Monopole HVDC Systems by Half-Bridge MMC," in *2020 IEEE Energy Conversion Congress and Exposition (ECCE)*, 2020, pp. 3383-3388.

[121] F. Palone, M. Marzinotto, and L. Buono, "Temporary overvoltage mitigation in symmetrical monopole VSC-MMC HVDC links," in *2017 AEIT International Annual Conference*, 2017, pp. 1-6.

[122] S. Wenig, M. Goertz, M. Suriyah, and T. Leibfried, "Active DC fault management of a bipolar full-bridge MMC-HVDC scheme with metallic return," in *2016 IEEE International Energy Conference (ENERGYCON)*, 2016, pp. 1-6.

[123] D. L. Dickmander, S. Y. Lee, G. L. Desilets, and M. Granger, "AC/DC harmonic interactions in the presence of GIC for the Quebec-New England Phase II HVDC transmission," *IEEE Transactions on Power Delivery,* vol. 9, no. 1, pp. 68-78, 1994.

[124] L. Weixia, W. Jun, L. Lianguang, M. Guanglei, W. Liying, and X. Chao, "Harmonic analysis of the converter stations modulated by GIC in HVDC transmission lines," in *2008 International Conference on Electrical Machines and Systems*, 2008, pp. 4244-4249.

[125] B. Kovan and F. d. León, "Mitigation of Geomagnetically Induced Currents by Neutral Switching," *IEEE Transactions on Power Delivery,* vol. 30, no. 4, pp. 1999-2006, 2015.

[126] M. Yang, D. Deswal, and F. d. León, "Mitigation of Half-Cycle Saturation of Adjacent Transformers During HVDC Monopolar Operation—Part I: Mitigation Principle and Device Design," *IEEE Transactions on Power Delivery,* vol. 34, no. 6, pp. 2232-2239, 2019.

[127] I. Babaeiyazdi, M. Rezaei-Zare, and A. Rezaei-Zare, "Wind Farm Operating Conditions Under Geomagnetic Disturbance," *IEEE Transactions on Power Delivery,* vol. 35, no. 3, pp. 1357-1364, 2020.

[128] S. Gao and M. Barnes, "Making VSC-HVDC control robust to geomagnetically induced current," in *2016 IEEE Power and Energy Society General Meeting (PESGM)*, 2016, pp. 1-5.

[129] H. Saad *et al.*, "Dynamic Averaged and Simplified Models for MMC-Based HVDC Transmission Systems," *IEEE Transactions on Power Delivery,* vol. 28, no. 3, pp. 1723-1730, 2013.

[130] J. Peralta, H. Saad, S. Dennetiere, J. Mahseredjian, and S. Nguefeu, "Detailed and Averaged Models for a 401-Level MMC–HVDC System," *IEEE Transactions on Power Delivery,* vol. 27, no. 3, pp. 1501-1508, 2012.

[131] H. Saad *et al.*, "Modular Multilevel Converter Models for Electromagnetic Transients," *IEEE Transactions on Power Delivery,* vol. 29, no. 3, pp. 1481-1489, 2014.

[132] Y. Li and F. Wang, "Arm inductance selection principle for modular multilevel converters with circulating current suppressing control," in *2013 Twenty-Eighth Annual IEEE Applied Power Electronics Conference and Exposition (APEC)*, 2013, pp. 1321-1325.

[133] "Working Group B4.57, "Guide for the Development of Models for HVDC Converters in a HVDC Grid," *CIGRE Technical Brochure,* vol. 604, 2014.

[134] A. Lindberg, *PWM and control of two and three level high power voltage source converters*. Royal Institute of Technology, 1995.

[135] L. Zhang, "Modeling and control of VSC-HVDC links connected to weak AC systems," Ph.D. dissertation, KTH, Stockholm, 2010.

[136] M. Hamzeh, S. Emamian, H. Karimi, and J. Mahseredjian, "Robust Control of an Islanded Microgrid Under Unbalanced and Nonlinear Load Conditions," *IEEE Journal of Emerging and Selected Topics in Power Electronics*, vol. 4, no. 2, pp. 512-520, 2016.

[137] H. Karimi, M. Karimi-Ghartemani, and K. Sheshyekani, "Robust Control of Three-Phase Voltage Source Converters Under Unbalanced Grid Conditions," *IEEE Transactions on Power Electronics,* vol. 34, no. 11, pp. 11278-11289, 2019.

[138] H. Karimi, Y. Seyedi, and M. Karimi-Ghartemani, "A Robust and Simple Phase-Locked Loop for Unbalanced Power Grid Applications," in *2019 IEEE 28th International Symposium on Industrial Electronics (ISIE)*, 2019, pp. 29-34.

[139] Y. H. Lo, Y. C. Chen, K. L. Lian, H. Karimi, and C. Z. Wang, "An Iterative Control Method for Voltage Source Converters to Eliminate Uncharacteristic Harmonics Under

Unbalanced Grid Voltages for High-Power Applications," *IEEE Transactions on Sustainable Energy,* vol. 10, no. 3, pp. 1419-1429, 2019.

[140] S. M. Hoseinizadeh, H. Karimi, M. Karimi-Ghartemani, and S. Ouni, "A Multivariable Phase-Locked Loop-Integrated Controller for Enhanced Performance of Voltage Source Converters Under Weak Grid Conditions," *IEEE Transactions on Industrial Electronics,* vol. 69, no. 10, pp. 10079-10089, 2022.

[141] S. Silwal, M. Karimi-Ghartemani, H. Karimi, M. Davari, and S. M. H. Zadeh, "A Multivariable Controller in Synchronous Frame Integrating Phase-Locked Loop to Enhance Performance of Three-Phase Grid-Connected Inverters in Weak Grids," *IEEE Transactions on Power Electronics,* vol. 37, no. 9, pp. 10348-10359, 2022.

[142] Q. Tu and Z. Xu, "Impact of Sampling Frequency on Harmonic Distortion for Modular Multilevel Converter," *IEEE Transactions on Power Delivery,* vol. 26, no. 1, pp. 298-306, 2011.

[143] K. Li and C. Zhao, "New Technologies of Modular Multilevel Converter for VSC-HVDC Application," in *2010 Asia-Pacific Power and Energy Engineering Conference,* 2010, pp. 1-4.

[144] B. Bahrani, S. Debnath, and M. Saeedifard, "Circulating Current Suppression of the Modular Multilevel Converter in a Double-Frequency Rotating Reference Frame," *IEEE Transactions on Power Electronics,* vol. 31, no. 1, pp. 783-792, 2016.

[145] T. Qingrui, X. Zheng, H. Huang, and Z. Jing, "Parameter design principle of the arm inductor in modular multilevel converter based HVDC," in *2010 International Conference on Power System Technology*, 2010, pp. 1-6.

[146] S. Rohner, S. Bernet, M. Hiller, and R. Sommer, "Modelling, simulation and analysis of a Modular Multilevel Converter for medium voltage applications," in *2010 IEEE International Conference on Industrial Technology,* 2010, pp. 775-782.

[147] A. Antonopoulos, L. Angquist, H. P. J. t. E. C. o. P. E. Nee, and Applications, "On dynamics and voltage control of the Modular Multilevel Converter," pp. 1-10, 2009.

[148] H. Saad, Y. Fillion, S. Deschanvres, Y. Vernay, and S. Dennetière, "On Resonances and Harmonics in HVDC-MMC Station Connected to AC Grid," *IEEE Transactions on Power Delivery,* vol. 32, no. 3, pp. 1565-1573, 2017.

[149] A. Jamshidifar and D. Jovcic, "Small-Signal Dynamic DQ Model of Modular Multilevel Converter for System Studies," *IEEE Transactions on Power Delivery,* vol. 31, no. 1, pp. 191-199, 2016.

[150] J. Lyu, X. Cai, and M. Molinas, "Frequency Domain Stability Analysis of MMC-Based HVdc for Wind Farm Integration," *IEEE Journal of Emerging and Selected Topics in Power Electronics,* vol. 4, no. 1, pp. 141-151, 2016.

[151] M. Beza, M. Bongiorno, and G. Stamatiou, "Analytical Derivation of the AC-Side Input Admittance of a Modular Multilevel Converter With Open- and Closed-Loop Control Strategies," *IEEE Transactions on Power Delivery,* vol. 33, no. 1, pp. 248-256, 2018.

[152] L. Bessegato, K. Ilves, L. Harnefors, and S. Norrga, "Effects of Control on the AC-Side Admittance of a Modular Multilevel Converter," *IEEE Transactions on Power Electronics,* vol. 34, no. 8, pp. 7206-7220, 2019.

[153] Y. Chen, L. Xu, A. Egea-Àlvarez, B. Marshall, M. H. Rahman, and A. D. Oluwole, "MMC Impedance Modeling and Interaction of Converters in Close Proximity," *IEEE Journal of Emerging and Selected Topics in Power Electronics,* vol. 9, no. 6, pp. 7223-7236, 2021.

[154] M. Cespedes and J. Sun, "Impedance Modeling and Analysis of Grid-Connected Voltage-Source Converters," *IEEE Transactions on Power Electronics,* vol. 29, no. 3, pp. 1254-1261, 2014.

[155] H. Tao, H. Hu, X. Zhu, Y. Zhou, and Z. He, "Harmonic Instability Analysis and Suppression Method Based on αβ- Frame Impedance for Trains and Network Interaction System," *IEEE Transactions on Energy Conversion,* vol. 34, no. 2, pp. 1124-1134, 2019.

[156] Y. Li, T. An, D. Zhang, X. Pei, K. Ji, and G. Tang, "Analysis and Suppression Control of High Frequency Resonance for MMC-HVDC System," *IEEE Transactions on Power Delivery,* vol. 36, no. 6, pp. 3867-3881, 2021.

[157] K. Ilves, A. Antonopoulos, S. Norrga, and H. P. Nee, "Steady-State Analysis of Interaction Between Harmonic Components of Arm and Line Quantities of Modular Multilevel Converters," *IEEE Transactions on Power Electronics,* vol. 27, no. 1, pp. 57-68, 2012.

[158] C. Bajracharya, M. Molinas, J. Suul, and T. Undeland, *Understanding of Tuning Techniques of Converter Controllers for VSC-HVDC*. 2008.

[159] A. Rezaei-Zare, L. Marti, A. Narang, and A. Yan, "Analysis of Three-Phase Transformer Response due to GIC Using an Advanced Duality-Based Model," *IEEE Transactions on Power Delivery,* vol. 31, no. 5, pp. 2342-2350, 2016.

[160] *IEEE Recommended Practice and Requirements for Harmonic Control in Electric Power Systems*, IEEE Standard 519, 2014.